THE INFLUENCE OF AN ELECTRIC FIELD ON THE TRANSPORT PROPERTIES OF POLAR GASES

J. J. DE GROOT

THE INFLUENCE OF AN ELECTRIC FIELD ON THE TRANSPORT PROPERTIES OF POLAR GASES

PROEFSCHRIFT

TER VERKRIJGING VAN DE GRAAD VAN DOCTOR
IN DE WISKUNDE EN NATUURWETENSCHAPPEN AAN DE
RIJKSUNIVERSITEIT TE LEIDEN,
OP GEZAG VAN DE RECTOR MAGNIFICUS DR. C. SOETEMAN,
HOOGLERAAR IN DE FACULTEIT DER LETTEREN,
TEN OVERSTAAN VAN EEN COMMISSIE UIT DE SENAAT
TE VERDEDIGEN OP DONDERDAG 24 JUNI 1971
TE KLOKKE 16.15

DOOR

JOHANNES JACOBUS DE GROOT
GEBOREN TE OEGSTGEEST IN 1941

1971
KONINKLIJKE DRUKKERIJ VAN DE GARDE N.V.
ZALTBOMMEL

Promotor: PROF. DR. J. J. M. BEENAKKER

Dit proefschrift is tot stand gekomen mede onder leiding van
DR. C. J. N. VAN DEN MEIJDENBERG

Aan mijn ouders
Aan Lène

Dit werk is onderdeel van het programma van de Stichting voor Fundamenteel Onderzoek der Materie (F.O.M.) en is mogelijk gemaakt door financiële steun van de Nederlandse Organisatie voor Zuiver Wetenschappelijk Onderzoek (Z.W.O.).

PREFACE

Since 1960 the influence of external magnetic and electric fields on the transport properties of dilute gases has been intensively investigated by the Leiden Molecular Physics Group. This thesis deals with the investigations on the electric field effects performed so far at Leiden.

The first chapter describes the methods to measure the change of the viscosity and the heat conductivity in an electric field. The experimental results for a selected group of polar molecules are discussed. It is interesting to note that the heat conductivity of strongly polar gases increases when an electric field is applied, while the viscosity always decreases. The two existing theories for polar symmetric top molecules are compared. A synthesis of both theories is worked out and the result is shown to describe the experimental results satisfactorily.

In chapter II the reliability of the heat conductivity measurements is investigated by studying both the electric and the magnetic field effects for the heat conductivity of NF_3. It is shown that the experimental data are internally consistent.

Chapter III contains a study of the anomalous behaviour of the heat conductivity of strongly polar gases. Experiments on polar-nonpolar gas mixtures show evidence of two types of contributions; one giving rise to a decrease, the other to an increase in the heat conductivity when an electric field is applied. The latter contribution can be related to the electric dipole-dipole interactions between the molecules.

Analogous to the Stark effect, the field behaviour of the transport properties may be linear (first order) or quadratic (second order) in the field. Due to the inversion doubling of ammonia, NH_3 may show such a second

order behaviour, as is experimenrally verified for a gasmixture of NH_3 and nonpolar gas N_2. This subject is discussed in the last chapter.

Part of this work (chapter I) resulted from a close cooperation with the Molecular Physics Group at Genova. The investigations on the viscosity have been performed by F. Tommasini, A. C. Levi and G. Scoles, at the "Istituto di Fisica dell'Universita di Genova". The formal theory as given in chapter I, appendix A, has been worked out by A. C. Levi.

CONTENTS

CHAPTER I

VISCOSITY AND THERMAL CONDUCTIVITY OF POLAR GASES IN AN ELECTRIC FIELD

Synopsis

The influence of an electric field on the viscosity and thermal conductivity of gases of polar molecules has been investigated both theoretically and experimentally. The two different methods to solve the kinetic equation for polar symmetric top molecules, *i.e.* the perturbative method, employed by Mikhaĭlova and Maksimov, and the variational method, employed by Levi, McCourt and Tip, have both been refined. The improved methods now yield the same result: the field dependence of the electric effect is essentially the same as obtained by Mikhaĭlova and Maksimov whereas the terms contributing to the effect are essentially those given by Levi, McCourt and Tip. Measurements on the viscosity coefficient η_3 and the thermal conductivity coefficient λ'' are described. The hot-wire method which has been used for the thermal conductivity measurements is thoroughly discussed. The experimental results extend to the linear molecule NO, the oblate symmetric top molecules: NF_3, CHF_3, $CHCl_3$, $N(CH_3)_3$, the prolate symmetric top molecules: CH_3F, CH_3Cl, CH_3Br, CH_3CN and the slightly asymmetric top molecules: CH_3NH_2, C_2H_5Cl, C_2H_5CN, CH_3NO_2.

The data for η_3 are in direct agreement with the improved theory, taking one term into account. The behaviour of λ'' can also be explained on the basis of the improved theory, but generally two terms have to be taken into account, including one term due to non-invertible collisions. The cross-sections derived from the η_3 data agree with the cross-sections obtained from nonresonant absorption.

1. *Introduction.* It is at present well known, both experimentally[1,2]) and theoretically[3,4]), that the transport coefficients of all polyatomic gases change when they are placed in an external magnetic field and that the study of such changes may prove very useful in obtaining information about the non-spherical part of the intermolecular interactions. For a survey of the various investigations we refer to refs. 5 and 6.

In this paper we present the study of the influence of an electric field on

the transport properties of many polar gases, most of which are symmetric tops, in order to compare the results with the existing theories of the phenomenon[7,8]).

The polar gases are of great interest since various problems concerning reorientation and inelastic collisions in such systems remain open, in particular the relative importance of resonant collisions. Therefore the present results should be compared with those of other methods such as the study of the temperature dependence of the transport properties[9,10]), light scattering[43]), the direct study of collisions with molecular beams[11]) and the results of microwave spectroscopy: pressure broadening[12]), non-resonant absorption[13]) and the double resonance technique[14]).

TABLE I

Scheme of coefficients connecting the viscous pressure tensor $\boldsymbol{\Pi}$ of a polyatomic gas to the velocity gradient S in the presence of an electric field $\boldsymbol{E} = (E, 0, 0)$

	S_{xx}	S_{yy}	S_{zz}	S_{yz}	S_{zx}	S_{xy}
$\overset{\circ}{\Pi}{}^s_{xx}$	$-2\eta_1$	0	0	0	0	0
$\overset{\circ}{\Pi}{}^s_{yy}$	0	$-2\eta_2$	$-2(\eta_1 - \eta_2)$	0	0	0
$\overset{\circ}{\Pi}{}^s_{zz}$	0	$-2(\eta_1 - \eta_2)$	$-2\eta_2$	0	0	0
$\overset{\circ}{\Pi}{}^s_{yz}$	0	0	0	$-2(2\eta_2 - \eta_1)$	0	0
$\overset{\circ}{\Pi}{}^s_{zx}$	0	0	0	0	$-2\eta_3$	0
$\overset{\circ}{\Pi}{}^s_{xy}$	0	0	0	0	0	$-2\eta_3$

TABLE II

Scheme of coefficients connecting the heatflux through a polyatomic gas to the temperature gradient in the presence of an electric field $\boldsymbol{E} = (E, 0, 0)$

	$(\nabla T)_x$	$(\nabla T)_y$	$(\nabla T)_z$
q_x	$-\lambda^{//}$	0	0
q_y	0	$-\lambda^{\perp}$	0
q_z	0	0	$-\lambda^{\perp}$

The transport coefficients in the general phenomenological transport equations have a tensorial character. For an isotropic medium the transport coefficients behave like scalars. In an external field, however, an isotropic medium, such as a gas of neutral molecules, may become anisotropic and the transport coefficients may show tensorial properties.

The scheme for all the transport coefficients possible in a magnetic field is given in ref. 15. The corresponding scheme in an electric field is the same except for the absence of transverse effects due to the different space symmetry. On the other hand in the electric case cross effects between viscosity and thermal conductivity are possible[7]). The component schemes for the viscosity and thermal conductivity are shown in tables I and II. In the present study the coefficients η_3 and $\lambda^{//}$ will be considered.

The electric field effect is due to the precession of the molecular electric dipole around the direction of $\boldsymbol{E}$ which destroys most of the tensor polarization originated by collisions. Normally, the polarization has a negative influence upon the collisions which cause it, so that its destruction enhances the collision probability and reduces the mean free path, producing thereby a decrease in all the transport coefficients. Indeed the viscosity always decreases in an electric field, as will be seen, with the sole exception of ammonia; in the thermal conductivity a few very strongly polar gases show an increase.

After an unsuccessful attempt by Ray[16]) as early as 1922, an electric field effect was first measured by Cioară[17]) on the viscosity of mixtures of methyl alcohol and propionaldehyde with methane in 1961. There was no further investigation concerning viscosity, apart from some qualitative measurements by Amme[18]), until 1967 when Gallinaro *et al.*[19]) published results for chloroform and ethyl chloride.

The history of the electric field effect on the thermal conductivity is more complicated. Apart from the early attempts of the pioneer in this field, H. Senftleben[20]), which were vitiated by electrostriction, it was not until 1965 that Senftleben[21]) himself discovered an effect in the thermal conductivity of ethyl chloride and chloroform. He also found indications for an anomalous behaviour of the methyl and benzyl cyanides, namely an increase instead of a decrease in λ. In 1966 Gorelik and Sinitsyn[22]) measured the effect on ethyl chloride, ethyl alcohol and nitrogen trifluoride. In 1967 De Groot *et al.*[23]) confirmed Senftleben's measurements on the cyanides and also found a striking dependence of the electric field effect on the molecular dipole moment. New measurements were reported by Gorelik *et al.* on nitrogen trifluoride[24]) and by Borman *et al.* on various polar gases[25]). A disagreement between the results of Gorelik *et al.*[24]) and De Groot *et al.*[23]) will be discussed in chapter II[26]).

In section 2 the two existing theories[7,8]) are compared and the result of an improved theory is presented. In section 3 the experimental apparatus and results for the viscosity are described. Section 4 is devoted to the apparatus and the results for the thermal conductivity. In section 5 the results are analysed using a comparison with theory, while section 6 is devoted to discussion and conclusions. In appendix A the improvements in the theoretical methods are worked out. In the appendices B, C and D

some non-obvious calculations are presented that are needed in order to analyse the theoretical and experimental results.

2. *Theory*. Theories of the electric Senftleben–Beenakker effects have been given by Mikhaïlova and Maksimov[7]), hereafter referred to as MM, and by Levi, McCourt and Tip[8]), hereafter referred to as LMT. These theories both start from the Chapman–Enskog equations, obtained from the transport equation by assuming approximate local equilibrium and linearizing in the macroscopic gradients. There are, however, several important differences between these theories:

a) The MM theory is classical, while the LMT theory is quantummechanical: thus the transport equation for MM is a classical generalization of the Boltzmann equation to polyatomic gases, while for LMT it is a generalization of the Waldmann–Snider[27,28]) equation;

b) MM solve the Chapman–Enskog equations by an iteration-perturbation procedure, LMT by taking scalar products inside a finite set, which is equivalent to a variational principle;

c) MM take for their perturbation approach as unperturbed part of the collision operator the collision operator of spherical Maxwell molecules; no such assumption is needed in a variational approach;

d) MM use an expansion in spherical tensors, LMT in Cartesian tensors.

Point *a*) is a priori in favour of LMT, but is rather academic for the heavy molecules which are dealt with in the present article, since all quantum averages coincide with the classical averages to a good approximation. Point *b*) is crucial: it leads to very different averaging procedures in the two theories with respect to the relative orientation of angular momentum and dipole moment, hence, as will be shown, to very different shapes of the dispersion curves. In appendix A it will be seen that the variational procedure can be refined to give the same shape for the dispersion curve as the iterative procedure. Point *c*) is a weak point of the MM theory, inhibiting a correct treatment of reorientation collisions which are very important for the viscosity; however, it is possible to modify the MM theory to include all inelastic collisions correctly, by using as unperturbed collision operator the diagonal part (with respect to the tensor basis chosen) of the total collision operator[29]). Point *d*) is purely formal and does not involve any real change.

In this section only the outline and the results of the refined theories will be discussed. In quantum-mechanical language, a state of a symmetric-top molecule is defined by three quantum numbers j, k, m (neglecting the inversion degeneracy). The rotational Hamiltonian,

$$\mathscr{H}_{\mathrm{rot}} = \frac{\hbar^2}{2I_{\mathrm{A}}}\left\{J^2 + \left(\frac{I_{\mathrm{A}}}{I_{\mathrm{C}}} - 1\right)J_\zeta^2\right\}, \tag{1}$$

where the eigenvalues of J^2 are $j(j+1)$, those of J_ζ are k, and those of J_x are m, determines the local equilibrium distribution matrix:

$$f_{eq} = \left(\frac{\beta}{2\pi m}\right)^{\frac{3}{2}} \frac{n}{Q} \exp(-W^2 - \beta \mathscr{H}_{rot}), \tag{2}$$

where $\beta = (kT)^{-1}$, $W = (\beta/2m)^{\frac{1}{2}}\, \boldsymbol{p}$, Q is the one-particle rotational partition function and n is the number density.

The exact distribution matrix is given by

$$f = f_{eq}(1 + \Phi). \tag{3}$$

The field has practically no influence on f_{eq}, but it does affect Φ. The field Hamiltonian is diagonal to a good approximation and is given by

$$\mathscr{H}_{field} = -dEJ^{-2}J_\zeta J_x. \tag{4}$$

Since the field energy depends on the quantum number m, Φ tends to become diagonal in m at high fields. This gives rise to a change in the transport properties.

In the case of the thermal conductivity Φ is given by

$$\Phi = -\frac{1}{T}\, \boldsymbol{A} \cdot \nabla T, \tag{5}$$

where $\boldsymbol{A}$ satisfies the Chapman–Enskog equation

$$-\left(\frac{2kT}{m}\right)^{\frac{1}{2}} \left\{ W^2 - \frac{5}{2} + \frac{\hbar^2\beta}{2I_A}\left[J^2 - \langle J^2\rangle + \left(\frac{I_A}{I_C} - 1\right)(J_\zeta^2 - \langle J_\zeta^2\rangle)\right]\right\} \boldsymbol{W}$$

$$= \mathscr{C}\boldsymbol{A} - \frac{\mathrm{i}}{\hbar}\,[\mathscr{H}_{field}, \boldsymbol{A}], \tag{6}$$

$\mathscr{C}$ being the collision superoperator†. In the case of the shear viscosity Φ is given by

$$\Phi = -\mathsf{B} : \mathsf{S}, \tag{7}$$

where S is the shear tensor (symmetric traceless part of the velocity gradient tensor), and B satisfies the Chapman–Enskog equation

$$-2[\boldsymbol{W}]^{(2)} = \mathscr{C}\mathsf{B} - \frac{\mathrm{i}}{\hbar}\,[\mathscr{H}_{field}, \mathsf{B}], \tag{8}$$

where the symbol $[\ ]^{(q)}$ indicates a natural tensor of rank q (symmetric traceless in all pairs of indices).

It is possible to solve the Chapman–Enskog equations (6) and (8) in two ways. MM use the perturbation approach, which consists in splitting $\mathscr{C}$ into

† $\mathscr{C} = \mathscr{J}_0$, the collision superoperator defined in eq. (14) of ref. 8 and eq. (4) of ref. 30.

two parts

$$\mathscr{C} = \mathscr{C}^{(0)} + \varepsilon\mathscr{C}^{(1)} \tag{9}$$

such that the eigenvalues and the tensorial eigenfunctions of $\mathscr{C}^{(0)}$ are known, and then in expanding $\boldsymbol{A}$ and $\boldsymbol{B}$ in these eigenfunctions. They chose for $\mathscr{C}^{(0)}$ the collision integral for Maxwell molecules; however, it is probably better to choose first a complete set of tensors and then to take $\mathscr{C}^{(0)}$ to be that part of $\mathscr{C}$ diagonal in this set[29]). When this is done, observing also that the superoperator $\mathscr{F}$ defined by

$$\mathscr{F}X = -\frac{\mathrm{i}}{\hbar}[\mathscr{H}_{\text{field}}, X] \tag{10}$$

is tensorially diagonal in the set, the eqs. (6) and (8) being of the form

$$(\mathscr{C}^{(0)} + \mathscr{F} + \varepsilon\mathscr{C}^{(1)})\, X = K \tag{11}$$

can be solved by iteration. The zeroth order equation is

$$X = (\mathscr{C}^{(0)} + \mathscr{F})^{-1} K \tag{12}$$

and the general solution is obtained as a power series in ε; X and K are expanded in the set and the result depends on the off-diagonal matrix elements of $\mathscr{C}$. The lowest non-vanishing order for the electric field effects is the second. Of course, only a small number of tensors is actually used. On the other hand, LMT use a variational approach. Again a complete set of tensors is chosen, but only a small set of these is kept; the eqs. (6) and (8) are then solved approximately by taking scalar products with the tensors of the small set. Up to this point the two methods are completely equivalent. The difference arises from the fact that the tensorial behaviour is not all that matters: the quantities $\boldsymbol{A}$ and $\boldsymbol{B}$ do not depend only on the directions of $\boldsymbol{W}$ and $\boldsymbol{J}$, but also on their magnitudes and on J_ζ^2. By its very nature, the variational procedure is forced to introduce an additional expansion in orthogonal polynomials depending on those scalar quantities and (usually) to keep only a finite number of them.

This problem does not arise in the perturbative procedure. The original LMT theory introduces only two polynomials as coefficients of each tensor considered. This amounts to that approximation where the matrix representing $\mathscr{F}$ is replaced by a matrix made up of two-by-two blocks. The perturbative procedure, on the other hand, keeps the complete matrix automatically and is therefore somewhat more refined. As is shown in appendix A, it is also possible to obtain the correct results using a variational theory, by introducing in the variational set all possible polynomials times the relevant tensors. Thus the "improved variational theory" and the "improved perturbation theory" give the same results, the tensors being those of LMT and the field dependence being given by the MM integrals. (In appendix A a more thorough discussion of these points is given.) From here on these

equivalent theories will be indicated as the "improved theory" IT. In the following, the word "term" will be used to indicate an element of the basis set for the (operator) space, *i.e.* a product of tensors and polynomials.

The important terms are, first of all, those which occur in the Chapman–Enskog equations; secondly those which are coupled to those of the first group via the collision superoperator but feel also the effect of the field, *i.e.* do not belong to the null space of $\mathscr{F}$. In the original LMT theory a third group was also introduced, composed of tensors twinned to those of the second group via $\mathscr{F}$. In the perturbative theory or in the improved variational theory this third group does not appear explicitly because the effect of the field is treated exactly.

For the viscosity the only term of the first group is $[\boldsymbol{W}]^{(2)}$, the most important term of the second group is probably $[\boldsymbol{J}]^{(2)}$ †. This has recently been proven experimentally for nitrogen, with very high accuracy, by Hulsman and Burgmans[32]). The term $[\boldsymbol{J}]^{(2)}$ is not considered by MM because their inconvenient choice of the unperturbed collision operator hinders the treatment of cross sections vanishing in the elastic limit; however, an improved choice allows the study of this term within the framework of perturbation theory.

For the thermal conductivity the terms of the first group are $(W^2 - \frac{5}{2})\,\boldsymbol{W}$, $(J^2 - \langle J^2\rangle)\,\boldsymbol{W}$ and $(J_\zeta^2 - \langle J_\zeta^2\rangle)\,\boldsymbol{W}$; the most important terms of the second group are expected to be $\boldsymbol{W}[\boldsymbol{J}]^{(2)}$ (for the decrease in λ) and $\boldsymbol{W}\boldsymbol{J}$ (for the increase in λ). The latter term is connected to collisions without an inverse (a violation of the naive detailed balance) [30]).

The terms of the third group of the original LMT theory are simply those of the second group times J_ζ.

For the above mentioned terms of the second group the IT results for the shear viscosity and thermal conductivity coefficients are given by:

$$\begin{aligned}
\frac{\Delta\eta_1}{\eta_0} &= \frac{\eta_1 - \eta_0}{\eta_0} = 0,\\
\frac{\Delta\eta_2}{\eta_0} &= \frac{\eta_2 - \eta_0}{\eta_0} = -\tfrac{1}{2}\psi_{02} f_{02}(2\xi_{02}, x),\\
\frac{\Delta\eta_3}{\eta_0} &= \frac{\eta_3 - \eta_0}{\eta_0} = -\psi_{02} f_{02}(\xi_{02}, x),
\end{aligned} \tag{13}$$

and

$$\begin{aligned}
\frac{\Delta\lambda^{//}}{\lambda_0} &= \frac{\lambda^{//} - \lambda_0}{\lambda_0} = -\psi_{12} f_{12}(\xi_{12}, x) + 2\psi_{11} f_{11}(\xi_{11}, x),\\
\frac{\Delta\lambda^{\perp}}{\lambda_0} &= \frac{\lambda^{\perp} - \lambda_0}{\lambda_0} = -\psi_{12}\{\tfrac{1}{2} f_{12}(\xi_{12}, x) + f_{12}(2\xi_{12}, x)\} + \psi_{11} f_{11}(\xi_{11}, x),
\end{aligned} \tag{14}$$

† For ammonia other terms such as $[\boldsymbol{W}]^{(2)}\,\boldsymbol{J}$ may be important [30, 31]).

where the parameters ψ, determining the saturation values, are:

$$\psi_{02} = \left[\begin{smallmatrix}200\\020\end{smallmatrix}\right]^2 [200]^{-1} [020]^{-1};$$

$$\psi_{12} = \frac{25}{8} \frac{k^2T}{m} \frac{\Lambda_{12}^2}{[120]_{\text{sph}}}; \qquad \psi_{11} = \frac{25}{8} \frac{k^2T}{m} \frac{\Lambda_{11}^2}{[110]_{\text{sph}}}, \tag{15}$$

with

$$\Lambda_{12} = \frac{\hbar^2}{5I_A kT} \{(\langle J^4\rangle - \langle J^2\rangle^2)\left[\begin{smallmatrix}1002\\120\end{smallmatrix}\right][1002]^{-1}$$
$$+ (x-1)(\langle J_\zeta^4\rangle - \langle J_\zeta^2\rangle^2)\left[\begin{smallmatrix}1003\\120\end{smallmatrix}\right][1003]^{-1}\} - \left[\begin{smallmatrix}1001\\120\end{smallmatrix}\right][1001]^{-1},$$

$$\Lambda_{11} = \frac{\hbar^2}{5I_A kT} \{(\langle J^4\rangle - \langle J^2\rangle^2)\left[\begin{smallmatrix}1002\\110\end{smallmatrix}\right][1002]^{-1}$$
$$+ (x-1)(\langle J_\zeta^4\rangle - \langle J_\zeta^2\rangle^2)\left[\begin{smallmatrix}1003\\110\end{smallmatrix}\right][1003]^{-1}\}. \tag{16}$$

The parameter x equals I_A/I_C, where the moments of inertia I_A and I_C refer to axes perpendicular and parallel to the figure axis respectively. The field functions f_{pq}, determining the field dependence, are:

$$f_{pq}(\xi_{pq}, x) = \frac{1}{\langle [\boldsymbol{J}]^{(q)} \bigcirc^q [\boldsymbol{J}]^{(q)}\rangle}$$
$$\times \left\langle [\boldsymbol{J}]^{(q)} \bigcirc^q [\boldsymbol{J}]^{(q)} \frac{(\hbar^{-1}J_\zeta J^{-2}(2I_A kT)^{\frac{1}{2}}\xi_{pq})^2}{1 + (\hbar^{-1}J_\zeta J^{-2}(2I_A kT)^{\frac{1}{2}}\xi_{pq})^2} \right\rangle, \tag{17}$$

where p and q are the rank in $\boldsymbol{W}$ and $\boldsymbol{J}$ of the expansion terms respectively. The field parameters ξ are†:

$$\xi_{02} = \frac{2}{15} \frac{dE\langle J^4\rangle}{n(2I_A kT)^{\frac{1}{2}}[020]};$$

$$\xi_{12} = \frac{1}{15} \frac{dE\langle J^4\rangle}{n(2I_A kT)^{\frac{1}{2}}[120]_{\text{sph}}}; \qquad \xi_{11} = \frac{1}{6} \frac{dE\langle J^2\rangle}{n(2I_A kT)^{\frac{1}{2}}[110]_{\text{sph}}}. \tag{18}$$

The relevant collision brackets are given in table III. For the definition of the collision brackets the operator $\mathscr{R}_0 = -\mathscr{C}/n$ is used, so that all brackets are independent of the density n and the diagonal brackets $[pqi]$ are positive.

It may be clarifying to notice that the field functions f are approximately of the type

$$f_{pq} = \frac{1}{\langle J^{2q}\rangle} \left\langle J^{2q} \frac{(\omega/\omega_{pq})^2}{1 + (\omega/\omega_{pq})^2} \right\rangle, \tag{19}$$

† These field parameters differ by a factor $\sqrt{2}$ from those given by MM[7]). This difference is due to a mistake in the transformation of $\gamma(0)$ in eq. (2.13) to the non-dimensional γ in eq. (3.1) in the paper of MM.

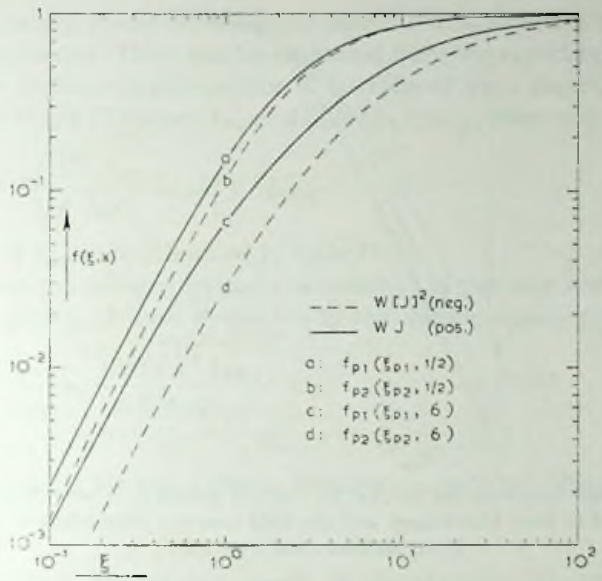

Fig. 1. The field dependence of the negative $[\boldsymbol{J}]^{(2)}$ and $\boldsymbol{W}[\boldsymbol{J}]^{(2)}$ terms, f_{02} and f_{12} $(= f_{02})$, and the positive $\boldsymbol{WJ}$ term, f_{11}, for $x = \frac{1}{2}$ and $x = 6$ according to the improved theory (IT).

TABLE III

List of collision brackets used in the text
$[A\,;\,B] = \langle A\mathscr{R}_0 B\rangle$; $\mathscr{R}_0 = -\mathscr{C}/n^*$; ϵ is the Levi-Civita tensor

$[1001] = \frac{1}{3}[(W^2 - \frac{5}{2})\, W_\alpha;\, (W^2 - \frac{5}{2})\, W_\alpha]$	$[{}^{1001}_{120}] = \frac{1}{5}[(W^2 - \frac{5}{2})\, W_\alpha;\, W_\beta[\boldsymbol{J}]^{(2)}_{\beta\alpha}]$
$[1002] = \frac{1}{3}[(J^2 - \langle J^2\rangle)\, W_\alpha;\, (W^2 - \frac{5}{2})\, W_\alpha]$	$[{}^{1002}_{120}] = \frac{1}{5}[(J^2 - \langle J^2\rangle)\, W_\alpha;\, W_\beta[\boldsymbol{J}]^{(2)}_{\beta\alpha}]$
$[1003] = \frac{1}{3}[(J_\zeta^2 - \langle J_\zeta^2\rangle)\, W_\alpha;\, (J_\zeta^2 - \langle J_\zeta^2\rangle)\, W_\alpha]$	$[{}^{1003}_{120}] = \frac{1}{5}[(J_\zeta^2 - \langle J_\zeta^2\rangle)\, W_\alpha;\, W_\beta[\boldsymbol{J}]^{(2)}_{\beta\alpha}]$
$[200] = \frac{1}{5}[[\boldsymbol{W}]^{(2)}_{\alpha\beta};\, [\boldsymbol{W}]^{(2)}_{\beta\alpha}]$	$[{}^{1002}_{110}] = -\frac{1}{6}\varepsilon_{\alpha\beta\gamma}[(J^2 - \langle J^2\rangle)\, W_\gamma;\, W_\beta J_\alpha]$
$[120]_{\mathrm{sph}} = \frac{1}{15}[[\boldsymbol{J}]^{(2)}_{\alpha\beta}\, W_\gamma;\, W_\gamma[\boldsymbol{J}]^{(2)}_{\beta\alpha}]$	$[{}^{1003}_{110}] = -\frac{1}{6}\varepsilon_{\alpha\beta\gamma}[(J_\zeta^2 - \langle J_\zeta^2\rangle)\, W_\gamma;\, W_\beta J_\alpha]$
$[123]_{\mathrm{sph}} = \frac{1}{15}[J_\zeta[\boldsymbol{J}]^{(2)}_{\alpha\beta}\, W_\gamma;\, J_\zeta W_\gamma[\boldsymbol{J}]^{(2)}_{\beta\alpha}]$	$[{}^{200}_{020}] = \frac{1}{5}[[\boldsymbol{W}^{(2)}]_{\alpha\beta};\, [\boldsymbol{J}]^{(2)}_{\beta\alpha}]$
$[110]_{\mathrm{sph}} = \frac{1}{9}[J_\alpha W_\beta;\, W_\beta J_\alpha]$	
$[113]_{\mathrm{sph}} = \frac{1}{9}[J_\zeta J_\alpha W_\beta;\, J_\zeta W_\beta J_\alpha]$	
$[020] = \frac{1}{5}[[\boldsymbol{J}]^{(2)}_{\alpha\beta};\, [\boldsymbol{J}]^{(2)}_{\beta\alpha}]$	
$[023] = \frac{1}{5}[J_\zeta[\boldsymbol{J}]^{(2)}_{\alpha\beta};\, J_\zeta[\boldsymbol{J}]^{(2)}_{\beta\alpha}]$	

* $\mathscr{C} = \mathscr{J}_0$, the collision superoperator defined in eq. (14) ref. 8.

where $\omega = J_\zeta J^{-2}\hbar^{-1}\,\mathrm{d}E$ is the precession frequency and $1/\omega_{pq}$ the time scale at which the relevant process takes place. The calculation of the field functions $f_{12} = f_{02}$ and f_{11} is elaborated in appendix B. There it is shown that the field functions in the classical limit depend only on ξ and on x. For two typical values of x, $f_{02} = f_{12}$ and f_{11} have been drawn in fig. 1 and for a

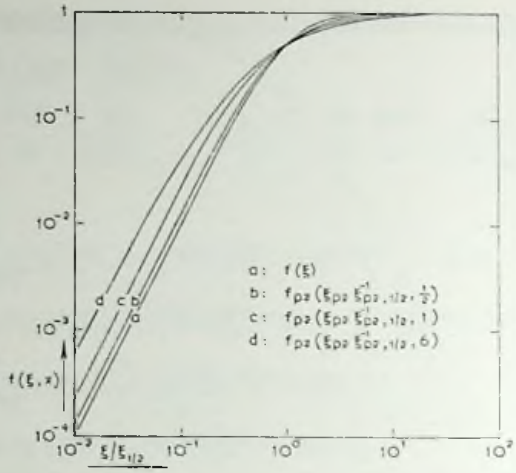

Fig. 2. The field functions f_{02} ($= f_{12}$) for various values of x according to IT, horizontally scaled to their half-values, and the field function f according to the theory of Levi, McCourt and Tip (LMT).

number of x values the half values $\xi_{pq,\frac{1}{2}}$, defined by $f_{pq}(\xi_{pq,\frac{1}{2}}, x) = \frac{1}{2}$, are given in table IV. The differences between the curves representing a particular field function for different values of x and also the differences between f_{12} and f_{11} for a given value of x are a consequence of the averaging over all precession frequencies (see eq. (19)). To show clearly the differences in shape for different values of x, in fig. 2 the various functions f_{02} have been plotted in such a way that all curves meet when the function has the value $\frac{1}{2}$. For comparison the field dependence given by LMT, $f(\xi) = \xi^2/(1 + \xi^2)$, has also been drawn in fig. 2. The LMT field function $f(\xi)$ is insensitive to the value of x, since the field parameters ξ represent average precession frequencies in themselves. Roughly speaking the IT and MM theories give the average of a function while LMT gives a function of the average.

TABLE IV

$\xi_{pq,\frac{1}{2}}$ for different values of $x = I_A/I_C$ $f_{pq}(\xi_{pq,\frac{1}{2}}, x) = \frac{1}{2}$		
x	$\xi_{02,\frac{1}{2}} = \xi_{12,\frac{1}{2}}$	$\xi_{11,\frac{1}{2}}$
0.5	3.2	3.0
1.0	4.1	3.4
6.0	13.2	8.5
14.0	21.5	13.0
20.0	26.5	15.5

For the analysis of the experimental results it will be useful to introduce collision frequencies. These can be evaluated from the experimental data as follows: the collision superoperator $\mathscr{C}$ is replaced by a negative constant $-\omega_{pq}$; then in the IT theory $\xi_{pq} = dE(2kTI_A)^{-\frac{1}{2}}/\omega_{pq}$ from which is derived

$$\frac{\omega_{pq}}{p} = d\left(\frac{E}{p}\right)_{pq,\frac{1}{2}} (2I_A kT)^{-\frac{1}{2}}\, \xi^{-1}_{pq,\frac{1}{2}}. \tag{20}$$

The values of $\xi_{pq,\frac{1}{2}}$ are tabulated in table IV.

To compare the collision frequencies obtained in this way with the elastic collision frequency, defined by $\omega_c = p/\eta$, the collision numbers

$$Z_{pq} = \frac{\omega_c}{\omega_{pq}} = \frac{(2kTI_A)^{\frac{1}{2}}\, \xi_{pq,\frac{1}{2}}}{d(E/p)_{pq,\frac{1}{2}}\, \eta} \tag{21}$$

are introduced.

The expressions for the collision frequencies and the collision numbers will be used in section 6.

3. *Experimental method and results for the viscosity.* The experimental method has already been outlined in ref. 19 and is basically the same as that described in ref. 2. It is a differential method using a Wheatstone bridge arrangement of flow resistances as shown in fig. 3. The only difference with the method described in ref. 2 is that the viscosity of the flowing gas is changed in all the four resistances by applying the same electric field to C_1, C_3 and C_2, C_4 alternately. Such a technique cannot easily be

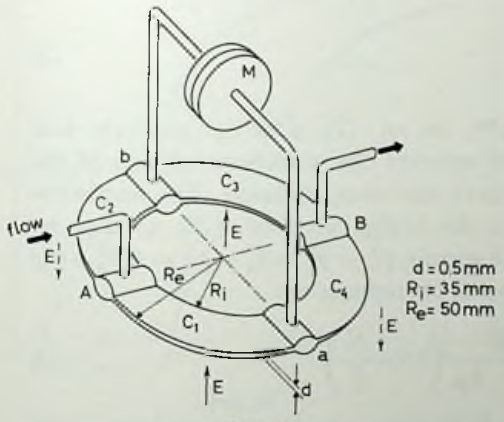

Fig. 3

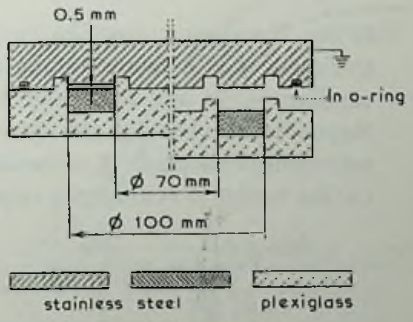

Fig. 4

Fig. 3. Apparatus for the measurement of $\eta_3(E)$. M: micro membrane manometer; C_1, C_2, C_3, C_4: flow resistances of the Wheatstone bridge.

Fig. 4. Cross section of the apparatus for the measurement of $\eta_3(E)$.

applied for the measurements in a magnetic field due to the presence of stray fields. A cross section of the bridge is shown in fig. 4. In the upper part of the apparatus four holes have been drilled, at 90° from each other. Two are for the gas inlet and outlet and two are used to connect the balance detector, *viz.* an Atlas Micro Membrane Manometer (M.M.M.). As can easily be seen from fig. 4 the elements of the flow resistances have a rectangular cross section (0.05×1.5 cm^2).

Neglecting the fluid compressibility and the height of the cross section in comparison with the width and calling x the field direction and z the flow direction, the only non-vanishing component of the velocity gradient is $\partial v_z/\partial x$. Therefore, according to the scheme in table I the quantity of interest in these measurements is $\Delta\eta_3/\eta_0 = (\eta_3 - \eta_0)/\eta_0$. Applying the field first to C_1, C_2, then to C_2, C_4 the M.M.M. gives a signal difference δp, proportional, as will be seen, to $\Delta\eta_3/\eta_0$ and depending on $(E/\bar{p})$ where E is the electric field strength and $\bar{p} = \frac{1}{2}(p_A + p_B)$. The M.M.M. signal is recorded on a chart recorder and is converted into pressure readings following the calibration given by the manufacturer.

The electric field is always present in two flow resistances, so that the overall flow resistance of the bridge does not change with the alternation of the field *i.e.* p_A and p_B are constant. For such an arrangement and if $p_a - p_b \ll p_a$ (in our case $p_a - p_b$ never exceeds $2 \times 10^{-3}\, p_a$) the Hagen–Poiseuille equation, neglecting the Reynolds term, gives:

$$\frac{\Delta\eta_3}{\eta_0}\left(\frac{E}{\bar{p}}\right) = \frac{p_a(p_A^2 - p_B^2)\,\delta p}{2(p_A^2 - p_a^2)(p_a^2 - p_B^2)}\left(1 + \frac{K}{\bar{p}}\right), \tag{1}$$

where

$$K = \frac{3}{d}\sqrt{\frac{\pi}{2}\frac{RT}{M}}\,\eta_0\,\frac{2 - f}{f} \tag{2}$$

is the Knudsen correction factor[33]). In eq. (2), d is the capillary half thickness, f is a factor taking into account the surface roughness of the capillary walls and R, T and M have the usual meaning. The maximum Reynolds number for the flow in the bridge was $\mathcal{R}e = 30$, so that no turbulence took place. If, as usually happens, $p_A^2 - p_a^2 = p_a^2 - p_B^2 = \frac{1}{2}(p_A^2 - p_B^2)$ *i.e.* the bridge is symmetric, expression (1) reduces to:

$$\frac{\Delta\eta_3}{\eta_0}\left(\frac{E}{\bar{p}}\right) = \frac{2p_a}{p_A + p_B}\,\frac{\delta p}{p_A - p_B}\left(1 + \frac{K}{\bar{p}}\right). \tag{3}$$

The Knudsen correction factor K has been determined experimentally in the following way. Measurements have been performed at different pressures, yielding dispersion-like curves which for the lowest values of the pressure do not overlap. The experimental values $(\Delta\eta/\eta)_{\text{meas.}}$ obtained at a

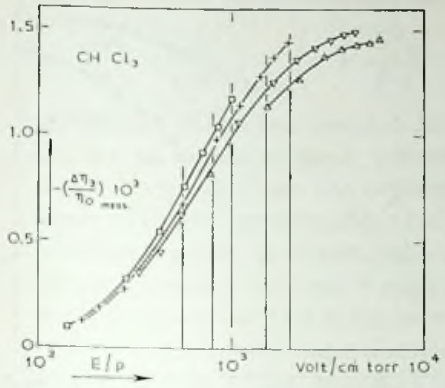

Fig. 5

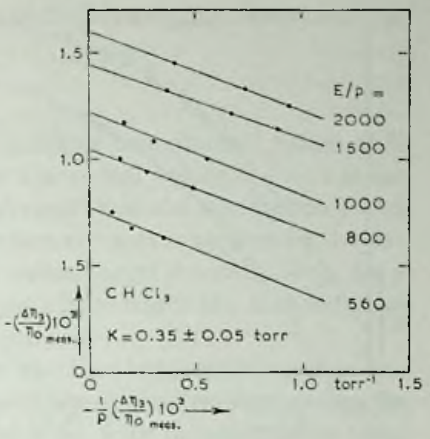

Fig. 6

Fig. 5. The measured relative viscosity change $(\Delta\eta_3/\eta_0)_{\text{meas.}}$ as a function of E/p for $CHCl_3$.

□ 7 torr; + 3.6 torr; ▽ 1.83 torr; △ 1.3 torr.

Fig. 6. $\Delta\eta_3/\eta_0$ *vs.* $(1/p)(\Delta\eta_3/\eta_0)_{\text{meas.}}$ for different E/p values.
The slope of the straight lines determines the Knudsen correction factor K for $CHCl_3$.

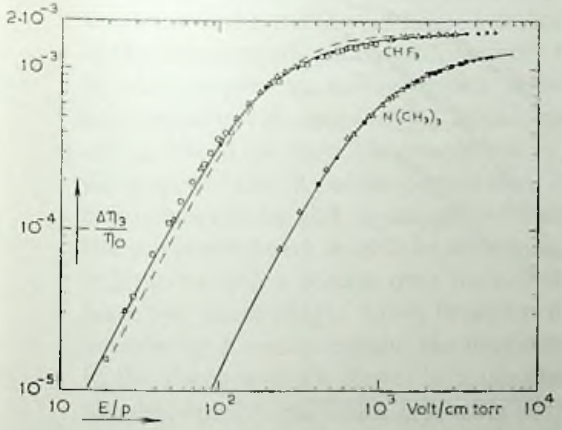

Fig. 7a

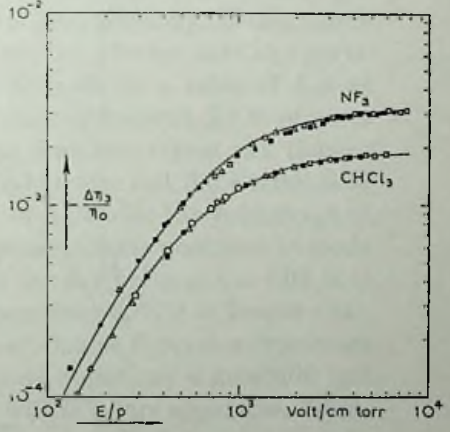

Fig. 7b

Figs. 7a and 7b. $\Delta\eta_3/\eta_0$ *vs.* E/p for the oblate symmetric top molecules.

●, □, ■, △, ○ pressures in the range from 1 to 10 torr;

———— $\psi_{02}f_{02}(\xi_{02}, \frac{1}{2})$;

---------- $\psi f(\xi)$.

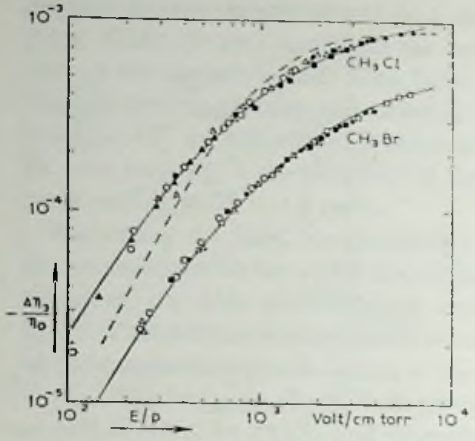

Fig. 8a

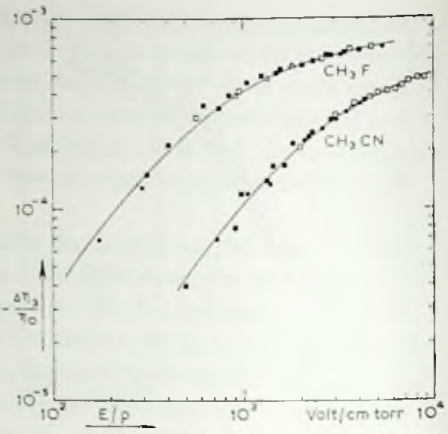

Fig. 8b

Fig. 8a and 8b. $\Delta\eta_3/\eta_0$ *vs.* E/p for the prolate symmetric top molecules.
●, □, ■, △, ○ pressures in the range from 1 to 10 torr;
———— $\psi_{02}/_{02}(\xi_{02}, x)$; x proper to the molecule;
---------- $\psi f(\xi)$.

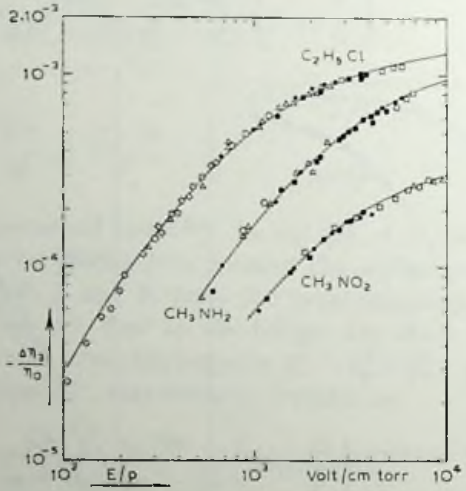

Fig. 9. $\Delta\eta_3/\eta_0$ *vs.* E/p for the asymmetric top molecules.

C_2H_5Cl: □, ■, ●, △, ○, ◇ pressures in the range from 1 to 20 torr;
CH_3NH_2: □, ●, ■, △, ○ pressures in the range from 1 to 10 torr;
CH_3NO_2: △, □, ●, ■ pressures in the range from 3 to 7 torr;
———— $\psi_{02}/_{02}(\xi_{02}, x)$; x proper to the molecule.

fixed $E/\bar{p}$ value are plotted as a function of $(1/\bar{p})(\Delta\eta/\eta)_{\text{meas.}}$. Since

$$\frac{\Delta\eta}{\eta} = \left(\frac{\Delta\eta}{\eta}\right)_{\text{meas.}} \left(1 + \frac{K}{\bar{p}}\right),$$

the slope of the plots is equal to K. The obtained experimental values of K are, for all measured gases, 2 times the theoretical values if $f = 1$ is assumed in eq. (2). From the experimental conditions the assumption $f = 1$ seems not to be unreasonable. The Knudsen correction applied to the experimental points to obtain saturation values never exceeds 30%. As a typical example figs. 5 and 6 show the plots from which the Knudsen correction factor K for $CHCl_3$ has been determined.

The experimental points, corrected for the Knudsen conditions if necessary, are shown in figs. 7a and 7b for the oblate symmetric tops, in figs. 8a and 8b for the prolate symmetric tops and in fig. 9 for the asymmetric tops.

4. *Experimental method and results for the heat conductivity.* 4*a*. Experimental method and apparatus. The change of the heat conductivity in an electric field with the field parallel to the temperature gradient can be measured with the parallel-plate method where a voltage difference is applied between the plates, or with the hot-wire method where the voltage difference is applied between wire and cylinder. It is worthwhile to compare first the utility of both methods for the measurement of the field effect.

Since the field effect on the heat conductivity is a function of E/p, the measuring range in both methods is limited by the maximum value of E/p that can be obtained. The maximum value of E is determined by electrical breakdown whereas the minimum value of p is determined by the magnitude of the Knudsen effects allowed. In order to get the relevant data in a parallel plate apparatus, measurements should be made to a value of E/p at least equal to two times $(E/p)_{\frac{1}{2}}$. Because of this requirement, for most gases one is forced to make measurements in the Knudsen region and thus to allow quite large Knudsen corrections. In a hot-wire cell the electric field is inhomogeneous and an integrated value of $\Delta\lambda/\lambda$ over the field range of the cell is measured. As will be seen later, measurements need now be made only up to such a voltage over the cell that the E/p value at the wire is at least two times $(E/p)_{\frac{1}{2}}$. From breakdown experiments[34]) it is known that, outside the Knudsen region, the maximum attainable E/p value (minimum in the Paschen–Back curve) in a parallel-plate apparatus is generally half the value of the maximum E/p value at the wire in a wire apparatus. When, therefore, an equivalent criterion for the Knudsen limit is used in both apparatus, the accessible range of E/p values is roughly a factor 2 larger in the wire apparatus.

For the Knudsen limit in the wire apparatus the mean free path of the gas molecules must be compared with the diameter of the wire and in the

parallel plate apparatus with the distance of the plates. The pressure, corresponding to the Knudsen limit, will therefore be higher in a hot-wire apparatus than the equivalent pressure in a parallel plate apparatus. An advantage of the higher pressures is that spurious effects of the wall of the apparatus are less likely to be significant (*e.g.* impurities from the walls and pressure changes during the measurements). A third advantage of the hot wire method compared with the parallel plate method is the much lower heat leak. This is the more important since the polar gases to be investigated have in general a very small heat conductivity coefficient. The disadvantage of the wire apparatus is, of course, the inhomogeneity of the field.

All our measurements have been done with hot-wire cells, similar to the cell used by Senftleben, but differing in minor details. In such an arrangement the wire is heater, thermometer and ground electrode at the same time. A schematic diagram of the apparatus is given in fig. 10. The mantle of the

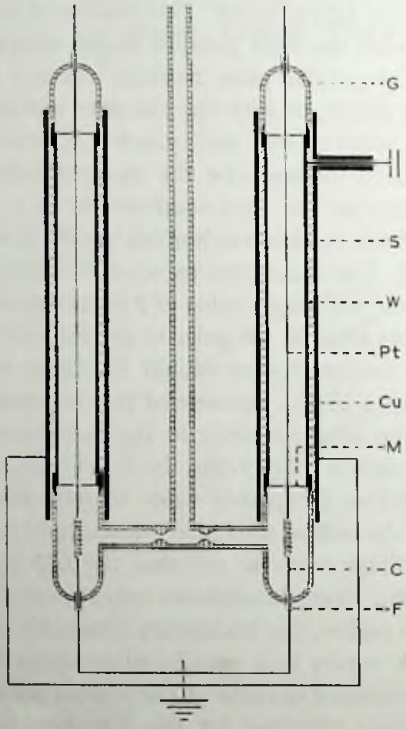

Fig. 10. Apparatus for the measurement of $\lambda//(E)$.
The electric field is applied between wire and cylinder.
G: glass caps; S: stainless steel cylinder; W: wax layer;
Pt: platinum wire, radius 25 μm; Cu: grounded copper cylinder;
M: mica spacer; C: platinum wire, radius 100 μm; F: feed-through.

cell consists of a stainless-steel tube 15 cm long and 1.5 cm in diameter, which is coated inside with a rhodium layer and closed at both ends with glass caps containing the feed-throughs of the wire. To avoid electrostriction in the oil of the thermostat, the outside of the mantle has first been covered with wax as an electrical isolating material and then painted with silver paint up to halfway along the glass caps. Since the silver layer is grounded it moreover reduces the leak current from the outer electrode to the wire. The platinum wire is kept in the centre by mica spacers at the ends of the mantle. Centring the wire is not only important for a symmetrical heat transport but also for avoiding electrostatic forces on the wire. The portion of the wire between the spacers has a diameter of 50 μm and a resistance $R(0)$ at 20°C of 7.96 ohm. Outside the spacers the diameter is 200 μm and at one end the wire has been spring-wound to stretch the thin part. Special care has been taken to maintain a high breakdown voltage, among other things by cleaning the surfaces of the electrodes and by restricting light from outside. In an earlier apparatus (apparatus I) the cells differ from those described (apparatus II) in the mounting of the outer electrode. In apparatus I a copper cylinder has been glued to the inside of a glass tube with an industrial glue (locktite) and the potential lead goes through the inlet tube to the top of the thermostat. The outside of the glass tube has again been silver-painted. The dimensions differ in the diameter of the outer cylinder, 2.4 cm instead of 1.5 cm and in the length, 137 mm instead of 150 mm. The change of the heat conductivity due to an electric field has been measured differentially by using the two identical cells and two variable resistances of about 100 Ω in a Wheatstone bridge. In one of the cells a positive or negative voltage is applied to the cylinder. Both cells are placed in a thermostat filled with kerosene. As the heat generated in the cells is small, temperature control of the bath is not necessary. A change in the heat conductivity in one cell due to the field effect gives rise to a change in temperature of the platinum wire and thus to a change of the wire resistance. The unbalance of the Wheatstone bridge is directly measured by means of a Keithly nanovoltmeter and recorded on a chart recorder. For the calibration, the deflection on the recorder due to a change of the wire temperature is compared with the change due to a variation of one of the variable resistances. With a temperature difference ΔT of about 10°C between wire and cylinder a resolving power $\delta T/\Delta T = 5 \times 10^{-7}$ is reached.

If one of the cells is replaced by a variable resistance, the wire resistance at various bridge currents can be determined. Then the absolute value of the heat conductivity can also be evaluated. The methods used to account for the temperature distribution along the wire and the various heat losses of the cell are explained in appendix D.

Finally we note that Knudsen effects and effects of electrostriction in the

gas have been avoided by limiting the pressure range in which the various gases have been measured. The only exception is NO where indeed Knudsen effects have been observed.

4b. Results for the polyatomic molecules. The relative change of the wire temperature $\delta T/\Delta T$ has been measured as a function of the voltage difference V over the cell at various gas pressures p for eleven different polar gases. Figs. 11, 12, 13 show double logarithmic plots of the measured values of $\delta T/\Delta T$ as a function of V/p for the oblate symmetric, the prolate symmetric and the asymmetric-top molecules respectively.

The gases CH_3CN, C_2H_5CN and CH_3NO_2 show an increase of the heat

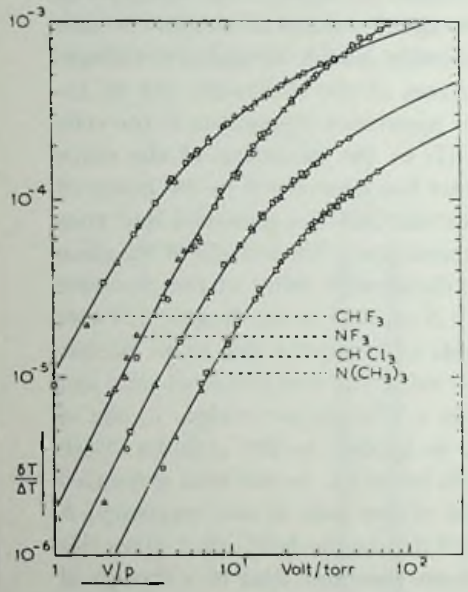

Fig. 11

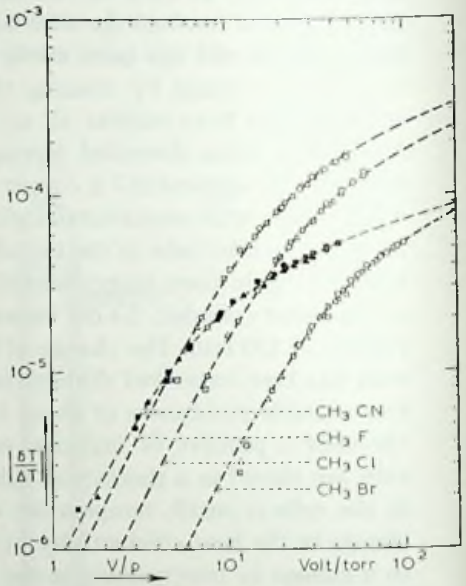

Fig. 12

Fig. 11. $\delta T/\Delta T$ *vs.* V/p for the oblate symmetric top molecules.

CHF_3:	o 14.9 torr;	△ 32.0 torr;	□ 206.4 torr;
NF_3:	o 22.9 torr;	△ 37.0 torr;	□ 83.5 torr;
$CHCl_3$:	o 19.0 torr;	△ 26.5 torr;	□ 38.5 torr;
$N(CH_3)_3$:	o 7.2 torr;	△ 10.2 torr;	□ 13.5 torr;

———— $\varphi_{12}F_{12}(\xi_{12}, \frac{1}{2})$.

Fig. 12. $\delta T/\Delta T$ *vs.* V/p for the prolate symmetric top molecules.
Open points indicate a decrease of λ'';
full points indicate an increase of λ''.

CH_3CN:	● 16.5 torr;	▲ 28.5 torr;	■ 32.5 torr;
CH_3F:	o 9.6 torr;	△ 14.7 torr;	□ 20.7 torr;
CH_3Cl:	o 6.8 torr;	△ 10.0 torr;	□ 13.0 torr;
CH_3Br:	o 4.0 torr;	△ 6.0 torr;	□ 8.6 torr;

-------- $\varphi F(\xi)$.

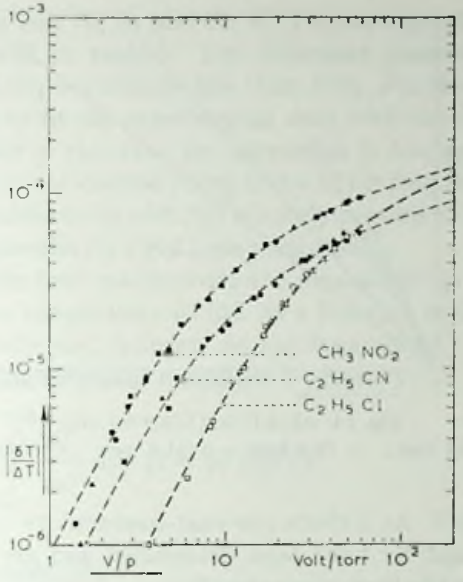

Fig. 13. $\delta T/\Delta T$ *vs.* V/p for the asymmetric top molecules.
Open points indicate a decrease of $\lambda'/\!/$;
full points indicate an increase of $\lambda'/\!/$.

CH_3NO_2: ● 10.4 torr; ▲ 14.2 torr; ■ 17.7 torr;
C_2H_5CN: ● 10.4 torr; ▲ 17.0 torr; ■ 18.8 torr;
C_2H_5Cl: ○ 12.2 torr; △ 16.7 torr; □ 41.0 torr;
--------- $\psi F(\xi)$.

conductivity when the electric field is applied (positive effect); all the other gases show a decrease (negative effect).

For each gas measurements of δT have been done for at least three different pressures, whereas ΔT has been measured at one or more of the highest pressures. Since for all gases the points constitute a single curve, Knudsen effects in $\delta T/\Delta T$ are below the limit of accuracy. For the sake of distinctness only three different pressure series are presented in the graphs, *i.e.* the highest, the lowest and one pressure in between. For all measured gases the correction factor $f = -(\delta T/\Delta T)_{sat}^{-1}(\Delta\lambda'/\!/\lambda)_{sat}$, accounting for the various heat losses, varies between the limits 1.03 and 1.01 (see appendix D). Some of the gases have been measured in apparatus I, the others in apparatus II. For most gases positive as well as negative voltages have been applied to the cylinder. The results are found to be independent of the polarity. The temperature difference ΔT between wire and cylinder varied between 5°C–15°C. The absolute values of the heat conductivity coefficients, λ_0, have been determined for all measured gases using eq. (4) of appendix D. The results

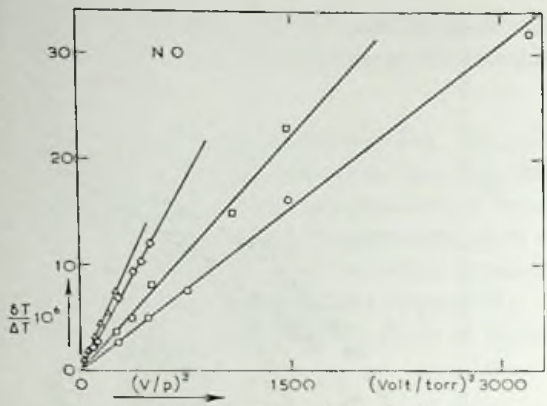

Fig. 14. $\delta T/\Delta T$ *vs.* $(V/p)^2$ for NO.
○ 9.1 torr; □ 15.6 torr; ◇ 31.4 torr; △ 50.0 torr.

are listed in table V. As a check the heat-conductivity coefficients of D_2, Ne, O_2, N_2, Ar and Kr have been determined and are found to deviate less than 2% from the literature values[35]).

For a number of other gases the sign of the effect has been determined, but as the effects appeared to be very small no attempts have been made to obtain saturation curves. These results are included in table V.

4*c*. Results for NO. Because of its exceptional molecular state some measurements have also been performed on the linear polar molecule NO. This gas is in a $^2\Pi$ state at room temperature so that the total angular momentum is not perpendicular to the molecular axis as for most linear molecules. This gives rise to a first-order electric effect $\Delta\lambda/\lambda = f(E/p)$ in contrast to other linear molecules which should show a second-order electric effect $\Delta\lambda/\lambda = f(E^2/p)$ comparable to the second-order Stark effect[3]). Due to the small effective electric dipole moment along the J axis ($d_{\text{eff}} \approx 0.016$ D) only the first part of the curve could be measured. For small values of ξ it follows from the discussion in appendix C:

$$\frac{\delta T}{\Delta T} = \frac{C_1}{a}\left(\frac{\Delta\lambda''}{\lambda}\right)_{\text{sat}} \xi^2(R_1) = \left(\frac{\Delta\lambda''}{\lambda}\right)_{\text{sat}} \frac{C_2}{a^3 R_1^2}\left(\frac{V}{p}\right)^2,$$

where C_1 and C_2 are dependent on the molecular properties of NO. A plot of the measured $\delta T/\Delta T$ *versus* $(V/p)^2$ is shown in fig. 14. The different slopes for different pressures, ranging from 10–50 torr, are apparently due to Knudsen effects.

5. *Analysis of the results.* In the case of the viscosity the theoretical curves representing the IT functions $f_{02}(\xi_{02}, x)$ fit the experimental data with great accuracy for both the prolate and the oblate symmetric-top

molecules (figs. 7a and 7b, 8a and 8b, 9). The corresponding IT parameter values are reported in table V. The estimated error in the quantities $(\Delta\eta_3/\eta_0)_{\text{sat}}$ and $(E/p)_{\frac{1}{2}}$ is certainly less than 10%. For the oblate molecules it is also possible to fit the experimental data with simple LMT functions $f(\xi)$, although even in this case the agreement is less accurate than with $f_{02}(\xi_{02}, x)$. In fig. 7a the dashed curve is the $f(\xi)$ fitting the data for CHF_3. For prolate molecules the fit with $f(\xi)$ is hardly possible as may be seen from fig. 8a, where the results for CH_3Cl are presented.

In the case of the heat conductivity the measurements yield the relative change of the wire temperature $\delta T/\Delta T$ as a function of the voltage difference V between wire and cylinder. As has been shown in appendix C the relation between the measured quantities is given by

$$\frac{\delta T}{\Delta T} = -\frac{1}{a}\int_{\xi(R_2)}^{\xi(R_1)} \frac{\Delta\lambda''}{\lambda_0}\, \mathrm{d}(\ln \xi) = \psi F(\xi(R_1)) \tag{C.6}$$

and

$$\frac{\Delta\lambda''}{\lambda_0} = -a\,\frac{\mathrm{d}(\delta T/\Delta T)}{\mathrm{d}\ln(V/p)}, \tag{C.8}$$

where $a = \ln(R_2/R_1)$ and R_2 and R_1 are the cylinder and wire radius respectively. Therefore, two procedures can be followed to extract the parameters of the field effect, $(\Delta\lambda''/\lambda_0)_{\text{sat}}$ and $(E/p)_{\frac{1}{2}}$, from the measurements:

a) The theoretical curve $\Delta\lambda''/\lambda_0$ *versus* ξ can be integrated, according to eq. (C.6), to yield $\delta T/\Delta T$ as a function of $\xi(R_1)$. The various theoretical curves obtained in this way can then be compared with the experimental data.

b) The experimental curve $\delta T/\Delta T$ *versus* V/p can be differentiated according to eq. (C.8) to yield $\Delta\lambda''/\lambda_0$ as a function of $E(R_1)/p$. This curve can then be compared with the various theoretical curves for the field effect.

Both methods are equivalent for it is clear from fig. 15, for example, that an extrapolation of the curve $\Delta\lambda''/\lambda_0$ *versus* E/p from say 90% to saturation is, as far as accuracy is concerned, comparable to extrapolation of the curve $\delta T/\Delta T$ as a function of V/p from 25% to saturation (see also appendix C). For the presentation of the results and for estimation of the accuracy of the extracted parameters the first method has the advantage that the original measured data and their spread are shown in the graphs where the theoretical and the experimental curves are compared.

In fig. 15 for the oblate molecule $CHCl_3$ ($x = 0.51$) the solid curves represent the best fitting IT function $f_{12}(\xi_{12}, \frac{1}{2})$, the dotted curves the best fitting LMT function $f(\xi)$. These curves are only slightly different for our measuring range and therefore both curves fit within the limits of accuracy. The resulting parameters are independent of whether the fit is made with

TABLE V

Systematic survey of the experimental results and the relevant molecular quantities

Gas	$\left(\frac{\Delta\eta_3}{\eta_0}\right)_{sat} \times 10^3$	$\left(\frac{E}{p}\right)_{\frac{1}{2}}^{\eta}$	$\left(\frac{\Delta\lambda'/}{\lambda_0}\right)_{sat} \times 10^3$	$\left(\frac{E}{p}\right)_{\frac{1}{2}}^{\lambda}$	d	$\frac{(2kTI_A)^{\frac{1}{2}}}{\hbar}$	$\varkappa = \frac{I_A}{I_C}$	M	η_0	λ_0 [b]
		V/cm torr		V/cm torr	debije				μ poise	mW/cm K
NF_3	−3.3	840	−3.5	980	0.234	24.2	0.55	71	200 [a]	0.180
CHF_3	−1.72	225	−1.65	280	1.64	24.5	0.55	70	163	0.143
$CHCl_3$	−1.95	700	−0.93	800	1.013	43.4	0.51	120	103	0.083
$N(CH_3)_3$	−1.35	1150	−0.64	1300	0.612	26.7	0.60	59	92 [a]	0.158
CH_3F	−0.86	1100	−0.67 *	770*	1.86	15.5	6.0	34	90 [a]	0.155
CH_3Cl	−1.18	1700	−0.57 *	1150*	1.87	21.8	11.6	50.5	107	0.105
CH_3Br	−0.60	2800	−0.23 *	1700*	1.80	25.4	16	95	133	0.086
CH_3J			− [c]		1.65		20.8	142		
H_2O			− [c]		1.85			18		
D_2O			− [c]		1.86			20		
CH_3COCH_3			+ [c]		2.90			58		
CH_3Cl	−1.18	1700	−0.57 *	1150*	1.87	21.8	11.6	50.5	107	0.105
CH_3CN	−0.68	3800	+0.132*	260*	3.92	26.0	17.3	41	70	0.096
C_2H_5Cl	−1.5	1700	−0.32 *	1200*	2.03	34.4	5.9	64.5	96	0.117
C_2H_5CN			+0.14 *	360*	3.96		6.2	55		0.096
$C_6H_5CH_3$			− [c]		0.36			92		
C_6H_5CN			+ [c]		4.40			103		
CH_3NH_2	−1.4	5000			1.24			31		
CH_3NO_2	−0.42	4400	+0.22 *	305*	3.46		1.9	61	80 [a]	0.089

* LMT parameters; [a] Evaluated from λ_0; [b] Obtained from the present measurements;
[c] Only the sign could be determined since the effect is small in the measuring range.

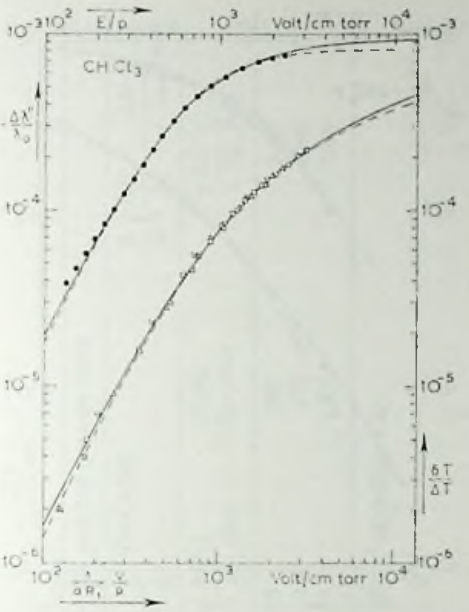

Fig. 15. $\Delta\lambda^{//}/\lambda_0$ at the wire *vs.* E/p at the wire for $CHCl_3$ (full points). $\delta T/\Delta T$ *vs.* E/p ($= (1/aR_1)(V/p)$) at the wire for $CHCl_3$ (open points).

———— $\psi_{12}F_{12}(\xi_{12}, \frac{1}{2})$ and $\psi_{12}F_{12}(\xi_{12}, \frac{1}{2})$ resp.;
--------- $\psi F(\xi)$ and $\psi F(\xi)$ resp.

the $\delta T/\Delta T$ curve or with the differentiated curve $\Delta\lambda^{//}/\lambda_0$. According to the IT theory $(\Delta\lambda^{//}/\lambda_0)_{sat} = (0.93 \pm 0.03)\ 10^{-3}$, $(E/p)_{\frac{1}{2}} = 800 \pm 50$ V/cm torr and according to the LMT theory $(\Delta\lambda^{//}/\lambda_0)_{sat} = (0.84 \pm 0.02)\ 10^{-3}$, $(E/p)_{\frac{1}{2}} = 680 \pm 30$ V/cm torr. As can be seen from fig. 15 the different values for $(\Delta\lambda^{//}/\lambda_0)_{sat}$ are a result of the different asymptotic behaviour of the theoretical curves (see also appendix B). The difference in $(E/p)_{\frac{1}{2}}$ values is mainly a consequence of the difference in $(\Delta\lambda^{//}/\lambda_0)_{sat}$. The comparison for the other oblate molecules leads to similar conclusions as those drawn for $CHCl_3$. The IT parameter values for the oblate molecules are listed in table V and the corresponding curves are shown in fig. 11. For the prolate molecules the situation is different. Fig. 16 shows, for example, the results for the molecule CH_3F ($x = 6.0$). Here the solid curves represent the IT function $f_{12}(\xi_{12}, 6)$ with the parameter values $(\Delta\lambda^{//}/\lambda_0)_{sat} = 1.0 \times 10^{-3}$ and $(E/p)_{\frac{1}{2}} = 1600$ V/cm torr. The deviations are clearly outside the limits of accuracy. It is therefore not very appropriate to characterize the data with IT parameter values. The LMT parameter values are independent of whether the fit is made with $\Delta\lambda^{//}/\lambda_0$ or $\delta T/\Delta T$ and are found to be $(\Delta\lambda^{//}/\lambda_0)_{sat} = (0.67 \pm 0.02) \times 10^{-3}$ and $(E/p)_{\frac{1}{2}} = 770 \pm 20$ V/cm torr.

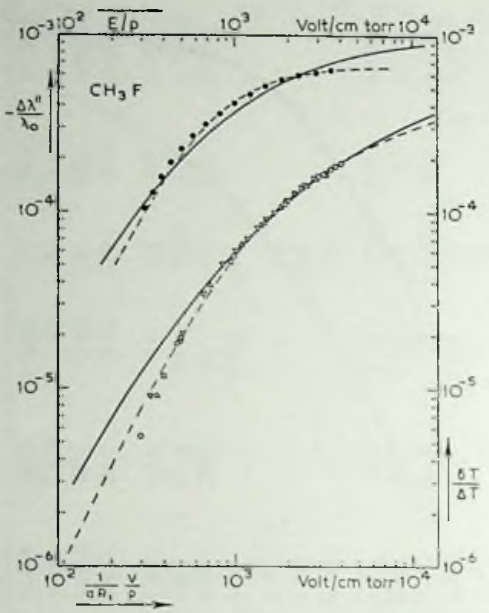

Fig. 16. $\Delta\lambda''/\lambda_0$ at the wire *vs.* E/p at the wire for CH_3F (full points). $\delta T/\Delta T$ *vs.* E/p $(= (1/aR_1)(V/p))$ at the wire for CH_3F (open points).
———— $\psi_{12}F_{12}(\xi_{12}, 6)$ and $\psi_{12}F_{12}(\xi_{12}, 6)$ resp.;
--------- $\psi F(\xi)$ and $\psi F(\xi)$ resp.

The comparison for the other prolate tops and the slightly asymmetric tops leads to similar conclusions as those for CH_3F. Therefore the results for all prolate and slightly asymmetric tops are characterized by the LMT parameter values. These parameter values are listed in table V and marked by a star. In figs. 12 and 13 the corresponding LMT curves are shown.

Some of the present results can be compared with those reported by Senftleben[21]), Gorelik *et al.*[24]) and Borman *et al.*[25]). Senftleben employed the hot wire method in an arrangement similar to ours, *i.e.* with a radial inhomogeneous field. Quantitative results were presented for $CHCl_3$ and C_2H_5Cl, and for CH_3CN and C_6H_5CN an increase in λ was reported. Unfortunately Senftleben equated the relative change of the wire temperature directly to the relative change in the heat conductivity of the gas $(\delta T/\Delta T = \Delta\lambda/\lambda)$ instead of using eq. (C.6). As a consequence Senftleben's paper does not contain the necessary information on the geometry of his cells, *i.e.* wire and cylinder diameters. An exact comparison with his results is therefore not possible. Gorelik *et al.* and Borman *et al.* also use the hot wire method but the field is that of a parallel plate capacitor with the plates, situated inside or outside the cell, parallel to the wire. In these arrangements the change of the heat conductivity is assumed to be

TABLE VI

Comparison between the results of refs. 24 and 25, and the present work

Gas	Gorelik *et al.*[24]) Borman *et al.*[25])		This work		$\frac{1}{2}\left\{\frac{\Delta\lambda^{//}}{\lambda_0}+\frac{\Delta\lambda^{\perp}}{\lambda_0}\right\}_{sat}$
	$10^4 \times \frac{1}{2}\left\{\frac{\Delta\lambda^{//}}{\lambda_0}+\frac{\Delta\lambda^{\perp}}{\lambda_0}\right\}_{sat}$	$(E/p)_1$ V/cm torr	$10^4 \times \left(\frac{\Delta\lambda^{//}}{\lambda_0}\right)_{sat}$	$(E/p)_1$ V/cm torr	$\left(\frac{\Delta\lambda^{//}}{\lambda_0}\right)_{sat}$
NF_3	120.[a]	2000[a]	35	990	3.43
$CHCl_3$	26.8	500	9.3	800	2.88
C_2H_5Cl	11.7	425	3.2*	1200*	3.65

[a] Parameters obtained by representing the data with[24]) $2.5 - 1.5\xi^{-1}\sinh^{-1}\xi - 0.5\xi^{-1}\sinh^{-1}2\xi$.

* LMT parameters.

$\frac{1}{2}(\Delta\lambda^{//}/\lambda_0 + \Delta\lambda^{\perp}/\lambda_0)$. In ref. 22 only preliminary results are reported. In ref. 25 Borman *et al.* describe measurements on a number of polar molecules. It may first be noted that the Moscow data, just like the Leiden data, do not show clear differences in field dependence between the oblate and prolate symmetric tops. Since the moments of inertia of most measured molecules were unknown, Borman *et al.* used the MM (= 1T) function $\frac{5}{4}\{\frac{3}{5}f_{12}(\xi_{12}, 1) + \frac{2}{5}f_{12}(2\xi_{12}, 1)\}$ to describe the field dependence and this curve fits all the data within the limits of accuracy. This is not necessarily in contradiction with our result that the Leiden data can be described with a single LMT curve. Unfortunately Borman *et al.* did not compare their results with LMT.

A comparison between the results of the Moscow group and the Leiden group can be made for the molecules NF_3, $CHCl_3$, C_2H_5Cl and CH_3CN. For the first three molecules the various parameter values are collected in table VI. It may be noted that all these data are derived from 1T functions except our data for C_2H_5Cl (LMT) and the Moscow data for NF_3 (special function[24]), see table VI). Taking these differences into account and assuming for the ratio $\frac{1}{2}(\Delta\lambda^{\perp} + \Delta\lambda^{//})/\Delta\lambda^{//}$ a value $\approx \frac{5}{4}$, a discrepancy of about a factor 2 in the saturation values of these gases remains to be explained. Moreover the differences in $(E/p)_{\frac{1}{2}}$ values appear rather erratic. To clarify the situation, we thoroughly investigated the change of the heat conductivity for NF_3 both in electric and magnetic fields with several different apparatus. The results, given in chapter II, are found to be internally consistent and in perfect agreement with theory and our previous results[23]). These experiments also show that the ratio $\frac{1}{2}(\Delta\lambda^{\perp} + \Delta\lambda^{//})/\Delta\lambda^{//} = 1.28$ for NF_3.

For CH_3CN the discrepancy is even more severe. Borman *et al.*[25]) report a change from a positive effect to a negative effect in the heat conductivity of CH_3CN. Such a behaviour is not observed by us nor mentioned by Senftleben †. The measurements of Borman extend to a homogeneous electric field yielding $\frac{1}{2}(\Delta\lambda^{//}/\lambda_0 + \Delta\lambda^{\perp}/\lambda_0)$, an inhomogeneous electric field yielding $\Delta\lambda^{//}/\lambda_0$ and also to a magnetic field $\Delta\lambda^{\perp}/\lambda_0$. Borman *et al.* showed that the electric field effects on CH_3CN can be described with the LMT theory, where a positive and a negative contribution is included. On the basis of their data we calculated the curve for the parallel field effect and this curve is shown in fig. 17 as curve 1; curve 2 in the same figure represents our results. We may remark that the curves are drawn as far as measurements have been performed. The difference is apparently not a consequence of the homogeneity of the field, because the change of sign was also observed by Borman *et al.*[25]) in an inhomogeneous field. The effect for the inhomogeneous field has a maximum at 130 V/torr and changes sign at a V/p

† Note added in proof: A behaviour as represented by curve 1 in fig. 17 has recently been observed in mixtures of CH_3CN with N_2 (see chapter III).

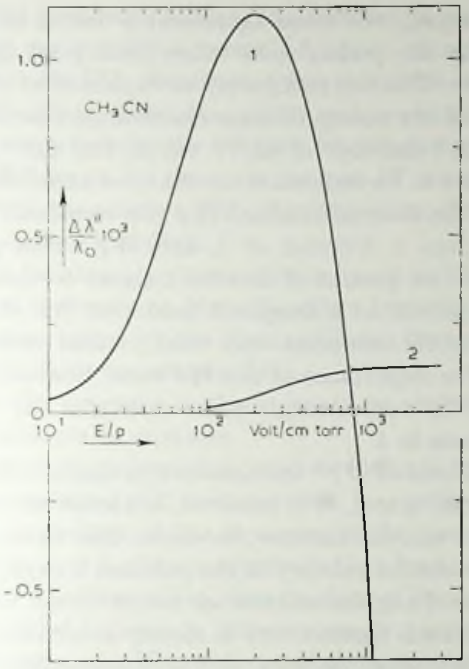

Fig. 17. $\Delta\lambda''/\lambda_0$ *vs.* E/p for CH_3CN.
curve 1: Borman *et al.* (ref. 25);
curve 2: present work.

value of 370 V/torr. In view of these results we did measurements up to 500 V/torr. Temperature differences between wire and cylinder of 20°C and 130°C were established, the latter temperature difference being also used by the Moscow group. No absolute values for $\Delta\lambda/\lambda$ were derived from these measurements because the Knudsen corrections were unknown but in the whole V/p range from 0–500 V/torr no maximum in the effect has been observed. From measurements in a homogeneous magnetic field we derived that $\Delta\lambda/\lambda$ is smaller than 10^{-5}, in the H/p range from $0 - 5 \times 10^4$ Oe/torr, although the Moscow group observed a maximum in $\Delta\lambda/\lambda$ of 5×10^{-4} already at H/p as low as 300 Oe/torr. We may point to the fact that the electric and magnetic measurements of the Moscow group are internally inconsistent. Comparing their E/p values at maximum $\Delta\lambda/\lambda$ or at $\Delta\lambda/\lambda = 0$ with the corresponding H/p values, a molecular g factor $g = 5$ is found, which value is an order of magnitude higher than the real values: $g^{//}=0.310$ and $g^{\perp} = -0.0317$ [36]).

6. *Conclusions.* It has been noted in the preceding section that the viscosity results agree well with the IT theory. As far as the thermal con-

ductivity is concerned, the same agreement is found for the oblate symmetric tops, while the prolate ones follow to a good approximation the steeper LMT curve. This can tentatively be explained as follows: Each term in the expansion of the nonequilibrium distribution function gives a contribution having the behaviour of an IT curve. For the viscosity, only the $[J]^{(2)}$ term appears to be important, so that the experiments give directly an IT curve. For the thermal conductivity two terms can be of importance, $W[J]^{(2)}$ which gives a decrease of λ, and WJ which gives an increase. This last term can be present if detailed balance is violated. It has been proved by experiments in a magnetic field that the $W[J]^{(2)}$ term dominates strongly for the nonpolar and weakly polar molecules (*e.g.* NF_3, NO, CO)[37,26]. The importance of the WJ term, however, is substantiated by the fact that the very strongly polar molecules like CH_3CN, CH_3NO_2 *etc.* show an increase in λ.

Both terms WJ and $W[J]^{(2)}$ are sensitive to elastic collisions (no change in internal quantum state), WJ, however, is almost insensitive to reorientation collisions; it can, for instance, be shown that those reorientation collisions where the relative velocity of the partners is negligible do not affect WJ at all because of angular-momentum conservation. On the other hand, $W[J]^{(2)}$ in the thermal conductivity is almost as sensitive to reorientation collisions as $[J]^{(2)}$ in the viscosity. If the elastic collisions are dominant the collision frequencies for WJ and $W[J]^{(2)}$ will be nearly equal and the $W[J]^{(2)}$ contribution will have only a slightly larger half value than the WJ contribution, due to its larger average precession frequency (see fig. 1 and table IV). When, however, reorientation collisions are dominant the collision frequency for $W[J]^{(2)}$ may be appreciably higher than the collision frequency of WJ and the difference in half values between the two terms will be much enhanced thereby.

For the weakly polar gas NF_3 the WJ contribution is negligible, as has been demonstrated by experiments in both electric and magnetic fields (chapter II). Presumably detailed balance holds here to a good approximation. For this molecule the $(E/p)_{\frac{1}{2}}$ values for η and λ are almost the same, showing that the $W[J]^{(2)}$ term and the $[J]^{(2)}$ term correspond to the same collision frequency. Indeed the elastic and reorientation collision frequencies are nearly equal, as is indicated by the fact that both $Z_{12} = 0.74$ and $Z_{02} = 0.86$ are close to unity. For the other oblate molecules the WJ term may become relatively more important. Since, however, on one hand WJ and $W[J]^{(2)}$ have nearly the same average precession frequency ($\xi_{12,\frac{1}{2}}/\xi_{11,\frac{1}{2}} \approx 1$, see table VII) and on the other hand the collision frequencies do not differ very much because reorientation collisions are not much more frequent than elastic collisions ($(E/p)_{\frac{1}{2}}^{\eta}/(E/p)_{\frac{1}{2}}^{\lambda} \approx 1$) both terms saturate at comparable field values. As a consequence, the resulting curve still has approximately the IT shape.

Consider now the prolate molecules. The relevant precession frequencies for such molecules are roughly a factor 1.5 apart, as is indicated by the ratio $\xi_{12,\frac{1}{2}}/\xi_{11,\frac{1}{2}}$ in table VII. Moreover, these molecules have larger dipole moments than the oblate molecules, which makes reorientation collisions more likely, increasing thereby the collision frequency for the $W[J]^{(2)}$ term (but not for the WJ term). In this case the two IT curves have different half-values and since the positive WJ contribution saturates earlier and is smaller, a steeper curve is obtained.

Finally there are the strongly polar molecules such as CH_3CN or CH_3NO_2 where the WJ term is dominant. Here the effect becomes positive and the half-value, being determined by the elastic-collision frequency, is therefore relatively small (see, however, chapter III).

The validity of the foregoing analysis should be checked by measuring also $\lambda^{\perp}$ or by experiments on mixtures.

In table V the data are presented in order to indicate the apparent regularities. It may be remarked that there seems to be a critical dipole moment $d_c \approx 2.5$ debije (independent of the structure of the molecules) such that all molecules having $d < d_c$ show a negative effect for λ, and all molecules having $d > d_c$ show a positive effect. Also the data of Borman *et al.* [25]) agree with this rule. Detailed balance is indeed strongly violated by molecules with large dipole moments. The three methyl halogenides CH_3F, CH_3Cl and CH_3Br have the same dipole moment and of course the same structure. The data show a regular increase in half-values with mass for both η and λ (due to increasing prolateness). The saturation values for λ decrease in absolute value in the same order, but no such regularity is observed for η.

In table VII the collision numbers, as calculated from formula (2.21) are given. Z_{02} is given for all symmetric-top molecules, and also for the nearly symmetric top C_2H_5Cl; the collision numbers

$$Z_{12} = Z_{02}\frac{(E/p)^{\eta}_{02\frac{1}{2}}}{(E/p)^{\lambda}_{12\frac{1}{2}}} \qquad \text{and} \qquad Z_{11} = \frac{\xi_{12,\frac{1}{2}}}{\xi_{11,\frac{1}{2}}}\frac{(E/p)^{\eta}_{02\frac{1}{2}}}{(E/p)^{\lambda}_{11\frac{1}{2}}}Z_{02}$$

are not considered because the measurements yield only a mixture of both. For the oblate molecules, however, $Z_{12} \approx Z_{02}$ ($\approx Z_{11}$), as has been pointed out before.

In the case of the viscosity a good deal of information can also be drawn from the saturation value, using eq. (2.15). (This is hardly possible for the thermal conductivity because of the very complicated structure of Λ_{11} and Λ_{12}, eq. (2.16).) Although the collision bracket $\left[\begin{smallmatrix}200\\020\end{smallmatrix}\right]$ is off-diagonal and does not really represent an average cross section, it can be taken as a measure of the energetically inelastic-collision frequency because it nearly vanishes in the absence of these collisions[38]), so that by introducing an energetically inelastic-collision number $Z' = [200]\left[\begin{smallmatrix}200\\020\end{smallmatrix}\right]^{-1}$ eq. (2.15) can be

TABLE VII

Collision numbers and cross sections obtained from η_3 and comparison between η_3 and $\lambda//$

Gas	d debye	$x = \frac{I_A}{I_C}$	$\xi_{02,\frac{1}{2}} = \xi_{12,\frac{1}{2}}$	$\xi_{11,\frac{1}{2}}$	$\frac{\xi_{12,\frac{1}{2}}}{\xi_{11,\frac{1}{2}}}$	$\frac{(E/p)^{\eta}_{\frac{1}{2}}}{(E/p)^{\lambda}_{\frac{1}{2}}}$	Z_{02}	$\frac{(\Delta\eta_3/\eta_0)_{sat}}{(\Delta\lambda//\lambda_0)_{sat}}$	Z'	σ_{η_0}[a] Å^2	σ_{02} Å^2
NF_3	0.234	0.55	3.3	3.05	1.08	0.86	0.86	0.94	16.2	61.5	71
CHF_3	1.64	0.55	3.3	3.05	1.08	0.80	0.56	1.04	18.1	75	131
$CHCl_3$	1.013	0.51	3.2	3.0	1.07	0.87	0.80	2.09	20.3	155	192
$N(CH_3)_3$	0.612	0.60	3.4	3.1	1.10	0.88	0.59	2.11	20.9	122	205
CH_3F	1.86	6.0	13.2	8.5	1.55	1.43	0.47	1.28	23.3	92	196
CH_3Cl	1.87	11.6	18.4	11.9	1.55	1.48	0.49	2.07	20.5	94	220
CH_3Br	1.80	16.0	22.5	13.9	1.62	1.65	0.36	2.61	24.5	107	294
C_2H_5Cl	2.03	5.9	13.1	8.4	1.56	1.42	0.56	4.68	19.4	122	213
CH_3CN	3.92	17.3	23.7	14.4	1.64	14.6	0.25	−5.15	19.3	134	533
CH_3NO_2	3.46	1.9				14.4		−1.91			

[a] Calculated from η_0; $\sigma = \frac{5}{4}\frac{kT}{\langle v_{rel}\rangle}\frac{\omega}{p}$, $\langle v_{rel}\rangle = \sqrt{8kT/\pi\mu}$, μ is reduced mass.

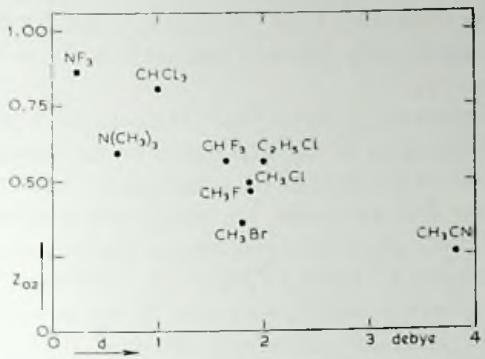

Fig. 18. The reorientation collision number Z_{02} as a function of the dipole moment d.

rewritten:

$$-\left(\frac{\Delta\eta_3}{\eta_0}\right)_{\text{sat}} = \frac{Z_{02}}{(Z')^2}.$$

The values of Z' so obtained are listed in table VII. It can be seen from table VII and fig. 18 that Z_{02} shows a definite decrease with increasing d, while Z' oscillates, staying constant in the average. This is reasonable. Indeed, a larger dipole moment will certainly increase the reorientation probability, but will not affect the energetically inelastic collisions which are essentially hard collisions, independent of the long-range part of the potential. It is also interesting to note that the absolute values of Z_{02} are smaller than unity: as has been pointed out before, reorientation collisions are extremely probable in polar gases, even more probable than the linear momentum-changing collisions that determine the viscosity η_0.

In table VII collision cross sections (defined on the basis of the assumption that the average collision frequencies are proportional to the average cross sections) are also reported. The values of such cross sections

TABLE VIII

Comparison between the collision frequencies obtained from η_3 and nonresonant microwave absorption

Gas	$\frac{\omega_{02}}{p}$	$\frac{\omega_{\text{nonresonant}}}{p}$	$\frac{\omega_{02}}{\omega_{\text{nonresonant}}}$
	$10^6\ \text{s}^{-1}\ \text{torr}^{-1}$	$10^6\ \text{s}^{-1}\ \text{torr}^{-1}$	
CHF_3	14.5	12.8	1.13
CH_3F	31.4	28.4	1.11
CH_3Cl	25.1	28.4	0.88
CH_3Br	27.8	24.1	1.15
CH_3CN	75.4	86.5	0.87

are independent of the value of the viscosity η_0 which for a number of gases is not known experimentally but is evaluated from λ_0: in those cases σ_{02} is more reliable than Z_{02}.

Finally, a comparison is made between the collision frequencies obtained from $(E/p)_{\frac{1}{4}}$, corresponding to Z_{02}, and the collision frequencies obtained by Birnbaum[39]) from measurements of nonresonant microwave absorption. This is possible for five gases and the comparison is given in table VIII. The collision bracket, which is of importance for nonresonant absorption is of the type: $(1/n)\langle J^{-2}J_\zeta \boldsymbol{J}\cdot\mathscr{C}J^{-2}J_\zeta \boldsymbol{J}\rangle$ and corresponds therefore to a reorientation cross section analogous to σ_{02}. It can indeed be seen that for all five gases the collision frequencies obtained from the nonresonant microwave absorption and this experiment are nearly equal, although the frequencies for the various gases are very different.

A similar comparison with resonant absorption is impossible because the resonant cross section, while also sensitive to reorientation, is strongly influenced by perturbations which can disturb the absorption process. The cross sections may therefore be an order of magnitude larger than for the nonresonant case[40]).

Acknowledgements. The authors wish to thank Dra. M. Wisse-Schouten and Mr. W. Schippers for their enthusiastic help with the heat-conductivity experiments. Dr. A. Tip and Dr. G. Cooper are gratefully acknowledged for useful discussions on the microwave absorption phenomena. The assistance of the technical and administrative staffs of the Kamerlingh Onnes Laboratorium and the Istituto di Fisica dell' Università di Genova is highly appreciated. The authors are indepted to Dr. G. Cooper for reading the manuscript.

This work resulted from a cooperation of the molecular physics groups of the Kamerlingh Onnes Laboratorium, Leiden, and the Istituto di Fisica dell' Università di Genova.

The work of the Leiden group is part of the research program of the "Stichting voor Fundamenteel Onderzoek der Materie (F.O.M.)" and has been made possible by financial support from the "Nederlandse Organisatie voor Zuiver-Wetenschappelijk Onderzoek (Z.W.O.)".

APPENDIX A

In this appendix the perturbative and the variational methods will be compared. The problem is to find approximations to the scalar product

$$X_1 = (K, X), \tag{1}$$

where K and X are vectors of a Hilbert space H, and X is the solution of

the equation

$$K = (\mathscr{C} + \mathscr{F})\, X. \tag{2}$$

$\mathscr{C}$ and $\mathscr{F}$ are linear operators in H (the "collision" and "field" operators). An orthonormal basis set $\{\Psi_n\}$ will be chosen in H, and the following assumptions made:

$$\Psi_1 \equiv K; \qquad \mathscr{C}_{1n} = \mathscr{C}_{n1} = 0 \text{ unless } n = 1, 2; \qquad \mathscr{C}_{nn} = \lambda_n \text{ real};$$
$$\mathscr{F}\Psi_1 = 0; \qquad \mathscr{F}_{22} = 0; \qquad \mathscr{F}\dagger = -\mathscr{F}. \tag{3}$$

Moreover, the off-diagonal elements of $\mathscr{C}$ will be assumed to be small in comparison to the diagonal ones.

a) Perturbative method. $\mathscr{C}$ can be split into two parts:

$$\mathscr{C} = \mathscr{C}^{(0)} + \varepsilon\mathscr{C}^{(1)} \tag{4}$$

such that $\mathscr{C}^{(0)}$ is diagonal, $\mathscr{C}^{(1)}$ is purely off-diagonal and ε is a small number. Then eq. (2) can be solved formally:

$$X = (\mathscr{C}^{(0)} + \mathscr{F} + \varepsilon\mathscr{C}^{(1)})^{-1} K$$
$$= (\mathscr{C}^{(0)} + \mathscr{F})^{-1} \{1 + \varepsilon\mathscr{C}^{(1)}(\mathscr{C}^{(0)} + \mathscr{F})^{-1}\}^{-1} K. \tag{5}$$

Taking the scalar product and expanding in ascending powers of ε one obtains

$$X_1 = (K, (\mathscr{C}^{(0)} + \mathscr{F})^{-1} K) - \varepsilon(K, (\mathscr{C}^{(0)} + \mathscr{F})^{-1}\mathscr{C}^{(1)}(\mathscr{C}^{(0)} + \mathscr{F})^{-1} K)$$
$$+\varepsilon^2(K, (\mathscr{C}^{(0)} + \mathscr{F})^{-1}\mathscr{C}^{(1)}(\mathscr{C}^{(0)} + \mathscr{F})^{-1}\mathscr{C}^{(1)}(\mathscr{C}^{(0)} + \mathscr{F}^{(1)})^{-1} K) - \ldots \tag{6}$$

Because of the conditions (3) the first term equals λ_1^{-1}, the second vanishes and the third equals:

$$\lambda_1^{-2}\mathscr{C}_{12}\mathscr{C}_{21}[(\mathscr{C}^{(0)} + \mathscr{F})^{-1}]_{22}. \tag{7}$$

The "field effect", *i.e.* the difference between X_1 and the same quantity computed in the absence of $\mathscr{F}$ is then

$$\Delta X_1 = \lambda_1^{-2}\mathscr{C}_{12}\mathscr{C}_{21}\{[(\mathscr{C}^{(0)} + \mathscr{F})^{-1}]_{22} - \lambda_2^{-1}\}$$
$$= -\lambda_1^{-2}\lambda_2^{-1}\mathscr{C}_{12}\mathscr{C}_{21}[(\mathscr{C}^{(0)} + \mathscr{F})^{-1}\mathscr{F}]_{22}. \tag{8}$$

This is the generalized MM result. It goes over to the LMT result in the following approximation: there exists Ψ_3 such that $\mathscr{F}_{2n} = 0$ unless $n = 3$; $\mathscr{F}_{23} = -\mathscr{F}_{32}$ is real. In this case eq. (8) is replaced by the simpler result

$$\Delta X_1 = -\lambda_1^{-2}\lambda_2^{-1}\mathscr{C}_{12}\mathscr{C}_{21}\frac{\mathscr{F}_{23}^2}{\mathscr{F}_{23}^2 + \lambda_2\lambda_3} \tag{9}$$

which easily can be proved at low fields by expanding both (8) and (9) in power series in the field and identifying the terms.

b) Variational method. In the variational method no splitting of $\mathscr{C}$ is necessary, but a certain partial set S of basis vectors is chosen and scalar products are taken with the elements of the set. Two choices are here in order: the first is Ψ_1, Ψ_2, Ψ_3; the second is Ψ_1, Ψ_2 and all the basis vectors Ψ_n coupled to Ψ_2, directly or indirectly, via $\mathscr{F}$. The variational equations have the form

$$\begin{aligned} 1 &= (\Psi_1, (\mathscr{C} + \mathscr{F})\, X), \\ 0 &= (\Psi_n, (\mathscr{C} + \mathscr{F})\, X), \qquad (n > 1), \qquad (\Psi_n \in S). \end{aligned} \tag{10}$$

By letting

$$X = \sum_n X_n \Psi_n, \tag{11}$$

the eqs. (10) become

$$\begin{aligned} 1 &= \lambda_1 X_1 + \mathscr{C}_{12} X, \\ 0 &= \mathscr{C}_{21} X_1 + \lambda_2 X_2 + \sum_{n>2} \mathscr{C}_{2n} X_n + \sum_{n>2} \mathscr{F}_{2n} X_n, \\ 0 &= \lambda_n X_n + \mathscr{C}_{n2} X_2 + \sum_{m \neq 2,n} \mathscr{C}_{nm} X_m + \mathscr{F}_{n2} X_2 + \sum_{m \neq 2,n} \mathscr{F}_{nm} X_m, \\ & \quad (n > 2). \end{aligned} \tag{12}$$

These equations can be simplified by neglecting all off-diagonal matrix elements of $\mathscr{C}$ except $\mathscr{C}_{12}$ and $\mathscr{C}_{21}$:

$$\begin{aligned} 1 &= \lambda_1 X_1 + \mathscr{C}_{12} X_2, \\ 0 &= \mathscr{C}_{21} X_1 + \lambda_2 X_2 + \sum_{n>2} \mathscr{F}_{2n} X_n, \\ 0 &= \lambda_n X_n + \mathscr{F}_{n2} X_2 + \sum_{m \neq 2,n} \mathscr{F}_{nm} X_m, \qquad (n > 2). \end{aligned} \tag{13}$$

Now the coefficients X_n can be split into a field-independent part and a change in the field:

$$X_n = X_n^0 + \Delta X_n. \tag{14}$$

The field-independent equations are

$$\begin{aligned} 1 &= \lambda_1 X_1^0 + \mathscr{C}_{12} X_2^0, \\ 0 &= \mathscr{C}_{21} X_1^0 + \lambda_2 X_2^0, \\ 0 &= X_n^0, \qquad (n > 2), \end{aligned} \tag{15}$$

with the approximate solution

$$X_1^0 = \lambda_1^{-1}, \qquad X_2^0 = -\lambda_1^{-1} \lambda_2^{-1} \mathscr{C}_{21}, \qquad X_n^0 = 0, \qquad (n > 2). \tag{16}$$

By subtracting (15) from (13) the equations

$$0 = \lambda_1 \Delta X_1 + \mathscr{C}_{12} \Delta X_2,$$

$$0 = \mathscr{C}_{21}\Delta X_1 + \lambda_2 \Delta X_2 + \sum_{n>2} \mathscr{F}_{2n} X_n, \tag{17}$$

$$0 = \lambda_n X_n + \mathscr{F}_{n2} X_2^0 + \mathscr{F}_{n2}\Delta X_2 + \sum_{m\neq 2,n} \mathscr{F}_{nm} X_m, \qquad (n>2),$$

are obtained, where the first term on the r.h.s. of the second equation is very small and can be neglected. The first equation gives

$$\Delta X_1 = -\lambda_1^{-1}\mathscr{C}_{12}\Delta X_2. \tag{18}$$

To solve the other equations for ΔX_2 first the simpler set Ψ_1, Ψ_2, Ψ_3 will be considered. In this case the equations reduce to

$$\begin{aligned} 0 &= \lambda_2 \Delta X_2 + \mathscr{F}_{23} X_3, \\ 0 &= \lambda_3 X_3 + \mathscr{F}_{32} X_2^0 + \mathscr{F}_{32}\Delta X_2, \end{aligned} \tag{19}$$

with the solution

$$\Delta X_2 = \frac{-\mathscr{F}_{23}^2}{\mathscr{F}_{23}^2 + \lambda_2\lambda_3} X_2^0, \tag{20}$$

whence, using (16) and substituting then into (18) one obtains the LMT result

$$\Delta X_1 = -\lambda_1^{-2}\lambda_2^{-1}\mathscr{C}_{12}\mathscr{C}_{21}\frac{\mathscr{F}_{23}^2}{\mathscr{F}_{23}^2 + \lambda_2\lambda_3}, \tag{21}$$

which coincides exactly with (9).

On the other hand it is also possible to use the more extended set, obtaining then, instead of (19), the equations

$$\begin{aligned} 0 &= \lambda_2 \Delta X_2 + (\mathscr{F}X)_2, \\ 0 &= \lambda_n X_n + (\mathscr{F}X^0)_n + (\mathscr{F}\Delta X_n), \qquad (n>2), \end{aligned} \tag{22}$$

equivalent to the operator equation on the subspace orthogonal to K:

$$0 = \mathscr{C}^{(0)}\Delta X + \mathscr{F}X^0 + \mathscr{F}\Delta X, \tag{23}$$

whose solution is

$$\Delta X = -(\mathscr{C}^{(0)} + \mathscr{F})^{-1}\mathscr{F}X^0. \tag{24}$$

In particular

$$\Delta X_2 = -[(\mathscr{C}^{(0)} + \mathscr{F})^{-1}\mathscr{F}]_{22} X_2^0. \tag{25}$$

Using (16) and substituting then into (18), the result

$$\Delta X_1 = -\lambda_1^{-2}\lambda_2^{-1}\mathscr{C}_{12}\mathscr{C}_{21}[(\mathscr{C}^{(0)} + \mathscr{F})^{-1}\mathscr{F}]_{22} \tag{26}$$

is obtained. This coincides exactly with the MM result (8). Thus the LMT is that approximation to the generalized MM result which is obtained by restricting the variational set to a finite set (in particular, a set of three vectors).

APPENDIX B

All field functions $f(\xi)$ occurring in the LMT theory have the simple dispersion form

$$f(\xi) = \frac{\xi^2}{1 + \xi^2}, \tag{1}$$

whereas in the IT theory the functions $f_{pq}(\xi_{pq}, x)$ are given by

$$f_{pq}(\xi_{pq}, x) = \frac{1}{\langle [\boldsymbol{J}]^{(q)} \odot^q [\boldsymbol{J}]^{(q)} \rangle} \times \left\langle [\boldsymbol{J}]^{(q)} \odot^q [\boldsymbol{J}]^{(q)} \frac{(\hbar^{-1} J_\zeta J^{-2} (2 I_A k T)^{\frac{1}{2}} \xi_{pq})^2}{1 + (\hbar^{-1} J_\zeta J^{-2} (2 I_A k T)^{\frac{1}{2}} \xi_{pq})^2} \right\rangle. \tag{2.17}$$

The functions describing the field dependence of the viscosity and thermal conductivity are f_{02} and f_{12}, f_{11} respectively. Taking the classical limit of eq. (2.17) the MM field functions are obtained[7]). As shown in section 2, eq. (2.19), the IT field functions in principle have the form of a simple (LMT) dispersion function weighted with J^{2q} and averaged with the Boltzmann factor. For this reason the IT functions do not only depend on ξ but also on the moments of inertia and on the rank q of $\boldsymbol{J}$. This fact is reflected in the different asymptotic behaviour of the field functions, *i.e.* in the low field range:

$$f(\xi) \sim \xi^2,$$

$$f_{p2}(\xi_{p2}, x) \sim \frac{2}{x(3x^{-2} + 4x^{-1} + 8)} \xi_{p2}^2, \tag{2}$$

$$f_{11}(\xi_{11}, x) \sim \frac{2}{(2 + x^{-1})(1 - x)} \left[1 - \frac{1}{(x^{-1} - 1)^{\frac{1}{2}}} \operatorname{tg}^{-1}(x^{-1} - 1)^{\frac{1}{2}} \right] \xi_{11}^2, \quad \text{for} \quad x \leq 1$$

$$\sim \frac{2}{(2 + x^{-1})(1 - x)} \left[1 - \frac{1}{2(1 - x^{-1})^{\frac{1}{2}}} \ln \left(\frac{1 + (1 - x^{-1})^{\frac{1}{2}}}{1 - (1 - x^{-1})^{\frac{1}{2}}} \right) \right] \xi_{11}^2, \quad \text{for} \quad x \geq 1$$

and in the high field range:

$$f(\xi) \sim 1 - \frac{1}{\xi^2},$$

$$f_{p2}(\xi_{p2}, x) \sim 1 - \frac{24 \sqrt{(\pi x)}}{(3x^{-2} + 4x^{-1} + 8)} \frac{1}{|\xi_{p2}|}, \tag{3}$$

$$f_{11}(\xi_{11}, x) \sim 1 - \frac{4 \sqrt{(\pi x)}}{(2 + x^{-1})} \frac{1}{|\xi_{11}|}.$$

The asymptotic behaviour of the function $f_{pq}(\xi_{pq}, x)$ has been calculated from eq. (2.17) by taking the classical limit.

In the classical limit the functions $f_{pq}(\xi_{pq}, x)$ can be expressed in an analytical form for two special cases, *i.e.*:
$x = \frac{1}{2}$, extreme oblate symmetric top

$$f_{p2}(\xi_{p2}, \tfrac{1}{2}) = \tfrac{1}{7}\left(\xi_{p2}^2 - \sqrt{2\pi}\,|\xi_{p2}|^3 - 3\xi_{p2}^4 - \sqrt{\frac{\pi}{2}}\,|\xi_{p2}|^5\right)$$
$$+ \tfrac{1}{7}\left(2\xi_{p2}^2 + 3\sqrt{\frac{\pi}{2}}\,|\xi_{p2}|^3 + 3\xi_{p2}^4 + \sqrt{\frac{\pi}{2}}\,|\xi_{p2}|^5\right)\cdot A(|\xi_{p2}|\,\tfrac{1}{2}\sqrt{2}),$$

$$f_{11}(\xi_{11}, \tfrac{1}{2}) = \tfrac{1}{2}\left(2\xi_{11}^2 + \sqrt{\frac{\pi}{2}}\,|\xi_{11}|^3\right)$$
$$- \tfrac{1}{2}\left(\sqrt{\frac{\pi}{2}}\,|\xi_{11}| + 2\xi_{11}^2 + \sqrt{\frac{\pi}{2}}\,|\xi_{11}|^3\right)\cdot A(|\xi_{p2}|\,\tfrac{1}{2}\sqrt{2}), \tag{4}$$

$x = 1$, spherical top

$$f_{p2}(\xi_{p2}, 1) = \tfrac{4}{15}(-6\sqrt{\pi}\,\xi_{p2}^{-1} + 12 - \tfrac{7}{2}\xi_{p2}^2 + \xi_{p2}^4)$$
$$+ \tfrac{4}{15}(6\xi_{p2}^{-2} - 6 + 3\xi_{p2}^2 - \xi_{p2}^4)\,A(|\xi_{p2}|),$$

$$f_{11}(\xi_{11}, 1) = \tfrac{2}{3}(-2\sqrt{\pi}\,|\xi_{11}|^{-1} + 4 - \xi_{11}^2)$$
$$+ \tfrac{2}{3}(2\xi_{11}^{-2} - 2 + \xi_{11}^2)\,A(|\xi_{11}|), \tag{5}$$

where $A(y) = \sqrt{\pi}\,y\,e^{y^2}\,\mathrm{erfc}(y)$ has the following limiting values[41]:

$$y \to \infty, \qquad A(y) \sim 1 - \frac{1}{2y^2} + \frac{3}{4y^4} - \frac{15}{8y^6}, \tag{6}$$

$$y \to 0, \qquad A(y) \sim \sqrt{\pi}\,y - 2y^2 + \sqrt{\pi}\,y^3 - \tfrac{4}{3}y^4 + \frac{\sqrt{\pi}}{2}\,y^5.$$

All functions $f_{pq}(\xi_{pq}, x)$ presented in the figures have been calculated numerically in the classical approximation and checked on their asymptotic behaviour with the aid of eqs. (2) and (3). The functions $f_{pq}(\xi_{pq}, \frac{1}{2})$ and $f_{pq}(\xi_{pq}, 1)$ have moreover been calculated with the aid of eqs. (4) and (5).

APPENDIX C

In a hot-wire apparatus with a voltage difference V between wire (radius R_1) and cylinder (radius R_2) the electric field $\boldsymbol{E}$ is parallel to the tempera-

ture gradient so that the heat-conductivity coefficient $\lambda(E)$ equals $\lambda^{//}(E)$. Denoting the radial distance from the centre of the wire by r and defining $a = \ln(R_2/R_1)$, the cylindrical symmetric electric field is given by

$$E(r) = \frac{V}{ar} \tag{1}$$

and consequently $\lambda^{//}(E)$ also depends on r. This fact has to be taken into account when solving the conduction equation. In the stationary state the conduction equation

$$\nabla\cdot(\lambda^{//}\nabla T) = \lambda^{//}\nabla^2 T + \nabla\lambda^{//}\cdot\nabla T = 0 \tag{2}$$

holds, and because of the cylindrical symmetry, integration yields

$$\frac{\mathrm{d}T}{\mathrm{d}r} = -\frac{c}{\lambda^{//}(r)\,r}, \qquad \text{where} \qquad c = \text{constant}.$$

Writing $\lambda^{//}(r) = \lambda_0 + \Delta\lambda^{//}(r)$ and noting that $\Delta\lambda^{//}/\lambda_0 \leq 10^{-2}$, the temperature difference between wire and cylinder is found to be

$$\Delta T + \delta T = \frac{ca}{\lambda_0} + \frac{c}{\lambda_0}\int_{R_2}^{R_1}\frac{\Delta\lambda^{//}}{\lambda_0}\,\frac{\mathrm{d}r}{r}, \tag{3}$$

where δT is the change of the wire temperature due to the presence of the electric field. Using eq. (1) the relative change of the wire temperature due to the electric field can be written in the form

$$\frac{\delta T}{\Delta T} = \frac{1}{a}\int_{R_2}^{R_1}\frac{\Delta\lambda^{//}}{\lambda_0}\,\frac{\mathrm{d}r}{r} = -\frac{1}{a}\int_{E(R_2)}^{E(R_1)}\frac{\Delta\lambda^{//}}{\lambda_0}\,\mathrm{d}(\ln E). \tag{4}$$

Since $\Delta\lambda^{//}/\lambda_0$ reaches saturation at high field values, it follows that

$$\left(\frac{\delta T}{\Delta T}\right)_{\mathrm{sat}} = -\left(\frac{\Delta\lambda^{//}}{\lambda_0}\right)_{\mathrm{sat}}. \tag{5}$$

The theoretical expression for the relative change of the wire temperature is obtained by substituting the theoretical expression for $\Delta\lambda^{//}/\lambda_0$ in eq. (4) and transforming E to the theoretical field parameter ξ. This transformation is simple since for all theoretical models $\xi = \alpha E/p$, where α is determined by the properties of the gas molecules, and eq. (4) becomes

$$\frac{\delta T}{\Delta T} = -\frac{1}{a}\int_{\xi(R_2)}^{\xi(R_1)}\frac{\Delta\lambda^{//}(\xi)}{\lambda_0}\,\mathrm{d}(\ln\xi). \tag{6}$$

Since $\xi(R_2) = R_1R_2^{-1}\xi(R_1)$, the theoretical expression for $\delta T/\Delta T$ is a function

of $\xi(R_1)$ only. On the other hand it is also possible to obtain $\Delta\lambda''/\lambda_0$ directly from the measured change in wire temperature by differentiating eq. (4) with respect to $\ln E(R_1)$. Noticing that $E(R_2) = (R_1/R_2)\, E(R_1)$ one obtains:

$$\frac{\Delta\lambda''(R_1)}{\lambda_0} - \frac{\Delta\lambda''(R_2)}{\lambda_0} = -a \frac{\mathrm{d}(\delta T/\Delta T)}{\mathrm{d}(\ln E(R_1))}. \tag{7}$$

For our cell $R_2/R_1 \approx 300$ and the relevant part of $\Delta\lambda''/\lambda_0$ *versus* E/p usually covers a range of E/p values of approximately two orders of magnitude; hence $\Delta\lambda''(R_2)/\lambda_0$ will be small compared to $\Delta\lambda''(R_1)/\lambda_0$ in the actual measuring range. By transforming $E(R_1)$ to the measured quantity V/p eq. (7) can now be written

$$\frac{\Delta\lambda''(R_1)}{\lambda_0} = -a \frac{\mathrm{d}(\delta T/\Delta T)}{\mathrm{d}(\ln(V/p))}. \tag{8}$$

Consequently the slope of the experimental curve $\delta T/\Delta T$ *versus* $\ln(V/p)$ yields the relative change of the heat conductivity at the wire.

A clear picture of the situation is obtained when comparing for example the dotted curves in fig. 15. The upper curve represents the field effect at the wire as a function of $E(R_1)/p = \alpha^{-1}\xi(R_1)$ for the case of a single dispersion term according to the LMT theory, *i.e.*

$$\frac{\Delta\lambda''(R_1)}{\lambda_0} = \left(\frac{\Delta\lambda''(R_1)}{\lambda_0}\right)_{\mathrm{sat}} \frac{\xi^2(R_1)}{1 + \xi^2(R_1)}. \tag{9}$$

The lower curve represents the corresponding relative change of the wire temperature as a function of $V(aR_1p) = \alpha^{-1}\xi(R_1)$:

$$\frac{\delta T}{\Delta T} = -\frac{1}{a}\int_{\xi(R_2)}^{\xi(R_1)} \frac{\Delta\lambda''}{\lambda_0}\frac{\mathrm{d}\xi}{\xi} = -\frac{1}{2a}\left(\frac{\Delta\lambda''}{\lambda_0}\right)_{\mathrm{sat}} \ln\left\{\frac{\xi^2(R_1) + 1}{R_1^2 R_2^{-2}\xi^2(R_1) + 1}\right\}. \tag{10}$$

A comparison shows that 95% saturation of $\Delta\lambda''/\lambda_0$ at the wire gives rise to only 25% saturation in $\delta T/\Delta T$. All the relevant information with respect to $\Delta\lambda''/\lambda_0$ is therefore contained in the portion of the curve $\delta T/\Delta T$ *versus* V/p up to about 30% saturation in $\delta T/\Delta T$; the remaining part of the curve merely duplicates the information obtained from the first part and shows how the saturation of $\Delta\lambda''/\lambda_0$ spreads out over the cell to the cylinder wall.

APPENDIX D

To account for the temperature distribution along the wire and the various heat losses of the cell, one may proceed as follows. The average temperature difference between wire and cylinder can be determined from

$\Delta T = (R(I) - R(0))/\beta R(0)$, where $R(0)$ is the resistance of the wire at 20°C (bath temperature) when the electric current I is zero, $R(I)$ is the resistance when the current I is switched on, and β is the temperature coefficient of the resistance at 20°C. Similarly the temperature change of the wire due to the electric field effect on the heat conductivity is given by $\delta T = \delta R(I)/\beta R(0)$ and the relative temperature change by

$$\frac{\delta T}{\Delta T} = \frac{\delta R(I)}{R(I) - R(0)}. \tag{1}$$

In order to relate $R(I)$ to the heat conductivity of the gas in the cell, the conduction equation subject to the various boundary conditions should be solved. This problem has been reinvestigated quite recently by Oldham and Luchsinger[42]). They solved the conduction equation for a cylindrical hot-wire cell, subject to the following conditions:

a) The heat conductivity is independent of the radial distance from the centre of the wire. This implies that the temperature dependence of λ over the temperature range of the cell is neglected.
b) The boundaries are kept at the same temperature, by virtue of the thermostat.
c) The heat generated in the wire is dissipated by conduction through the gas, by radiation to the walls and by conduction through the wire.

The exact solution of the conduction equation is then given by:

$$\frac{R(I) - R(0)}{R(0)} = \sum_{\substack{n=1 \\ n \text{ odd}}}^{\infty} \left[n^2 \left(n^2\kappa + \varepsilon - \frac{\pi^2}{8} + N_n \Lambda \right) \right]^{-1}, \tag{2}$$

where

$$\kappa = \frac{\pi^5 R_1^2 k}{8 I^2 R(0)\, \beta l}$$ is the reduced heat conduction along the wire,

$$\varepsilon = \frac{\pi^2 e \sigma T^3 R_1 l}{I^2 R(0)\, \beta}$$ is the reduced radiation term,

$$\Lambda = \frac{\pi^4 R_1 \lambda}{4 I^2 R(0)\, \beta}$$ is the reduced heat conduction through the gas,

$$N_n = n \left[\frac{K_1(nB)\, I_0(nA) + I_1(nB)\, K_0(nA)}{K_0(nB)\, I_0(nA) - I_0(nB)\, K_0(nA)} \right],$$

k = thermal conductivity of the wire material (for platinum $k = 0.70$ W cm^{-1} K^{-1}),
l = length of the wire (for apparatus II, $l = 150$ mm),
e = emissivity,
σ = Stefan-Boltzmann constant,
$K_0(y)$, $I_0(y)$, $K_1(y)$ and $I_1(y)$ are hyperbolic Bessel functions[41]),

$A = \pi R_2/l$ and $B = \pi R_1/l$ (for apparatus II, $R_1 = 25$ μm and $R_2 = 15$ mm). Before eq. (2) is employed it is noted to what extent each of the aforementioned three conditions is applicable to our apparatus and to our measurements of the electric field effect:

a) Only at saturation is the change of the heat conductivity in an electric field independent of the radius. The temperature difference ΔT employed in the present work varies from 5°C to 15°C.

b) The ends of the thin wire are thermally linked to the bath by mica spacers which are connected to the wall, and by thick platinum wires which are connected to the feed-throughs. Secondly, the outer wall is separated from the bath by a wax layer. A simple calculation shows that these deviations are not significant.

c) For the calculation of the heat loss due to radiation it is necessary to know the emissivity ε. This factor is strongly dependent on the surface conditions of the wire. Therefore this coefficient has been determined independently by measuring the resistance as a function of I for the evacuated cell using eq. (2) with $A = 0$. A value of $\varepsilon = 0.05$ has been found.

Calculating the variation $\delta R(I)$ due to a change of λ at constant I from eq. (2) and using eq. (1) the relative change of the wire temperature is found to be

$$\left(\frac{\delta T}{\Delta T}\right)_{\text{sat}} = -\frac{\delta A}{A}\left\{\sum_{n\ \text{odd}} \frac{1}{n^2}\ \frac{N_n A}{(n^2\kappa + \varepsilon - \pi^2/8 + N_n A)^2}\right\} \times\left\{\sum_{n\ \text{odd}} \frac{1}{n^2}\ \frac{1}{(n^2\kappa + \varepsilon - \pi^2/8 + N_n A)}\right\}^{-1} = -\frac{1}{f}\left(\frac{\Delta\lambda''}{\lambda_0}\right)_{\text{sat}}. \tag{3}$$

The factor f has been calculated as a function of λ for the constants of apparatus II and for $I = 50$ mA. Its value varies from $f = 1.03$ for $\lambda = 0.05$ mW cm^{-1} K^{-1} to $f = 1.01$ for $\lambda = 0.25$ mW cm^{-1} K^{-1}.

Strictly speaking eq. (3) is valid only when the field effect is saturated in the whole cell, *i.e.* λ is independent of r. Since, however, at saturation the correction is found to be less than 3% it may be concluded that the possible deformation of the curves $\delta T/\Delta T$ *vs.* V/p, due to heat losses, is not very significant. In order to apply a correction for the heat losses without solving the generalized conduction eq. (C.2) it is reasonable to assume that the correction factor f is independent of δT (and thus of V/p), which implies no deformation of the curves at all. The saturation values of the field effect, given in table V, have been corrected according to eq. (3). Also the heat conductivity of the gas can be determined with the aid of

eq. (2) by writing

$$\frac{R(I) - R(0)}{R(0)} = \frac{\pi^2/8}{\kappa + \varepsilon - \pi^2/8 + N_1 A} \cdot f_0^{-1}, \tag{4}$$

where the correction factor

$$f_0^{-1} = \left\{ \sum_{n \text{ odd}} \frac{1}{n^2} \frac{\kappa + \varepsilon - \pi^2/8 + N_1 A}{n^2 \kappa + \varepsilon - \pi^2/8 + N_n A} \right\} \left\{ \sum_{n \text{ odd}} \frac{1}{n^2} \right\}^{-1}.$$

has been calculated for our cell as a function of λ at $I = 50$ mA. The correction factor f_0 varied between $f_0 = 1.060$ for $\lambda = 0.05$ mW cm^{-1} K^{-1} and $f_0 = 1.032$ for $\lambda = 0.25$ mW cm^{-1} K^{-1}. The values of λ_0 given in table V have been calculated according to this scheme.

REFERENCES

1) Senftleben, H., Physik. Z. 31 (1930) 961.
2) Beenakker, J. J. M., Scoles, G., Knaap, H. F. P. and Jonkman, R. M., Phys. Letters 2 (1962) 5.
3) Kagan, Yu. and Maksimov, L. A., Soviet Physics–JETP 14 (1962) 604.
4) McCourt, F. R. and Snider, R. F., J. chem. Phys. 46 (1967) 2387.
5) Beenakker, J. J. M., Festkörperprobleme VIII, ed. O. Madelung, Vieweg Verlag (Braunschweig, 1968).
6) Beenakker, J. J. M. and McCourt, F. R., Ann. Rev. Phys. Chem. 21 (1970).
7) Mikhaĭlova, Yu. V. and Maksimov, L. A., Soviet Physics–JETP 24 (1967) 1265.
8) Levi, A. C., McCourt, F. R. and Tip, A., Physica 39 (1968) 165. (Commun. Kamerlingh Onnes Lab., Leiden, Suppl. No. 126b).
9) Vines, R. G. and Bennett, L. A., J. chem. Phys. 22 (1954) 360.
10) Mason, E. A. and Monchick, L., J. chem. Phys. 36 (1962) 1622.
11) Cross, R. J., Gislason, E. A. and Herschbach, D. R., J. chem. Phys. 45 (1966) 3582.
12) Birnbaum, G., J. chem. Phys. 46 (1967) 2455.
13) Boudouris, G., Riv. Nuovo Cimento 1 (1969) 1.
14) Battaglia, A., Gozzini, A. and Polacco, E., Nuovo Cimento 14 (1959) 1076.
15) De Groot, S. R. and Mazur, P., Nonequilibrium Thermodynamics, North-Holland Publishing Co. (Amsterdam, 1962).
16) Ray, S., Phil. Mag. 43 (1922) 1129.
17) Cioară, P., Studia Univ. Babeș-Bolyai, Ser. I, Fasc. 1 (1961) 291.
18) Amme, R., Phys. Fluids 7 (1964) 1387.
19) Gallinaro, G., Meneghetti, G. and Scoles, G., Phys. Letters 24A (1967) 451.
20) Senftleben, H., Physik. Z. 32 (1931) 550.
21) Senftleben, H., Ann. Physik 15 (1965) 273.
22) Gorelik, L. L. and Sinitsyn, V. V., JETP Letters 3 (1966) 91.
23) De Groot, J. J., Van Oosten, A., Van den Meijdenberg, C. J. N. and Beenakker, J. J. M., Phys. Letters 25A (1967) 348.
24) Gorelik, L. L., Rukavishnikov, V. I. and Sinitsyn, V. V., Phys. Letters 28A (1969) 737.
25) Borman, V. D., Gorelik, L. L., Nikolaev, B. I., Sinitsyn, V. V. and Troyan, V. I., Svoiet Physics–JETP 29 (1969) 959.

26) De Groot, J. J., Hermans, L. J. F., Van den Meijdenberg, C. J. N. and Beenakker, J. J. M., Phys. Letters **31A** (1970) 304.
27) Waldmann, L., Z. Naturforsch. **12a** (1957) 660.
28) Snider, R. F., J. chem. Phys. **32** (1960) 1051.
29) Tip, A., Levi, A. C. and McCourt, F. R., Physica **40** (1968) 435 (Commun. Kamerling Onnes Lab., Leiden, Suppl. No. **126c**).
30) Levi, A. C. and McCourt, F. R., Physica **38** (1968) 415 (Commun. Kamerlingh Onnes Lab., Leiden, Suppl. No. **126a**).
31) Korving, J., Physica **46** (1970) 619.
32) Hulsman, H. and Burgmans, A. L. J., Phys. Letters **29A** (1969) 629.
33) Kennard, E. H., Kinetic Theory of Gases, McGraw-Hill Book Co. (New York and London, 1938).
34) Llewellyn Jones, F., Handbuch der Physik, Springer-Verlag (Berlin, 1959), Vol. XXII, p. 1.
35) Data Book (Thermophysical Properties Research Center, Purdue University, Lafayette, Indiana, 1966), Vol. 2.
36) Pochan, J. M., Schoemaker, R. L., Stone, R. G., Flygare, W. H., J. chem. Phys. **52** (1970) 2478.
37) Hermans, L. J. F., Koks, J. M., Knaap, H. F. P. and Beenakker, J. J. M., Phys. Letters 30A (1969) 139.
38) Hess, S., and Waldmann, L., Z. Naturforsch. **23a** (1968) 1893.
39) Birnbaum, G., J. chem. Phys. **27** (1957) 360.
40) Birnbaum, G., Intermolecular Forces, ed. J. O. Hirschfelder, Advances in Chemical Physics, Vol. 12, John Wiley & Sons (New York, 1967), Ch. 9, p. 487.
41) Abramowitz, M. and Stegun, I. A., Handbook of Mathematical Functions, Natl. Bur. Std. (U.S.), Govt. Printing Office (Washington, D.C., 1964).
42) Oldham, K. B. and Luchsinger, E. B., Trans. Faraday Soc. **64** (1968) 1791.
43) Hess, S., Z. Naturforsch. **25a** (1970) 350.

CHAPTER II

ELECTRIC AND MAGNETIC FIELD EFFECTS ON THE HEAT CONDUCTIVITY OF GASEOUS NF_3

Synopsis

The change in the heat conductivity of gaseous NF_3 in external electric and magnetic fields has been measured with several different apparatus. The results are internally consistent and in agreement with theory.

Several sets of data reported on the change of the heat conductivity of gases in an electric field show large discrepancies[1–4]). To clarify the situation we investigated the change of the heat conductivity for NF_3 both in an electric field, $\Delta\lambda(\boldsymbol{E})$, and in a magnetic field, $\Delta\lambda(\boldsymbol{H})$. In this way it is possible to check the internal consistency of the data since it follows from general theoretical arguments that both effects have equal saturation values when the small contribution from K inverting collisions is neglected for the electric field effect[8]).

The electric field effect was measured in two different hot-wire apparatus. In both apparatus a voltage difference was applied between a cylinder (radius R_2) and its central wire (radius R_1). Consequently, field and temperature gradient are parallel and the coefficient $\Delta\lambda^{//}(E)$ is obtained. In such a geometry the field effect near the wire is connected to the relative change in wire temperature by (see chapter I)[5]) $\Delta\lambda^{//}(E)/\lambda = -fa\ \mathrm{d}(\delta T/\Delta T)/$ $/\mathrm{d}(\ln(E/p))$ where $a = \ln(R_2/R_1)$ and f is a correction factor to account for heat losses and possibly Knudsen effects. The two apparatus used differed in cylinder diameter and length; in both cases $f \approx 1.03$ and $\Delta T \approx 7$ K. For the magnetic field effects homogeneous fields were used, so that in this case $\Delta\lambda(\boldsymbol{H})/\lambda = -f\delta T/\Delta T$. Firstly the coefficients $\Delta\lambda^{//}(H)$ and $\Delta\lambda^{\perp}(H)$ were measured separately in a parallel plate apparatus ($f \approx 2$ and $\Delta T \approx 10$ K),

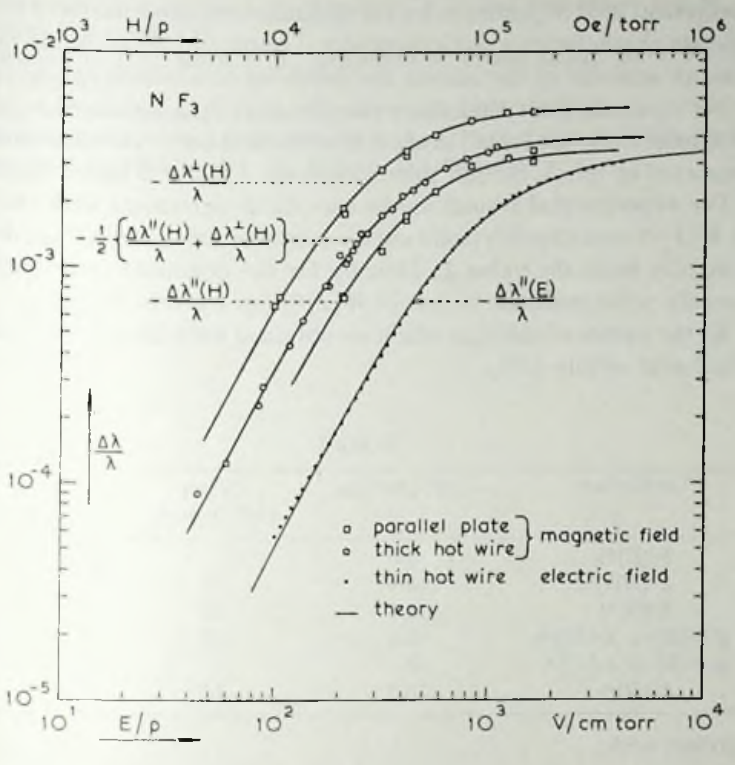

Fig. 1.

as described in ref. 6 and 7. Secondly, the combination $\frac{1}{2}\{\Delta\lambda^{//}(H) + \Delta\lambda^{\perp}(H)\}$ was measured in a thick hot wire apparatus. As hot wire a glass tube was used, heated inside with a platinum wire; here $f \approx 1.5$ and $\Delta T \approx 5$ K. The purity of the NF_3, was checked by mass-spectrometer to be better then 97%. All the results are represented in fig. 1.

The two different theoretical treatments of the electric field effect [8], and [9]), have been refined in chapter I and now yield the same field dependence. The change in heat conductivity is function of E/p, the ratio of field to pressure, but the functional behaviour depends also on the ratio of the moments of inertia of the molecule, as indicated in ref. 9. We calculated this field dependence using the moments of inertia of NF_3. The theory for the magnetic field effect should in fact be refined to account for the tensorial character of the rotational g-factor (magnetic field energy: $\mu_N(\vec{g}:JJ)\ J\cdot H/J^2$). As the components of the g-tensor for NF_3 are unknown we used the field dependence for the diamagnetic diatomic molecules. In fig. 1 the solid curves represent

the theoretical field dependence for the dominant contribution ($W[J]^{(2)}$). The parameters characterizing the experimental results are given in the table.

From an analysis of the results the following conclusions can be drawn:

a) Our research finds that the value for $(\Delta\lambda^{//}/\lambda)_{sat}$ measured in electric and magnetic fields are equal, in accordance with theory. A similar agreement was reported in ref. 3, though their values are a factor 3 higher than ours;

b) The experimental results are in reasonable agreement with the shape of the $W[J]^{(2)}$ contribution (solid curves) and the ratio $(\Delta\lambda^{\perp}/\Delta\lambda^{//})_{sat}$ deviates only slightly from the value $\frac{3}{2}$. Thus by far the dominant contribution for this weakly polar molecule is that of $W[J]^{(2)}$ (see *e.g.* refs. 10 and 6);

c) All the values of $(\Delta\lambda/\lambda)_{sat}$ which we obtained with the different methods are consistent within 10%.

TABLE I

Coefficient	$-10^3\cdot(\Delta\lambda/\lambda)_{sat}$	$(H/p)_{\frac{1}{2}}$ or $(E/p)_{\frac{1}{2}}$ (10^3 Oe/torr)	(V/cm torr)
$\lambda^{//}(E)$ [a]	3.5		980
$\lambda^{//}(H)$ [a]	3.4[5]	41	
$\lambda^{\perp}(H)$ [a]	5.4	29	
$\frac{1}{2}\{\lambda^{//}(H)+\lambda^{\perp}(H)\}$ [a]	4.0	37	
$\frac{1}{2}\{\lambda^{//}(E)+\lambda^{\perp}(E)\}$ [3]	12		1700
$\lambda^{\perp}(H)$ [3]	15.2	50	

[a] present work.

Consequently, the results obtained by Gorelik *et al.*[3], are far outside of our measuring accuracy. The measurements of ref. 3 were performed with hot-wire apparatus in homogeneous magnetic fields and slowly alternating electric fields under rather extreme conditions: $\Delta T \approx 130$ K and $f \approx 20$. Although a simplified expression was used in ref. 3 for the electric field effect, this explains only a minor part of the discrepancy.

REFERENCES

1) Gorelik, L. L. and Sinitsyn, V. V., JETP Lett. 3 (1966) 91.
2) De Groot, J. J., Van Oosten, A., Van den Meijdenberg, C. J. N. and Beenakker, J. J. M., Phys. Letters **25A** (1967) 348.
3) Gorelik, L. L., Rukavishnikov, V. I. and Sinitsyn, V. V., Phys. Letters **28A** (1969) 737.
4) Borman, V. D., Gorelik, L. L., Nikolayev, B. I., Sinitsyn, V. V. and Troyan, V. I. Sov. Phys. JETP **29** (1969) 959.
5) Tommasini, F., Levi, A. C., Scoles, G., De Groot, J. J., Van den Broeke, J. W., Van den Meijdenberg, C. J. N. and Beenakker, J. J. M., Physica **49** (1970) 299.

6) Hermans, L. J. F., Koks, J. M., Knaap, H. F. P. and Beenakker, J. J. M., Phys. Letters **30A** (1969) 139.
7) Hermans, L. J. F., Koks, J. M., Hengeveld, A. F. and Knaap, H. F. P., Physica **50** (1970) 410.
8) Levi, A. C., McCourt, F. R. and Tip, A., Physica **39** (1968) 165.
9) Mikhailova, Yu. V. and Maksimov, L. A., Sov. Phys. JETP **24** (1967) 1265.
10) Levi, A. C. and McCourt, F. R., Physica **38** (1968) 415.

CHAPTER III

HEAT CONDUCTIVITY OF POLAR–NONPOLAR GAS MIXTURES IN AN ELECTRIC FIELD

Synopsis

The change of the heat conductivity due to an electric field parallel to the temperature gradient, $\Delta\lambda^{//}(E)$, has been measured with a hot-wire apparatus for the gaseous systems CHF_3–N_2, CH_3F–N_2 and CH_3CN–N_2 at room temperature. The measurements clearly show the existence of two types of contributions to $\Delta\lambda^{//}(E)$, one giving rise to a positive effect, $\Delta\lambda^{//}(E) > 0$, the other to a negative effect, $\Delta\lambda^{//}(E) < 0$. It is found that the positive contribution is strongly connected to the dipole–dipole interactions. The occurrence of the positive contributions proves that the collision operator in the Waldmann–Snider equation is non-self-adjoint for polar gases. Effective collision cross sections have been calculated and are compared with those obtained by other methods.

1. *Introduction.* The effect of an external field on the transport properties of dilute polyatomic gases is well known (for a survey see refs. 1 and 2). Among the gases which have been studied in an external field some polar gases exhibit a special behaviour for the heat conductivity. While for most gases the transport coefficients decrease in an external field, the heat-conductivity coefficient of some strongly polar gases increases when an electric field is applied[3,4]). Further investigations on the heat-conductivity coefficient as a function of the electric field, $\lambda(\boldsymbol{E})$, revealed that in some cases the field effect, $\Delta\lambda(\boldsymbol{E})$, even changes from a positive effect, $\Delta\lambda(\boldsymbol{E}) > 0$, at low fields to a negative effect, $\Delta\lambda(\boldsymbol{E}) < 0$, at the higher fields[5,6]). These observations clearly suggest that for polar gases two contributions are present in $\lambda(\boldsymbol{E})$, one giving rise to a decrease, the other to an increase of the heat conductivity.

The positive contribution is of particular interest, as such a contribution is absent when the collision operator in the generalized Boltzmann equation

is self-adjoint[8,9]). The observed positive effect for the heat conductivity of the polar gases therefore implies that the collision operator is non-self-adjoint for these molecules. This means in a classical picture that for polar molecules a description of the collision term in the Boltzmann equation in terms of only direct and inverse collisions is insufficient.

In chapter I [7]) and ref. 4 a striking dependence of the saturation values of the field effect on the molecular electric dipole moment was found and it was therefore suggested that the positive contribution is strongly connected to the dipole–dipole interaction. If this is true, then the field effect for polar gases should be strongly influenced by the addition of a nonpolar gas. For this reason we investigated the change of the heat conductivity of some polar-nonpolar gas mixtures. Preliminary results of this study were given in ref. 6.

From the large variety of polar gases studied in chapter I, three typical examples of the symmetric top molecules were chosen *i.e.* CHF_3 an oblate symmetric top molecule with dipole moment $d = 1.64$ debye, CH_3F a prolate symmetric top molecule with $d = 1.87$D and CH_3CN a prolate symmetric top molecule with a very strong dipole moment $d = 3.94$ D. As a nonpolar component N_2 was preferred rather than one of the noble gases for the E/p range of the noble gases is more strongly limited by electrical breakdown. With N_2 as the nonpolar component it was possible to measure up to saturation of the field effect for all compositions of the systems CHF_3–N_2 and CH_3F–N_2.

In section 2 the theoretical formulation of the problem is given. The experimental method is outlined in section 3. The outline is rather extensive since measurements of $\lambda(\boldsymbol{E})$ are difficult and easily influenced by subtle differences in technique. The experimental results are given in section 4 and compared with theory in section 5. The final conclusions are stated in section 6.

2. *Theoretical formulation.* The general equation for the heat conduction of a polar gas in the presence of an external electric field $\boldsymbol{E} = (E, 0, 0)$ has the form:

$$\boldsymbol{q} = -\begin{vmatrix} \lambda^{//}(E) & 0 & 0 \\ 0 & \lambda^{\perp}(E) & 0 \\ 0 & 0 & \lambda^{\perp}(E) \end{vmatrix} \cdot \boldsymbol{\nabla} T, \tag{2.1}$$

where $\boldsymbol{q}$ is the heat flux, $\boldsymbol{\nabla} T$ the temperature gradient, $\lambda^{//}$ and $\lambda^{\perp}$ the heat-conductivity coefficients when the field is respectively parallel and perpendicular to the temperature gradient. In the absence of the field: $\lambda^{//} = \lambda^{\perp} = \lambda_0$.

From the theoretical treatments of the heat conductivity the following is recalled. In the non-equilibrium distribution function,

$$f = f_{c0}(1 - \boldsymbol{A} \cdot \boldsymbol{\nabla}(\ln T)),$$

$\boldsymbol{A}$ is expanded in terms of irreducible tensors made up of the molecular quantities: $\boldsymbol{W}$, the velocity, $\boldsymbol{J}$, the angular momentum, and for symmetric top molecules also of J_ζ, the component of $\boldsymbol{J}$ along the figure axis. The expansion terms containing $\boldsymbol{W}$ only, give the major contribution to the field free coefficient, λ_0, while the first expansion terms in both $\boldsymbol{J}$ and $\boldsymbol{W}$ or J_ζ, *i.e.* $\boldsymbol{WJ}$, $J_\zeta \boldsymbol{J}$ and $\boldsymbol{W}[\boldsymbol{J}]^{(2)}$ ($[\ ]^{(q)}$ denotes an irreducible tensor of rank q), are expected to be the most important in determining the field effect, $\Delta\lambda(\boldsymbol{E}) = \lambda(\boldsymbol{E}) - \lambda_0$. The $\boldsymbol{W}[\boldsymbol{J}]^{(2)}$ term gives rise to a decrease in the heat conductivity when an electric field is applied while the $\boldsymbol{WJ}$ term gives rise to an increase. The $J_\zeta \boldsymbol{J}$ term does not influence $\Delta\lambda^{//}$ but may contribute to $\Delta\lambda^{\perp}$ [10]). The odd terms in $\boldsymbol{J}$ are absent for parity reasons when the collision operator is self-adjoint [8]).

The effect of an electric field results from the precession of $\boldsymbol{J}$ during the free flight of the molecules. This precession destroys the $[\boldsymbol{W}]^{(p)}[\boldsymbol{J}]^{(q)}$ polarizations and the resulting effect in the heat conductivity will therefore be a function of $\omega\tau$, where ω is the precession frequency and τ is the mean free flight time. The expressions for the change of the heat conductivity for symmetric top molecules, obtained by solving the Waldmann–Snider equation with the Chapman–Enskog procedure, are (see ref. 10 and chap. I):

$$\Delta\lambda^{//}/\lambda_0 = 2\psi_{11}\langle f'_{11}(\omega\tau_{11})\rangle - \psi_{12}\langle f'_{12}(\omega\tau_{12})\rangle,$$
$$\Delta\lambda^{\perp}/\lambda_0 = \tfrac{1}{2}\Delta\lambda^{//}/\lambda_0 - \psi_{12}\langle f'_{12}(2\omega\tau_{12})\rangle. \tag{2.2}$$

The subscripts refer respectively to the rank in $\boldsymbol{W}$ and $\boldsymbol{J}$ of the expansion terms. Here ψ_{pq} are positive quantities which depend on the molecular interaction and determine the saturation value of the effect and (see ref. 11 and chap. I)

$$\langle f'_{pq}(\omega\tau_{pq})\rangle = \left\langle \frac{[\boldsymbol{J}]^{(q)} \bigcirc^{q} [\boldsymbol{J}]^{(q)}}{\langle [\boldsymbol{J}]^{(q)} \bigcirc^{q} [\boldsymbol{J}]^{(q)} \rangle_{J_\zeta \neq 0}} \frac{(\omega\tau_{pq})^2}{1 + (\omega\tau_{pq})^2} \right\rangle, \tag{2.3}$$

where ω is the precession frequency given by:

$$\omega = \frac{J_\zeta}{J(J+1)\,\hbar}\, dE, \tag{2.4}$$

with d and E the electric dipole moment and electric field, respectively. In eqs. (2.2) and (2.3) τ_{pq} are the characteristic relaxation times for the $[\boldsymbol{W}]^{(p)}[\boldsymbol{J}]^{(q)}$ polarizations given by:

$$\frac{1}{n\tau_{pq}} = \frac{\langle [\boldsymbol{J}]^{(q)}[\boldsymbol{W}]^{(p)} \bigcirc^{p+q} \mathscr{R}_0 [\boldsymbol{W}]^{(p)}[\boldsymbol{J}]^{(q)} \rangle}{\langle [\boldsymbol{J}]^{(q)}[\boldsymbol{W}]^{(p)} \bigcirc^{p+q} [\boldsymbol{W}]^{(p)}[\boldsymbol{J}]^{(q)} \rangle} \equiv \langle v_{\mathrm{rel}} \rangle\, \mathfrak{S}_{pq}, \tag{2.5}$$

n is the number density, $\mathscr{R}_0$ is the collision operator as defined in chap. I, $\mathfrak{S}_{pq}$ are generalized effective cross sections, and $\langle v_{\mathrm{rel}} \rangle$ is the average relative velocity given by $\langle v_{\mathrm{rel}} \rangle = (8kT/\pi\mu)^{\frac{1}{2}}$, where μ is the reduced mass. In the eqs. (2.2), (2.3) and (2.5) $\langle\ \rangle$ denotes an avarage over the equilibrium distri-

bution function. Since states with $J_\zeta = 0$ give rise to $\omega = 0$, these states have to be excluded from the averaging in the normalization factor, $\langle [J]^{(q)} \odot^q [J]^{(q)} \rangle$, in eq. (2.3). As can be seen from eq. (2.3), $\langle f'_{pq} \rangle$ is an average over a dispersion expression in $\omega\tau_{pq}$. This average is necessary because ω is different for molecules in different J_ζ and J states. At this point it is convenient to define a dimensionless field parameter, ξ_{pq}, which is independent of these quantum numbers:

$$\xi_{pq} = \frac{J(J+1)\,\hbar}{J_\zeta (2I_A kT)^{\frac{1}{2}}}\,\omega\tau_{pq} = \frac{\tau_{pq} p}{(2I_A kT)^{\frac{1}{2}}}\,\frac{dE}{p} = \frac{1}{\mathfrak{S}_{pq}}\left(\frac{\pi\mu}{16 I_A}\right)^{\frac{1}{2}}\frac{dE}{p}, \quad (2.6)$$

where I_A is the principal moment of inertia along an axis perpendicular to the figure axis and p is the pressure. After substituting eq. (2.6) in (2.3) one can perform the averaging and obtain $f_{pq} = \langle f'_{pq} \rangle$ as a function of ξ_{pq}, I_A and I_C. In the classical limit f_{pq} only depends on the moments of inertia via the ratio $I_A/I_C \equiv x$ and $f_{pq}(\xi_{pq}, x)$ has a less steep field dependence (weaker dispersion) with increasing value of x (chap. I).

In the literature on the electric field effect for polar symmetric top molecules sometimes a somewhat different expansion of the non-equilibrium distribution function is used[10]), resulting in a different type of averaging over the precession frequencies. The result can be written in the form:

$$f(\bar{\omega}_{pq}\tau'_{pq}) = \frac{(\bar{\omega}_{pq}\tau'_{pq})^2}{1 + (\bar{\omega}_{pq}\tau'_{pq})^2}, \quad (2.7)$$

where the quantities τ'_{pq} are defined analogously to the definition given by eq. (2.5) and the average precession frequencies $\bar{\omega}_{pq}$ are given by:

$$\bar{\omega}_{pq} = \hbar^{-1} \langle J_\zeta^2 J^{2q-2} \rangle (\langle J^{2q} \rangle \langle J_\zeta^2 J^{2q} \rangle)^{-\frac{1}{2}}\, dE$$

(see also eqs. (72) and (74) ref. 10). Functions of the type given by eq. (2.7) have often been used to analyse heat-conductivity data (chap. I and refs. 4, 5 and 12).

In eq. (2.7) the field effects are described in terms of an average precession frequency while in eq. (2.3) the contributions of molecules with different precession frequencies are averaged. It should be noted that in both expressions (2.3) and (2.7), the decay of a certain type of anisotropy in momentum space has been described with only one relaxation time (eq. (2.5)).

For a mixture of a polar and a nonpolar gas the expressions (2.2) and (2.3) remain formally the same (see ref. 13). In the expressions for f_{pq} one simply has to replace τ_{pq} by τ_{pq}^{mix}. The reciprocal of τ_{pq}^{mix} is linear in the mole fractions:

$$\frac{1}{\tau_{pq}^{\mathrm{mix}}} = X_p \frac{1}{\tau_{pq}^{\mathrm{p-p}}} + X_n \frac{1}{\tau_{pq}^{\mathrm{n-p}}}, \quad (2.8)$$

where X_p and X_n are the polar and nonpolar mole fractions, respectively.

Eq. (2.8) results from the fact that in a dilute gas mixture two types of interaction influence the decay of the $[\boldsymbol{W}]^{(p)}[\boldsymbol{J}]^{(q)}$ polarization of the polar molecules; *i.e.* the polar–polar (p–p) and nonpolar–polar (n–p) interactions.

For the analysis of the results it is useful to introduce the quantities $\xi_{pq,\frac{1}{2}}$, defined by $f_{pq}(\xi_{pq,\frac{1}{2}}, x) = \frac{1}{2}$, and from eq. (2.6) the corresponding quantities $(E/p)_{pq,\frac{1}{2}}$. Using eq. (2.2) the $(E/p)_{pq,\frac{1}{2}}$ value can be described as the E/p value at which $\Delta\lambda^{//}/\lambda_0 = \frac{1}{2}(\Delta\lambda^{//}/\lambda_0)_{\text{sat}}$ if only the $[\boldsymbol{W}]^{(p)}[\boldsymbol{J}]^{(q)}$ contribution was present. The interesting physical quantities $1/\tau_{pq}p$ or $\mathfrak{S}_{pq}$ can now be determined with the aid of eqs. (2.6) and (2.5):

$$\frac{1}{\tau_{pq}p} = \frac{d}{(2I_A kT)^{\frac{1}{2}}\,\xi_{pq,\frac{1}{2}}}\left(\frac{E}{p}\right)_{pq,\frac{1}{2}} = \frac{\langle v_{\text{rel}}\rangle\,\mathfrak{S}_{pq}}{kT}. \tag{2.9}$$

For the mixtures one finds by substituting eq. (2.8) in (2.9) that $(E/p)_{pq,\frac{1}{2}}$ is linear in the mole fractions:

$$(E/p)^{X_n}_{pq,\frac{1}{2}} = (E/p)^{X_n=0}_{pq,\frac{1}{2}}\,(X_p + X_n\gamma), \tag{2.10}$$

where

$$\gamma = \frac{\tau^{p-p}_{pq}}{\tau^{n-p}_{pq}} = \frac{(E/p)^{X_n=1}_{pq,\frac{1}{2}}}{(E/p)^{X_n=0}_{pq,\frac{1}{2}}} = \frac{\mathfrak{S}^{n-p}_{pq}}{\mathfrak{S}^{p-p}_{pq}}\left(\frac{m_n + m_p}{2m_n}\right)^{\frac{1}{2}}.$$

3. *Experimental method.* 3*a*. General. The measurements have been performed with a hot-wire apparatus in which an electric field is applied between the wire and the cylinder. The apparatus is an improved version of the two apparatuses described in chap. I. The present apparatus, see fig. 1, consists of a stainless-steel cylinder (length 16.7 mm, internal diameter 15 mm, thickness 1 mm) contained within a glass tube (length 280 mm, internal diameter 17.5 mm). The cylinder is glued to the glass tube with araldite at three points at each end of the cylinder. The platinum wire, diameter 50 μm, length 150 mm, is centred in the axis of the tube by two mylar spacers, 150 mm apart. To avoid electrostriction in the kerosene of the thermostat, the outside of the glass tube is covered with a layer of silverpaint which is electrical grounded.

Since the gases employed are chemically active both the apparatus and vacuum system have been constructed from glass, stainless steel and greaseless teflon stopcocks.

The influence of the electric field on the heat conductivity of the gas is measured differentially by using two identical cells and two variable resistances of about 100 Ω in a Wheatstone-bridge arrangement. The electric current through the wire is 50 mA and the resistance at 20°C is 7,96 Ω. Since the temperature coefficients of the thermometers, *i.e.* the Pt wire resistances, of both cells are equal to a very high degree, a temperature resolution of $\delta T \approx 1 \times 10^{-6}$ K and a resolving power of $\delta T/\Delta T = 2 \times 10^{-7}$

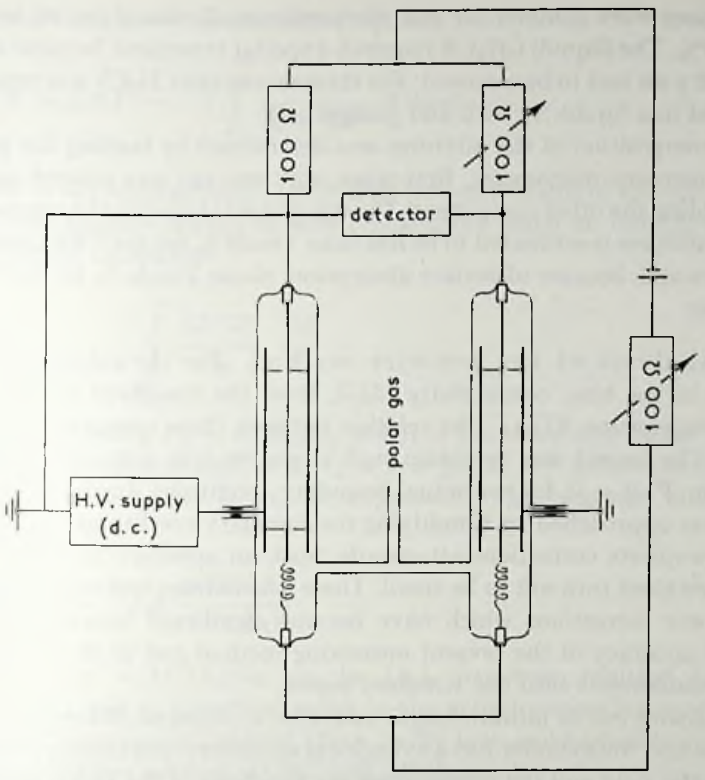

Fig. 1. A schematic diagram of the setup.

is achieved. As a matter of fact the resolving power is limited only by the thermal noise (Johnson noise) of the Wheatstone-bridge resistances. For further details on the measuring technique we refer to chap. I.

No spurious field effects were observed with a noble gas in the cells. The absence of other side effects such as electrostriction in the gas[14]) is apparent from the fact that all gases and gas mixtures investigated showed the expected unique E/p behaviour at the higher pressures. An extensive test performed with CHF_3 ($d = 1.64$ D, $M = 70$), yielded a unique E/p behaviour for pressures up to 200 torr and potential differences up to 1200 V. The results were also insensitive to the polarity of the field.

At the lower gas pressures (< 50 torr) Knudsen effects appeared. By allowing Knudsen corrections up to 40%, corresponding to a gas pressure $p \approx 2$ torr, a measuring range is obtained of about $0.2 < V/p < 200$V/torr, corresponding to a field to pressure ratio at the wire of $15 < E/p < 15 \times 10^3$ V cm^{-1} torr^{-1}. Pressures below 2 torr were avoided since at lower pressures the heat conductivity of the gas is influenced by the electric field resulting from the potential difference (≈ 0.5 V) between the ends of the wire, necessary for the heating of the wire.

All gases were commercial and the purity grade was given to be better than 99%. The (liquid) CH_3CN required a special treatment because the dissolved dry air had to be removed. For this purpose the CH_3CN was repeatedly solidified in a liquid-N_2 bath and pumped off.

The composition of the mixtures was determined by reading the pressure with a mercury manometer, first when only one gas was present and then after adding the other component. The experimental error in the compositions of the mixtures is estimated to be less than 1 mole % for the CHF_3 and CH_3F mixtures and, because of surface absorption, about 2 mole % for the CH_3CN mixtures.

3*b*. Analysis of the hot-wire method. For the calculation of the change in the heat conductivity, $\Delta\lambda/\lambda$, from the measured change in the wire temperature, $\delta T/\Delta T$, the relation between these quantities had to be found. The correct way to obtain such a relation is to solve the conduction equation, $\nabla \cdot \boldsymbol{q} = 0$, for the actual boundary conditions. In chap. I this problem was approached by simplifying the boundary conditions and applying the appropriate corrections afterwards. Such an approach is justified since the corrections turn out to be small. These calculations will now be repeated with some corrections which have become significant because of the increased accuracy of the present measuring method and of the extension of the measurements into the Knudsen region.

A hot-wire cell of infinite length and with a potential difference between the wire and the cylinder has a cylindrical symmetry and consequently both the electric field and the temperature are functions of the radial distance, r, only. Hence, the electric field, $\boldsymbol{E}$, is parallel to the temperature gradient and the heat-conductivity coefficient equals $\lambda''(E)$, see eq. (2.1). The conduction of the gas in the stationary state now satisfies the equation:

$$\nabla \cdot \{\lambda''(E, T)\, \nabla T\} = 0, \tag{3.1}$$

where $E = V/(ar)$ with $a = \ln(R_2/R_1)$ and R_1 and R_2 the radii of the wire and the cylinder, respectively.

In eq. (3.1) we have also taken into account the temperature dependence of λ. This dependence has been neglected in the earlier work†. If $\Delta T/T$ is small (about 1/30 in this experiment), one can write:

$$\lambda''(E, T) = \{\lambda_0 + \Delta\lambda''(E)\}(1 + \alpha t), \tag{3.2}$$

with $t = T(r) - T(R_2)$ and where $\alpha = (1/\lambda)(\partial\lambda/\partial T)$ and is assumed to be constant in the interval ΔT.

Solving eq. (3.1), for a cell of infinite length and in the case that heat

† For this reason the values of $(\Delta\lambda''/\lambda)_{\text{sat}}$ given in chap. I are about 2 to 3% too low.

losses are absent, one finds (see also chap. I):

$$\Delta T(1 + \tfrac{1}{2}\alpha\Delta T) = -c \int_{R_2}^{R_1} \frac{1}{\lambda_0 + \Delta\lambda''} \, \mathrm{d}(\ln r), \tag{3.3}$$

where $2\pi c$ is the constant radial heat flow per unit length of the cell. From eq. (3.3) the relative change in wire temperature when an electric field is applied can be calculated:

$$f_1 \frac{\delta T}{\Delta T} = -\frac{1}{a} \int_{E_2}^{E_1} \frac{\Delta\lambda''(E)}{\lambda_0} \frac{\mathrm{d}E}{E}, \tag{3.4}$$

where $E_1 = V/(aR_1)$, $E_2 = E_1 R_1/R_2$ and f_1 is the correction factor due to the temperature dependence of λ: $f_1 \approx 1 + \frac{1}{2}\alpha\Delta T$. By differentiating eq. (3.4) the field effect, $\Delta\lambda''/\lambda_0$, can be expressed in the measured quantities $\delta T/\Delta T$ and E_1 as

$$\frac{\Delta\lambda''(E_1)}{\lambda_0} = -f_1 a \frac{\mathrm{d}(\delta T/\Delta T)}{\mathrm{d}(\ln E_1)} \tag{3.5}$$

where the term $-\Delta\lambda''(E_2)/\lambda_0$ on the l.h.s. has been omitted because $E_2 = 0.003\, E_1$ and is, therefore, small in the actual measuring range.

From the behaviour of the field effect in the low- and high-field region a few simple relations between $\delta T/\Delta T$ and $\Delta\lambda''/\lambda_0$ result:

i) In the low-field region where $\Delta\lambda''/\lambda_0 \sim E^n$

$$\frac{\Delta\lambda''(E_1)}{\lambda_0} = -naf_1 \frac{\delta T}{\Delta T}, \tag{3.6}$$

so that on a double-logarithmic graph of $\delta T/\Delta T$ *vs.* E_1 and $\Delta\lambda/\lambda_0$ *vs.* E_1 both curves have the same initial slope but are vertically shifted by a factor naf_1.

ii) In the relatively high-field region where eq. (3.5) still holds:

$$\left(\frac{\Delta\lambda''(E_1)}{\lambda_0}\right)_{\mathrm{sat}} = -af_1 \frac{\mathrm{d}(\delta T/\Delta T)}{\mathrm{d}(\ln E_1)}, \tag{3.7}$$

so that $(\Delta\lambda''/\lambda_0)_{\mathrm{sat}}$ can be determined from the constant slope in a graph of $\delta T/\Delta T$ *vs.* $\ln E_1$ (see fig. 2).

iii) In the experimentally inaccessible, very high-field region, it follows from eq. (3.4) that:

$$f_1 \left(\frac{\delta T}{\Delta T}\right)_{\mathrm{sat}} = -\left(\frac{\Delta\lambda''}{\lambda_0}\right)_{\mathrm{sat}}. \tag{3.8}$$

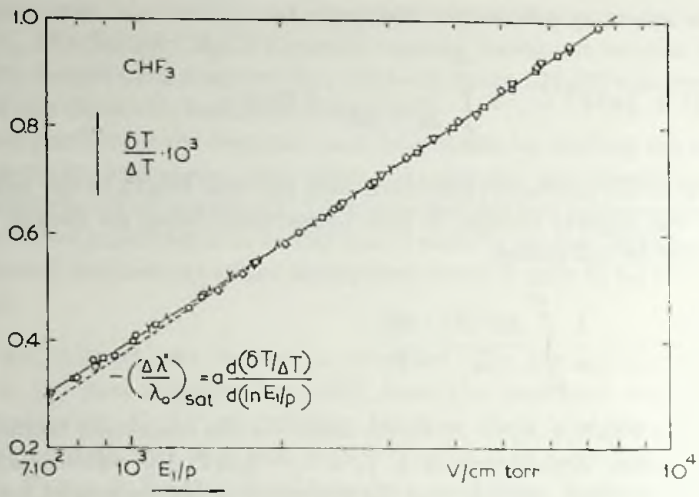

Fig. 2. Determination of $(\Delta\lambda^{//}/\lambda_0)_{sat}$ from the constant slope of $\delta T/\Delta T$ *vs.* $\ln(E_1/p)$ at high E_1/p values for CHF_3.
○ 20.5 torr, ⅄ 14.3 torr, Y 7.0 torr, □ 5.31 torr, ▽ 3.95 torr, ◇ 3.19 torr.

3*c*. Corrections. The above obtained solution of the conduction equation must be corrected for the finite length of the cell, the various heat losses and the fact that the current through the wire is kept constant rather than the heat input. The calculation of these corrections has been approached as follows.

First of all it is assumed that although the field direction is no longer parallel to the temperature gradient at the ends of the cell, still only $\lambda^{//}$ is involved so that eq. (3.1) remains unchanged. The conduction equation (3.1) is now solved taking into account the actual thermal boundary conditions but assuming that λ is independent of field and temperature. In this way the exact solution for the saturated field effect of a temperature-independent heat conductivity is obtained (see appendix D, chap. I), which can be written in the form:

$$f_2\left(\frac{\delta T}{\Delta T}\right)_{sat} = -\left(\frac{\Delta\lambda^{//}}{\lambda_0}\right)_{sat}, \tag{3.9}$$

where f_2 is a correction factor accounting for the finite length of the cell, the various heat losses and the constant current. Combining this solution with the previous solution, eq. (3.5), for the simplified boundary conditions with $\lambda = \lambda^{//}(E, T)$ a formula of practical use is now written as

$$\frac{\Delta\lambda''}{\lambda_0} = -fa\frac{\mathrm{d}(\delta T/\Delta T)}{\mathrm{d}(\ln E_1)}, \qquad \text{with} \quad f = f_1 f_2. \tag{3.10}$$

For an impression of the magnitude of the correction factors as calculated for the present apparatus the following values are given:

$\lambda_0 = 0.250$ mW cm^{-1} K^{-1}; $f_1 = 1.008$; $f_2 = 1.002$;

$\lambda_0 = 0.050$ mW cm^{-1} K^{-1}; $f_1 = 1.04$; $f_2 = 1.045$.

3*d*. Knudsen corrections. To obtain the field effect at high values of E/p, measurements have also been performed in the Knudsen region *i.e.* the low-pressure region where the wire diameter is no longer large in comparison with the mean free path of the molecules. In this region not only the field-free heat conduction but also the field effect shows deviations from the normal behaviour[15]). In the absence of the field the Knudsen correction for the wire temperature of a hot-wire cell with a constant heat input is of the form:

$$\Delta T_{\mathrm{meas}} = \Delta T(1 + K_{\Delta T}/p), \tag{3.11}$$

where $K_{\Delta T}$ is the Knudsen constant. Fig. 3 shows such a behaviour for CHF_3

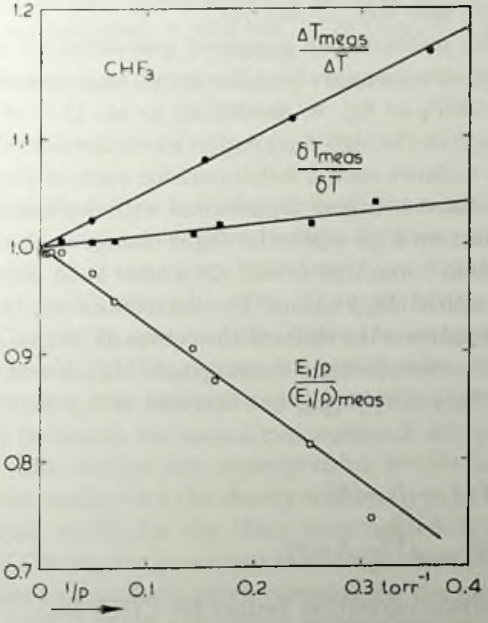

Fig. 3. The Knudsen corrections on ΔT_{meas}, δT_{meas} and $(E_1/p)_{\mathrm{meas}}$ *vs.* $1/p$ for CHF_3 according to the eqs. (3.11), (3.12) and (3.13).

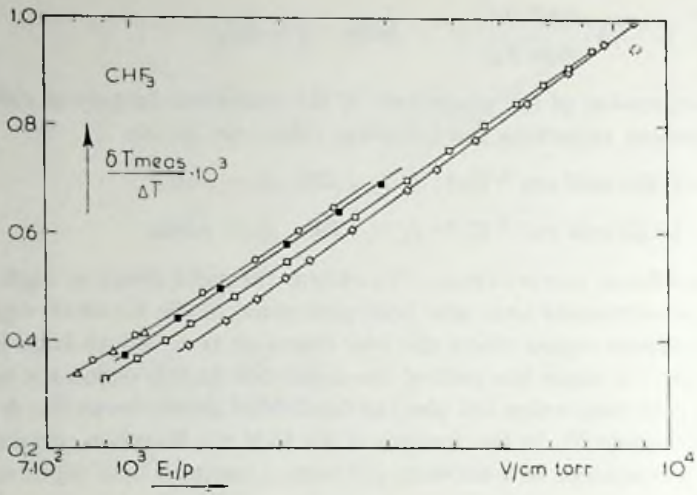

Fig. 4. Deviations from the unique E/p behaviour for CHF_3 due to Knudsen effects. After application of the Knudsen corrections the result shown in fig. 2 is obtained. △ 52.6 torr, ○ 20.5 torr, ■ 14.3 torr, □ 5.31 torr, ◇ 3.19 torr.

as obtained with the described apparatus. Similar corrections are found for the field effect (see also refs. 15 and 16).

For the hot-wire method both measured quantities, δT and E_1/p, have to be corrected. The corrections are best illustrated by a plot of δT *vs.* $\ln(E_1/p)$, as is shown for CHF_3 in fig. 4. According to eq. (3.7), $\delta T/\Delta T$ is a linear function of $\ln(E_1/p)$ in the high E_1/p region where the field effect is saturated at the wire. Fig. 4 shows such a behaviour for each of the lower pressures. The shift of these lines to higher E_1/p values with decreasing pressure is due to a Knudsen effect on E_1/p while the slight change in the slopes of the lines indicates a Knudsen correction on δT. Of course both Knudsen corrections appear at all measured E_1/p values. The corrections for the field effect are therefore determined from the shifts of the curves $\delta T/\Delta T$ *vs.* E_1/p for different low pressures on a double logarithmic graph. As an example fig. 3 shows $(\delta T)_{\text{meas}}/\delta T$ and $(E_1/p)/(E_1/p)_{\text{meas}}$ as a function of $1/p$ for CHF_3. Within the limits of accuracy the Knudsen corrections are described by:

$$\delta T_{\text{meas}} = \delta T\,(1 + K_{\delta T}/p), \tag{3.12}$$

$$E_1/p = (E_1/p)_{\text{meas}}(1 - K_E/p). \tag{3.13}$$

The specific Knudsen correction factors for CHF_3 are:

$K_{\Delta T} = 0.50$ torr, $K_E = 0.75$ torr and $K_{\delta T} = 0.10$ torr.

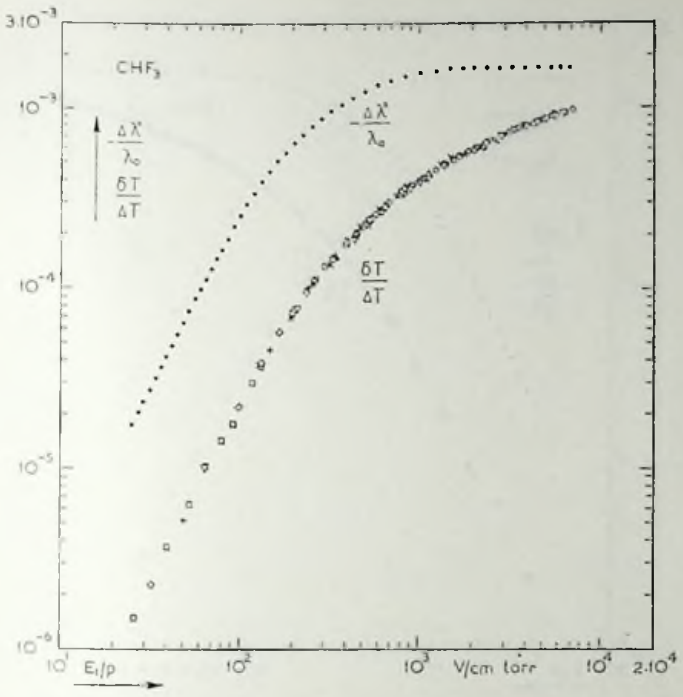

Fig. 5. $\delta T/\Delta T$ and the corresponding $\Delta\lambda''/\lambda_0$ *vs.* E_1/p for CHF_3
negative potential on the cylinder: □ 52.6 torr, ◇ 20.5 torr, ▽ 5.31 torr, △ 3.95 torr ○ 3.19 torr
positive potential on the cylinder: * 206.4 torr, + 135.1 torr, × 98.8 torr, ⅄ 14.3torr ϒ 7.0 torr.

The large value of K_E for the hot-wire method, has a similar origin as that for $K_{\Delta T}$ and is best understood by introducing a fictitious enlargement of the wire diameter. In eq. (3.4) the upper boundary $E_1 = V/(aR_1)$ must then be replaced by $E_1' = V/(aR_1')$ where $R_1' > R_1$. That part of the apparatus where the field effect is largest is now excluded from the integration and a large correction is the result. In this picture the small value of $K_{\delta T}$ is a direct consequence of the fact that the heat input is nearly kept constant.

4. *Results.* In this section the experimental results are presented. A comparison of these results with the theory will be given in the next section.

The experimental results for the three investigated systems CHF_3–N_2, CH_3F–N_2 and CH_3CN–N_2 are presented in the figs. 5–9, 11–15 and 17–22. Each of these figures shows for a given composition the measured values of $\delta T/\Delta T$ as a function of E_1/p and the corresponding curve $\Delta\lambda''/\lambda_0$. Since $\Delta\lambda''/\lambda_0$ is obtained by differentiating $\delta T/\Delta T$ with respect to $\ln(E_1/p)$ (see

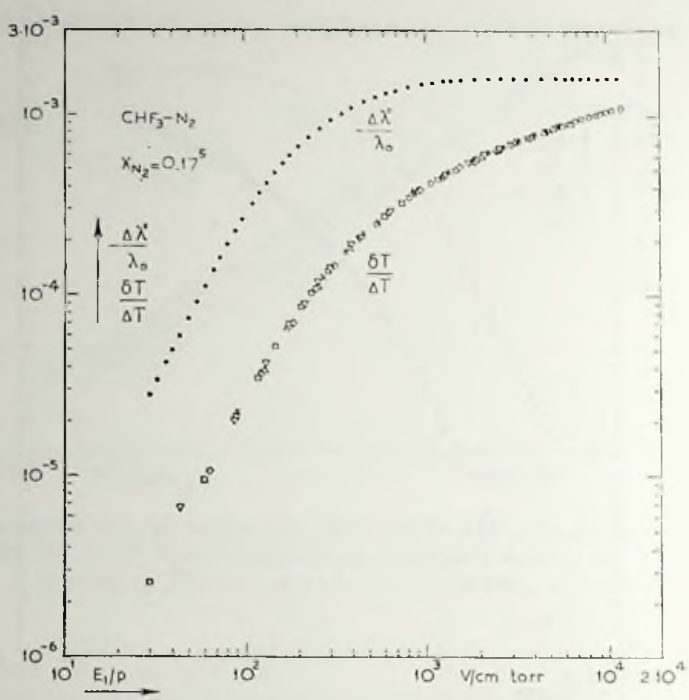

Fig. 6. $\delta T/\Delta T$ and the corresponding $\Delta\lambda''/\lambda_0$ *vs.* E_1/p for CHF_3–N_2; $X_{N_2} = 0.17^5$. □ 23.5 torr, ▽ 16.0 torr, ◇ 11.0 torr, × 7.49 torr, △ 5.09 torr, ○ 1.93 torr.

eq. (3.10)) an accurate determination of the relation between $\delta T/\Delta T$ and $\ln(E_1/p)$ is required. This is achieved by measuring many and precise values of $\delta T/\Delta T$; for each curve about 80 points with a mean scattering in the $\delta T/\Delta T$ values of either $\approx 1\%$ or 2×10^{-7} absolute. The actual differentiation was performed numerically by a polynomial fit. In the low- and high-field region the results were further checked using the relations (3.6) and (3.7).

Figs. 5–10 represent the results for the system CHF_3–N_2. For pure CHF_3 both negative and positive voltages were applied to the cylinder (see fig. 5). The results were found to be independent of the polarity, in agreement with the even in field character of the effect. Since breakdown generally occurs at the higher voltages when a negative potential is applied to the cylinder[17]), the latter polarity has mostly been used for the other gases. The measured field dependence of $\Delta\lambda''/\lambda_0$ is nearly the same for all compositions of the system. The characteristic quantities of the experimental curve, $(\Delta\lambda''/\lambda_0)_{\mathrm{sat}}$ and $(E/p)_{\frac{1}{2}}$, the experimental E/p value at half saturation, are tabulated in table I and graphically presented in fig. 10. The $(E/p)_{\frac{1}{2}}$ values are found to be linear in the concentration. When the nitrogen concentration

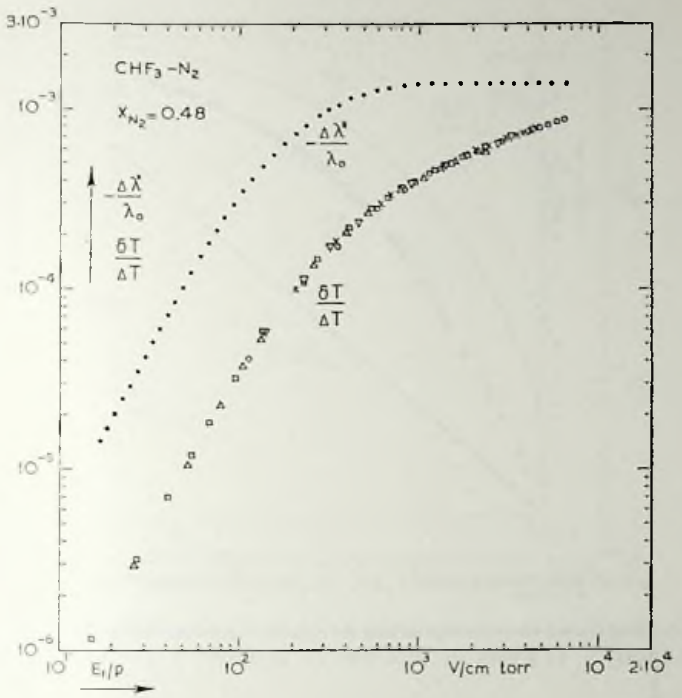

Fig. 7. $\delta T/\Delta T$ and the corresponding $\Delta\lambda^{//}/\lambda_0$ *vs.* E_1/p for CHF_3–N_2; $X_{N_2} = 0.48$. □ 51.4 torr, △ 26.5 torr, △ 15.2 torr, × 9.76 torr, ○ 5.68 torr.

reaches 100% the field effect still has a finite $(E/p)_{\frac{1}{2}}$ value while the magnitude of the effect, of course, becomes zero. The quantities $(\Delta\lambda^{//}/\lambda_0)_{sat}$ and $(E/p)_{\frac{1}{2}}$ for pure CHF_3 are 5% different from those in chap. I, due to the fact that less accurate corrections were employed in chap. I.

Figs. 11–16 present the results for the system CH_3F–N_2. As can be seen in fig. 11, pure CH_3F shows a distinct behaviour. The effect, $\Delta\lambda^{//}/\lambda_0$, is positive at low E/p values, changes sign and is negative at the higher E/p values. Such a behaviour for the electric field effect was first observed for $\frac{1}{2}(\Delta\lambda^{//} + \Delta\lambda^{\perp})$ in pure CH_3CN by Borman *et al.*[5]). The positive effect for CH_3F was overlooked in our earlier investigations as our resolving power was hardly sufficient to detect such small effects. (A change in sign of $\Delta\lambda^{//}/\lambda_0$ in the low E/p region will probably also occur for the other methyl halides, CH_3Cl and CH_3Br investigated in chap I). As can be seen in the figures, the shapes of the curves for the mixtures become gradually less steep with increasing concentration of the nonpolar component. The characteristic quantities $(\Delta\lambda^{//}/\lambda_0)_{max}$, $(E/p)_{max}$, $(E/p)_0$, *i.e.* the E/p value where $\Delta\lambda^{//}/\lambda_0 = 0$, $(\Delta\lambda^{//}/\lambda_0)_{sat}$ and $(E/p)_{\frac{1}{2}}$ are tabulated in table I and $(\Delta\lambda^{//}/\lambda_0)_{sat}$ and $(E/p)_{\frac{1}{2}}$ are plotted *vs.* X_{N_2} as shown in fig. 16. The $(E/p)_{\frac{1}{2}}$ values are to a good approxi-

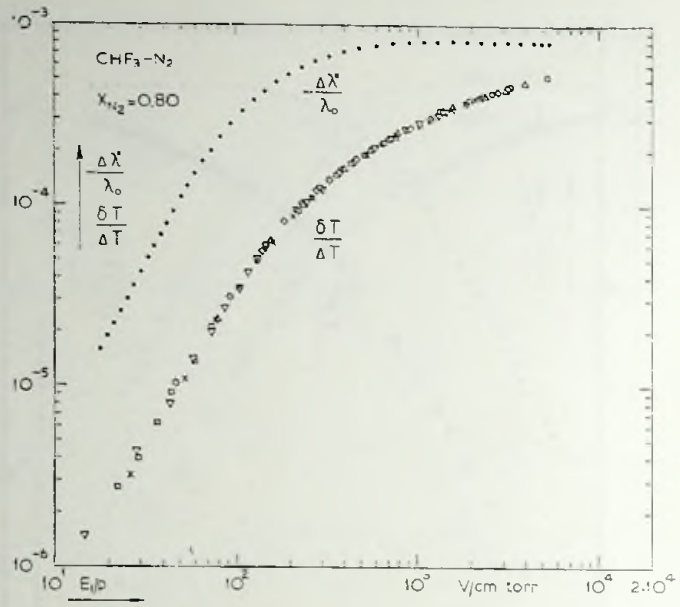

Fig. 8. $\delta T/\Delta T$ and the corresponding $\Delta\lambda''/\lambda_0$ *vs.* E_1/p for CHF_3–N_2; $X_{N_2} = 0.80$. □ 95.0 torr, ▽ 47.2 torr, × 26.5 torr, ◇ 15.0 torr, △ 7.78 torr, ○ 4.21 torr.

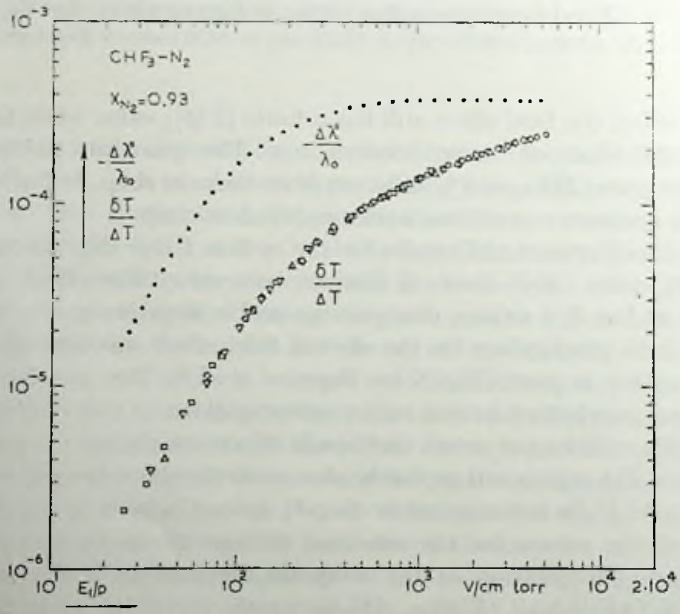

Fig. 9. $\delta T/\Delta T$ and the corresponding $\Delta\lambda''/\lambda_0$ *vs.* E_1/p for CHF_3–N_2; $X_{N_2} = 0.93$. □ 83.9 torr, △ 40.2 torr, △ 15.9 torr, ◇ 8.53 torr, ○ 4.78 torr.

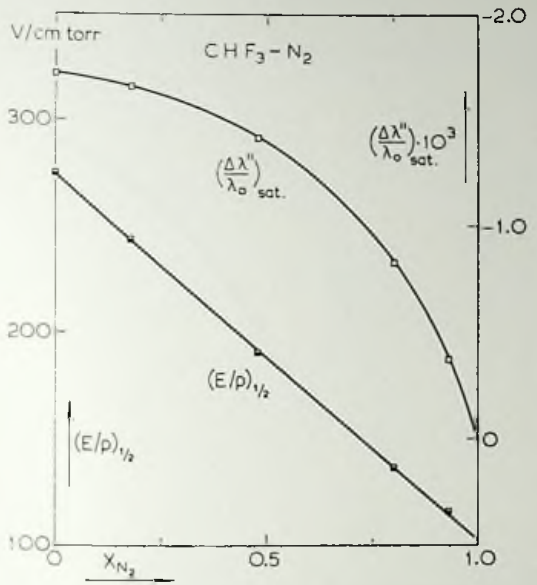

Fig. 10. $(\Delta\lambda''/\lambda_0)_{sat}$ and $(E/p)_{\frac{1}{2}}$ *vs.* X_{N_2} for the system CHF_3–N_2.

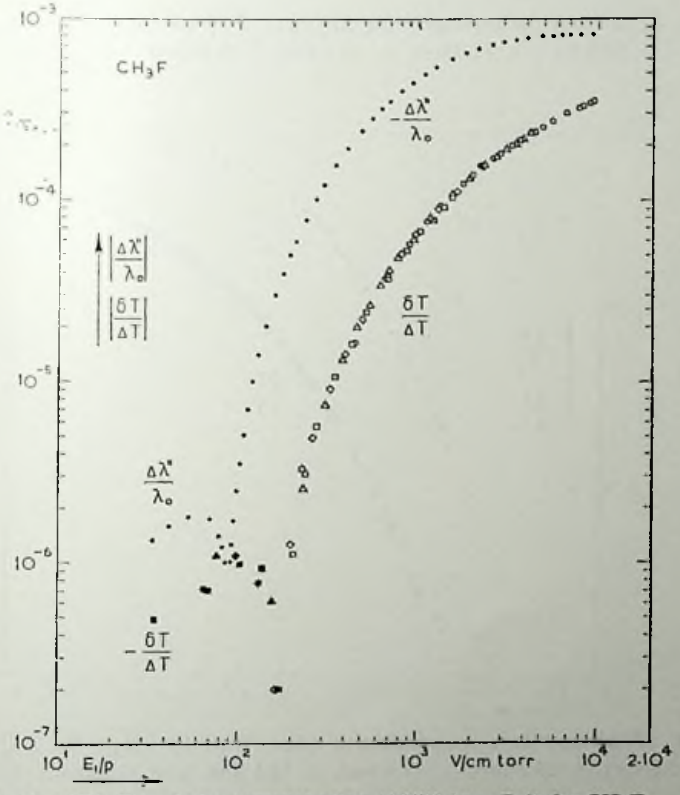

Fig. 11. $|\delta T/\Delta T|$ and the corresponding $|\Delta\lambda''/\lambda_0|$ *vs.* E_1/p for CH_3F.
■ □ 39.9 torr, ◆ ◇ 20.5 torr, ▲ △ 8.20 torr, ○ 2.06 torr.

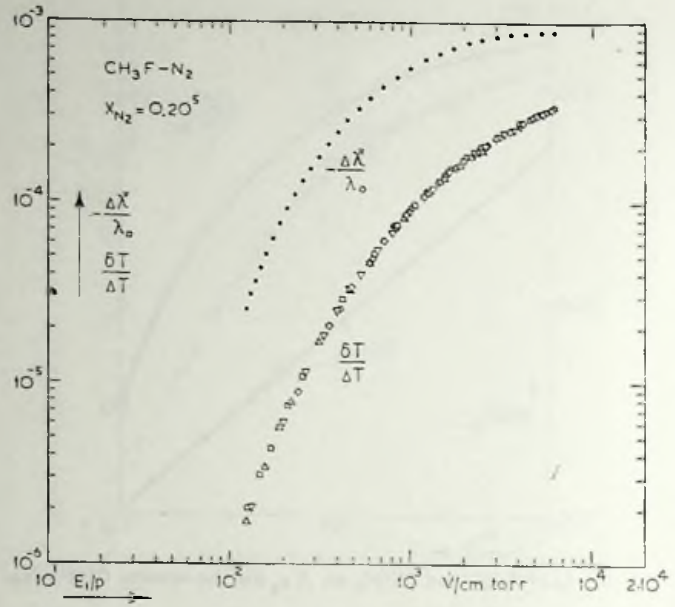

Fig. 12. $\delta T/\Delta T$ and the corresponding $\Delta\lambda''/\lambda_0$ *vs.* E_1/p for CH_3F–N_2; $X_{N_2} = 0.20^5$. □ 32.9 torr, △ 22.2 torr, ▽ 10.1 torr, ◇ 5.16 torr, ○ 2.35 torr.

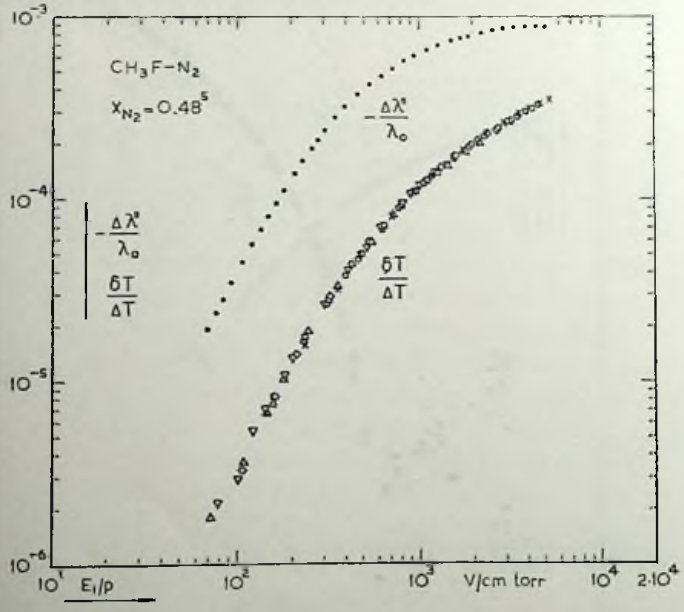

Fig. 13. $\delta T/\Delta T$ and the corresponding $\Delta\lambda''/\lambda_0$ *vs.* E_1/p for CH_3F–N_2; $X_{N_2} = 0.48^5$. □ 43.8 torr, ▽ 34.3 torr, △ 19.3 torr, ◇ 12.5 torr, ○ 8.30 torr, × 5.01 torr.

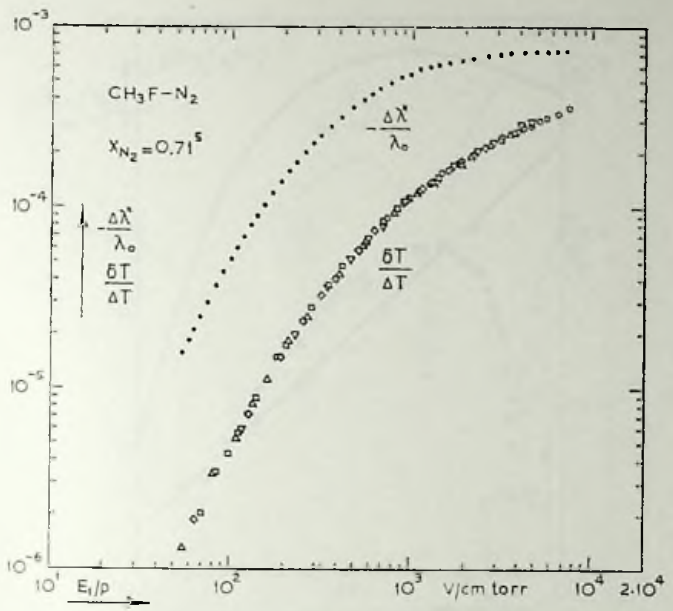

Fig. 14. $\delta T/\Delta T$ and the corresponding $\Delta\lambda''/\lambda_0$ *vs.* E_1/p for CH_3F–N_2; $X_{N_2} = 0.715$. □ 48.5 torr, △ 25.1 torr, ◇ 10.0 torr, ▽ 4.95 torr, ○ 2.33 torr.

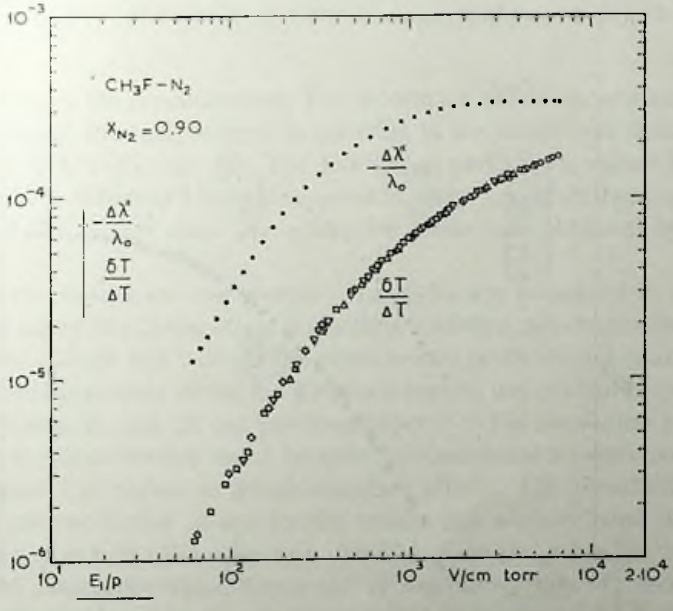

Fig. 15. $\delta T/\Delta T$ and the corresponding $\Delta\lambda''/\lambda_0$ *vs.* E_1/p for CH_3F–N_2; $X_{N_2} = 0.90$. □ 44.0 torr, ◇ 20.2 torr, ▽ 10.8 torr, △ 5.24 torr, ○ 2.64 torr.

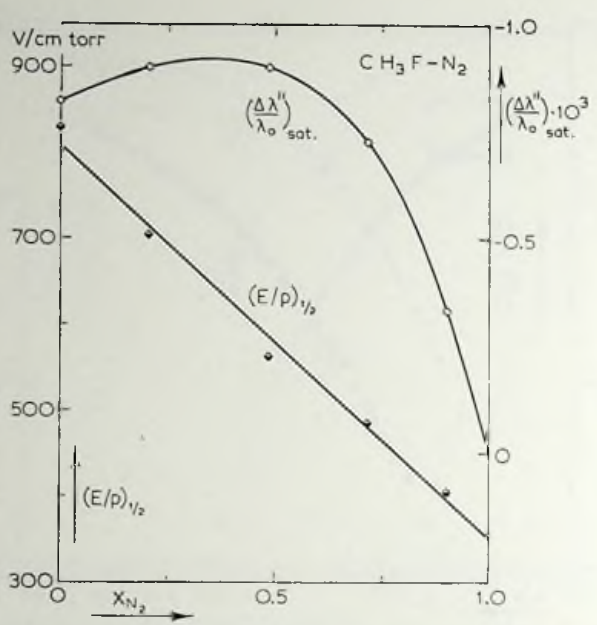

Fig. 16. $(\Delta\lambda''/\lambda_0)_{sat}$ and $(E/p)_{\frac{1}{2}}$ *vs.* X_{N_2} for the system CH_3F–N_2.

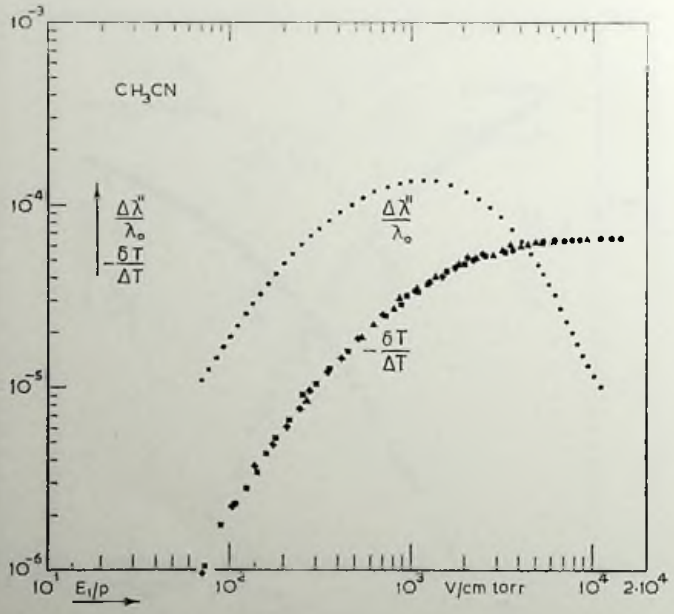

Fig. 17. $\delta T/\Delta T$ and the corresponding $\Delta\lambda''/\lambda_0$ *vs.* E_1/p for CH_3CN.
■ 37.5 torr, ◆ 19.7 torr, ▲ 7.74 torr, ● 1.89 torr.

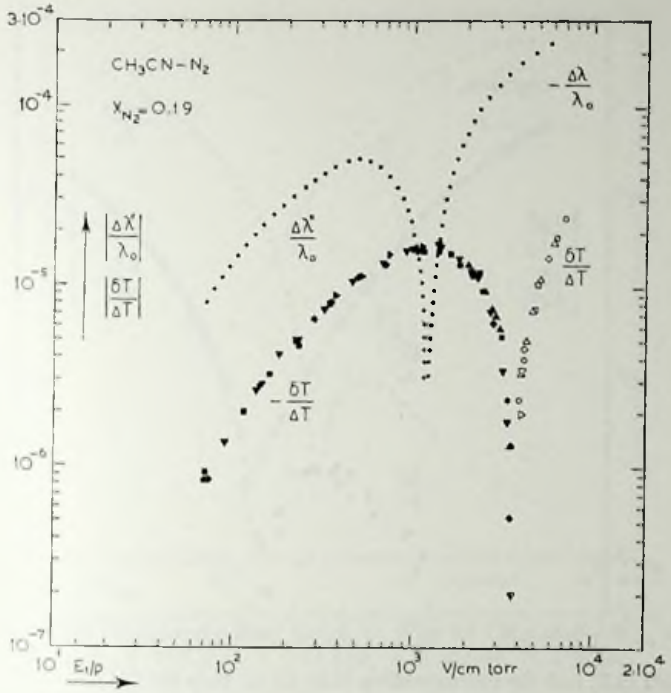

Fig. 18. $|\delta T/\Delta T|$ and the corresponding $|\Delta\lambda''/\lambda_0|$ *vs.* E_1/p for CH_3CN–N_2, $X_{N_2} = 0.19$. ■ 30.4 torr, ▼ ▽ 15.3 torr, ◆ ◇ 9.89 torr, ▶ ▷ 9.50 torr, ● ○ 6.25 torr.

mation linear in the concentration. The saturation values show a maximum as a function of the composition, in contrast to the monotonic decrease for the system CHF_3–N_2 (fig. 10). The $(\Delta\lambda''/\lambda_0)_{sat}$ and $(E/p)_i$ values for pure CHF_3 are 15% different from those given in chap. I, mainly because in the analysis of the former data the saturation value was obtained by extrapolation.

Finally the results for the system CH_3CN–N_2 are presented in the figs. 17–23. For pure CH_3CN the effect is positive, reaches a maximum and tends toward zero at high E/p values. The effect would probably not change sign, since the measurements in the far Knudsen region, not presented here, also show no change in sign. In our previous papers[4,7]) the maximum had been identified as the saturation value because no measurements were performed in the higher E/p region to avoid Knudsen effects. The possibility of an erroneous interpretation of our former results has already been suggested by Borman *et al.*[5,12]). We note that $(\Delta\lambda''/\lambda_0)_{max}$ in the table has the same value as the „saturation value" in our earlier communications[4,7]). A change in sign of $\Delta\lambda''/\lambda_0$ was found for the compositions $X_{N_2} = 0.19$ and 0.37 (figs. 18 and 19), whereas only a negative effect was observed for the higher N_2 compositions.

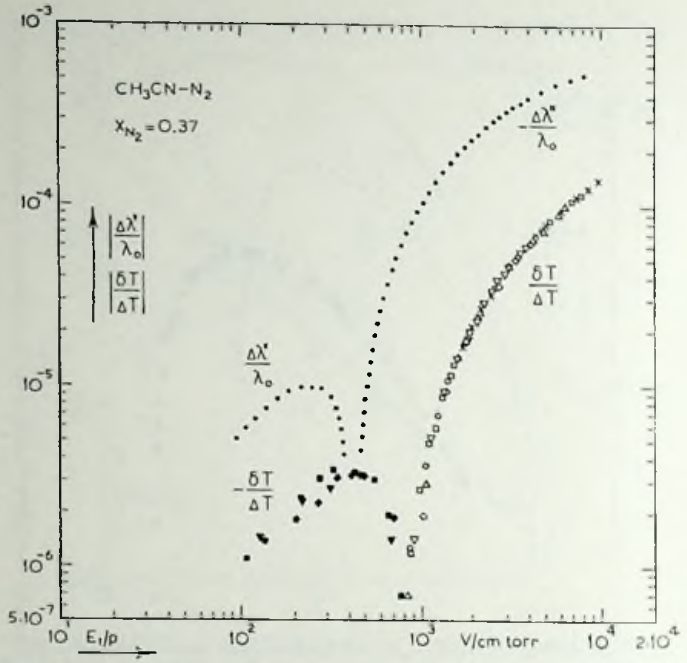

Fig. 19. $|\delta T/\Delta T|$ and the corresponding $|\Delta\lambda''/\lambda_0|$ *vs.* E_1/p for CH_3CN-N_2, $X_{N_2} = 0.37$. ■ □ 32.0 torr, ▼ ▽ 15.5 torr, ◆ ◇ 10.2 torr, △ 6.50 torr, ○ 4.00 torr, × 2.50 torr.

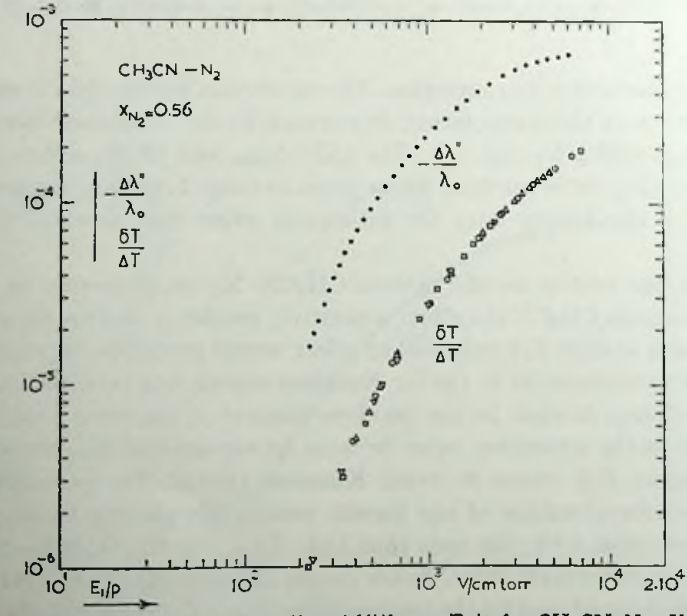

Fig. 20. $\delta T/\Delta T$ and the corresponding $\Delta\lambda''/\lambda_0$ *vs.* E_1/p for CH_3CN-N_2, $X_{N_2} = 0.56$ □ 31.1 torr, ▽ 20.9 torr, △ 10.9 torr, ○ 5.8 torr.

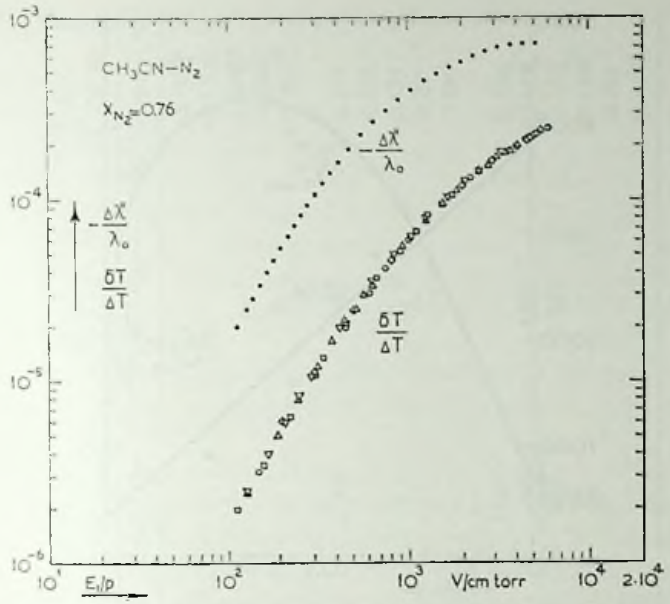

Fig. 21. $\delta T/\Delta T$ and the corresponding $\Delta\lambda''/\lambda_0$ *vs.* E_1/p for CH_3CN–N_2, $X_{N_2} = 0.76$. □ 31.2 torr, ▽ 16.7 torr, △ 11.1 torr, ◇ 6.80 torr, ○ 4.30 torr.

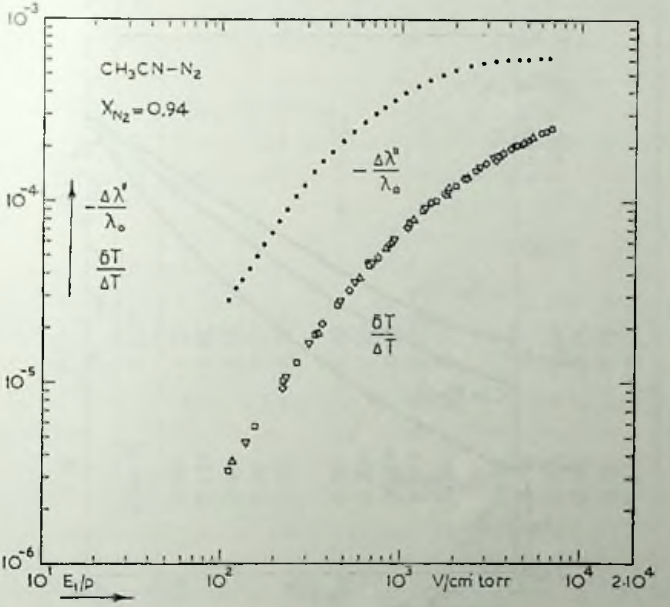

Fig. 22. $\delta T/\Delta T$ and the corresponding $\Delta\lambda''/\lambda_0$ *vs.* E_1/p for CH_3CN–N_2, $X_{N_2} = 0.94$. □ 31.4 torr, ▽ 15.2 torr, ◇ 9.22 torr, △ 5.70 torr, ○ 3.60 torr.

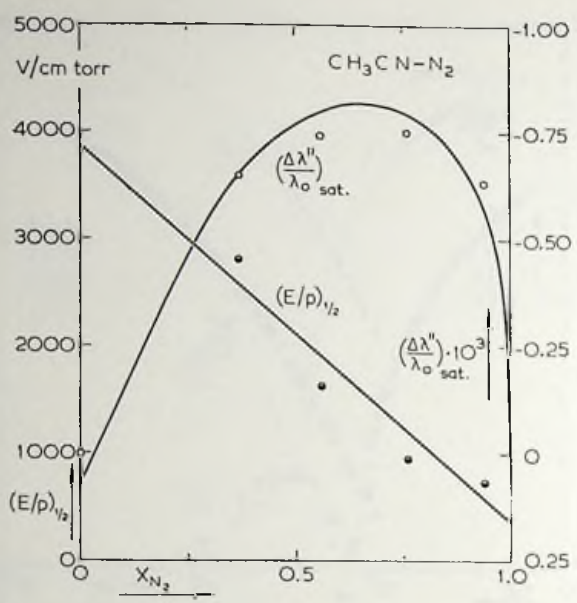

Fig. 23. $(\Delta\lambda''/\lambda_0)_{sat}$ and $(E/p)_{\frac{1}{2}}$ *vs.* X_{N_2} for the system CH_3CN–N_2:
points: extrapolation of experimental data;
solid lines: quantitative analysis (section 5*a*).

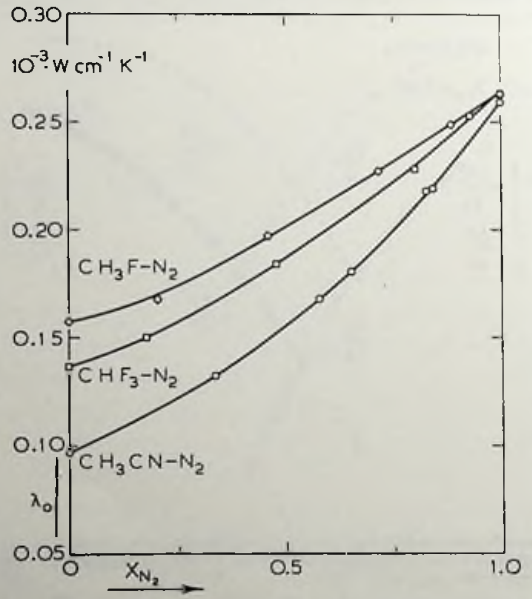

Fig. 24. Field-free heat-conductivity coefficient, λ_0, *vs.* X_{N_2} for the systems CHF_3–N_2, CH_3F–N_2 and CH_3CN–N_2 ($T \approx 297$ K).

TABLE I

System	X_{N_2}	$\left(\frac{\Delta\lambda''}{\lambda_0}\right)_{sat}$	$\left(\frac{\Delta\lambda''}{\lambda_0}\right)_{max}$	$\left(\frac{E}{p}\right)_i$	$\left(\frac{E}{p}\right)_{max}$	$\left(\frac{E}{p}\right)_0$	λ_0 (≈ 297 K)
	mole %	$\times 10^{-3}$	$\times 10^{-3}$	V cm^{-1} torr^{-1}	V cm^{-1} torr^{-1}	V cm^{-1} torr^{-1}	10^{-3} W cm^{-1} K^{-1}
CHF_3–N_2	0.00	−1.72		275			0.147
	0.17[5]	−1.66		244			0.150
	0.48	−1.42		191			0.184
	0.80	−0.83		137			0.228
	0.93	−0.37[5]		116			0.253
CH_3F–N_2	0.00	−0.82	≈ +0.002	820	≈ 60	≈ 90	0.157
	0.20[5]	−0.90		710			0.168
	0.48[5]	−0.90		562			0.197
	0.71[5]	−0.72[5]		485			0.227
	0.90	−0.33[5]		410			0.249
CH_3CN–N_2	0.00	≈ 0	+0.14		1150		0.096
	0.19		+0.05[2]		490	1200	0.115
	0.37	≈ −0.65	+0.01[0]	≈ 2800	245	420	0.137
	0.56	−0.74		1620			0.156
	0.76	−0.75		950			0.202
	0.94	−0.63		740			0.243

For the latter compositions, $X_{N_2} = 0.56$; 0.76; 0.94, the field dependence becomes gradually less steep (see figs. 20, 21 and 22).

Except for the compositions $X_{N_2} = 0.19$ and $X_{N_2} = 0.37$ a reasonable extrapolation of the data to saturation was possible. The obtained characteristic quantities are again given in table I and graphically represented as a function of composition in fig. 23. Like for the CH_3F–N_2 system the saturation values for the stysem CH_3CN–N_2 show a maximum as a function of the concentration but much more pronounced.

The values of the field-free heat conductivity, λ_0, for the three systems are represented in fig. 24 and listed in table I.

5*a*. *Discussion.* In this section the experimental results are discussed on the basis of the theoretical outline presented in section 2, for the three different systems.

The system CHF_3–N_2 ($I_A/I_C = x = 0.55$; $d = 1.64$ D)

The results for some compositions are shown on a semi log plot in fig. 25. The measured effects are negative and therefore $\boldsymbol{W}[\boldsymbol{J}]^{(2)}$ is dominant for this system. The solid curves in fig. 25 represent the field dependence of the $\boldsymbol{W}[\boldsymbol{J}]^{(2)}$ term, f_{12} (ξ_{12}, 0.55). As can be seen from the figure, the experimental field dependences fit the theoretical ones within the limits of the experimental accuracy. Although the differences in the shapes of the functions f and $f_{12}(\xi_{12}, 0.55)$ are small, $|f(\xi/\xi_{\frac{1}{2}}) - f_{12}(\xi_{12}/\xi_{12,\frac{1}{2}}, 0.5)| < 0.05$, the accurate measurements presented here do fit f_{12} better.

Since i) $\Delta\lambda^{//}/\lambda_0 < 0$, ii) the field dependence can be described with a single theoretical field function and iii) the measured $(E/p)_{\frac{1}{2}}$ values are linear in concentration (see fig. 10), it can be concluded that either the positive $\boldsymbol{WJ}$ contribution is negligible *i.e.* $\psi_{11} \approx 0$, or, because the shapes of $f_{12}(\xi_{12}, 0.55)$ and $f_{11}(\xi_{11}, 0.55)$ are nearly equal, both contributions have the same half value and $\psi_{12} > 2\psi_{11}$.

The system CH_3F–N_2 ($x = 6.0$, $d = 1.87$ D)

In fig. 26 the experimental curves for three compositions are shown and as a comparison the theoretical function $-10^{-3}\, f_{12}(\xi_{12}, 6)$ has also been drawn. The saturation values for all compositions are found to be negative; and therefore, $\boldsymbol{W}[\boldsymbol{J}]^{(2)}$ is also dominant for this system. However, since a small positive effect is found at low E/p values for pure CH_3F and the measured field dependence is steeper than $f_{12}(\xi_{12}, 6)$, the $\boldsymbol{WJ}$ polarization clearly contributes to the effect.

For a study of the field dependences the experimental curves for $X_{N_2} = 0$, $X_{N_2} = 0.90$ and the theoretical curve $f_{12}(\xi_{12}, 6)$ normalized to the same half-value and saturation value, have been drawn on a double log plot in fig. 27. Since the shapes of the experimental curves deviate from the shape of $f_{12}(\xi_{12}, 6)$ over the whole E/p region (see fig. 27) and the experimental half-values are linear in the concentration (see fig. 16), one can conclude that

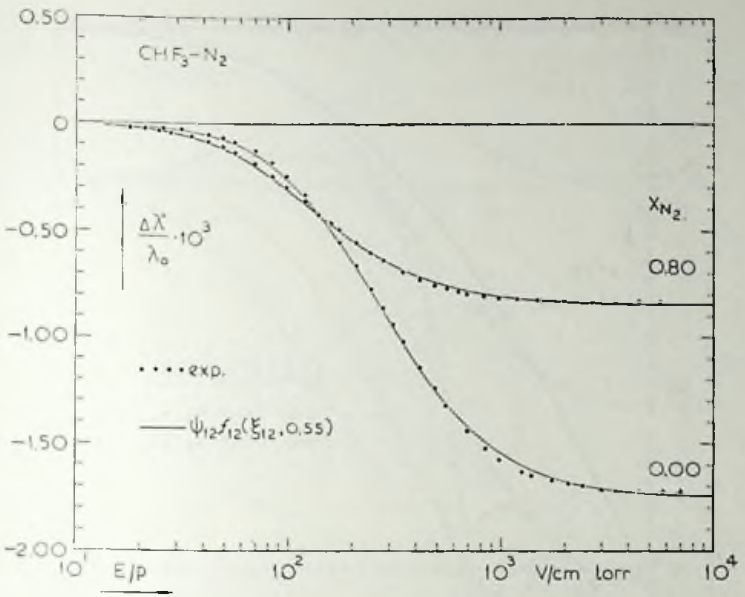

Fig. 25. $\Delta\lambda''/\lambda_0$ *vs.* E/p for two extreme CHF_3–N_2 compositions; solid lines: field dependence of the negative $W[J]^{(2)}$ term.

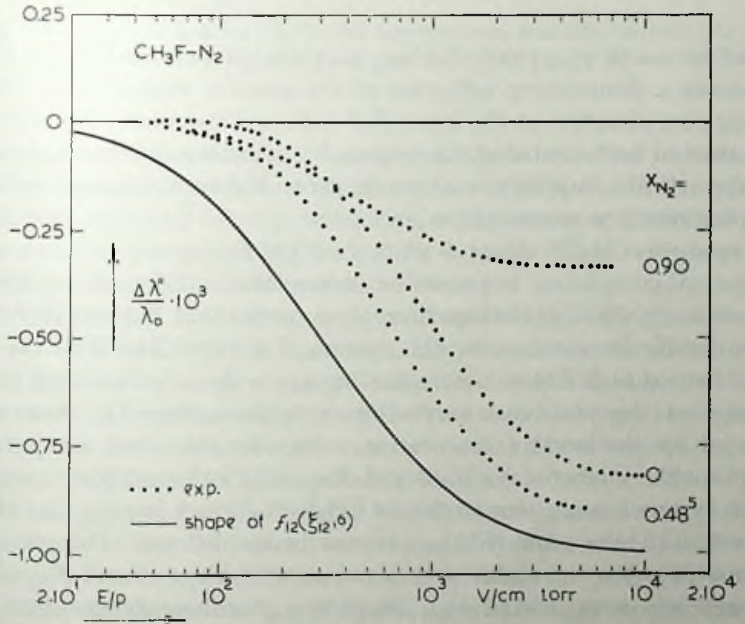

Fig. 26. $\Delta\lambda''/\lambda_0$ *vs.* E/p for three different CHF_3–N_2 compositions; solid lines: shape of the negative $W[J]^{(2)}$ term.

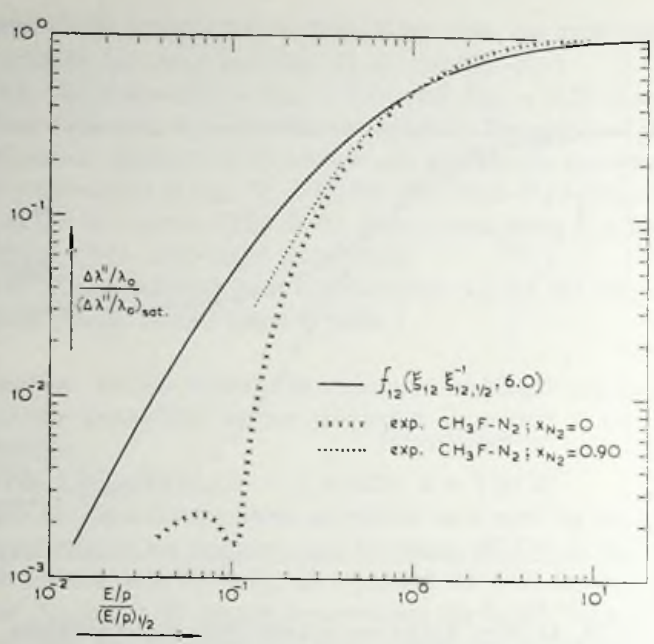

Fig. 27. Comparison between the theoretical field dependence for $W[J]^{(2)}$ and the experimental field dependence for CH_3F and CH_3F–N_2, $X_{N_2} = 0.90$.

the half-values $(E/p)_{11,\frac{1}{2}}$ and $(E/p)_{12,\frac{1}{2}}$ are rather close to each other. Fig. 27 also shows a diminishing influence of the positive contribution with increasing concentration at the lower E/p values. This means that either the half-values of both contributions approach each other even more closely or that the relative importance of the positive WJ term becomes less with increasing nitrogen concentration.

The system CH_3CN–N_2 ($x = 17.3$, $d = 3.94$ D)

A mutual comparison between the curves for the different compositions is shown in fig. 28. It is obvious from these results that WJ and $W[J]^{(2)}$ are of comparable importance for this system. For pure CH_3CN $\Delta\lambda''/\lambda_0$ tends toward zero at high E/p values, indicating $\psi_{12} \approx 2\psi_{11}$. A decreasing relative influence of the positive contribution with increasing X_{N_2}, however, is indicated by the negative saturation values for the other compositions. Except for the mixtures $X_{N_2} = 0$ and $X_{N_2} = 0.19$ the qualitative analysis for this system is analogous to that of CH_3F–N_2, which implies that also for this system $(E/p)_{11,\frac{1}{2}}$ and $(E/p)_{12,\frac{1}{2}}$ cannot be too different. This conclusion is compatible with the results for the compositions $X_{N_2} = 0$ and $X_{N_2} = 0.19$. Although $2\psi_{11} \approx \psi_{12}$ and $(E/p)_{11,\frac{1}{2}} \approx (E/p)_{12,\frac{1}{2}}$ for these compositions, a net effect results because the shape of the two field functions is different ($|f_{11}(\xi_{11}/\xi_{11,\frac{1}{2}}, 17) - f_{12}(\xi_{12}/\xi_{12,\frac{1}{2}}, 17| \lesssim 0.05$).

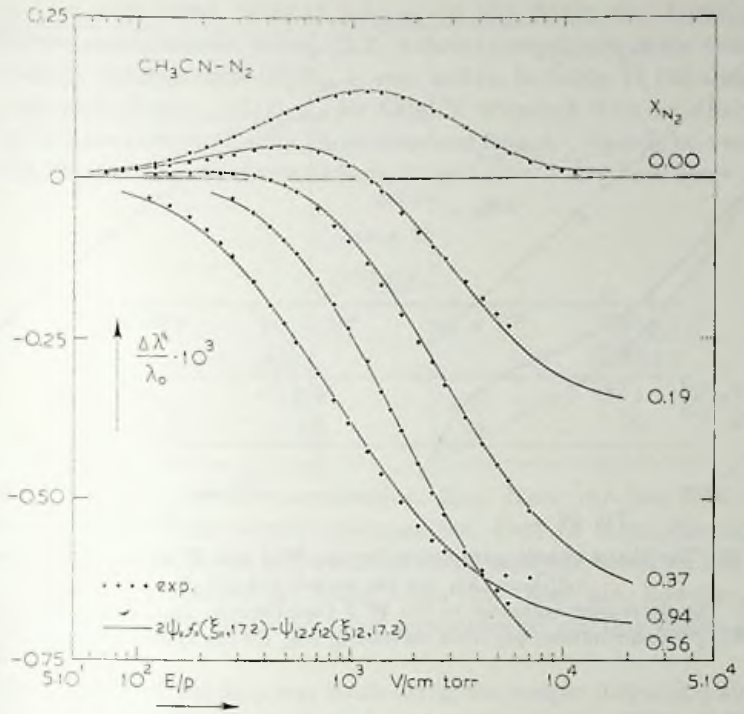

Fig. 28. $\Delta\lambda^{//}/\lambda_0$ *vs.* E/p for some CH_3CN-N_2 compositions. Field dependence of a combination of the positive $\boldsymbol{WJ}$ and negative $\boldsymbol{W}[\boldsymbol{J}]^{(2)}$ contribution.

The qualitative conclusions given above, agree with the results of a quantitative analysis performed for the system CH_3CN-N_2. In the appendix the method employed for the calculation of the separate contributions to $\Delta\lambda^{//}$ is given. Before presenting the results, however, some critical remarks concerning the analysis itself need to be made.

First the analysis is based upon the assumption that only the first-order terms, *i.e.* $\boldsymbol{WJ}$ and $\boldsymbol{W}[\boldsymbol{J}]^{(2)}$, contribute. In some cases calculated contributions turn out to be very large in comparison with the measured effects and in those circumstances higher-order terms may no longer be negligible. Secondly, distinct values for the ratio of both half-values, see appendix fig. 34, are only found for mixtures with additional characteristic points as *e.g.* $(\Delta\lambda^{//}/\lambda_0)_{max}$ and $(\Delta\lambda/\lambda_0)_0$. Finally, the obtained results strongly depend on the shape of the field functions employed for the analysis. The field functions f_{pq} are sensitive to the weighting factor $[\boldsymbol{J}]^{(q)} \odot^q [\boldsymbol{J}]^{(q)} \approx \boldsymbol{J}^{2q}$, see eq. (2.3), and the justification of this factor is still subject to discussion[18]).

The results of the analysis are shown in fig. 29 where the quantities $(E/p)_{11,\frac{1}{2}}$, $(E/p)_{12,\frac{1}{2}}$, $2\psi_{11}$ and ψ_{12} have been plotted as a function of the

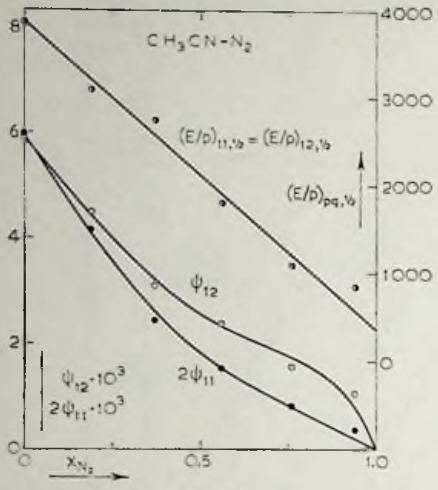

Fig. 29.

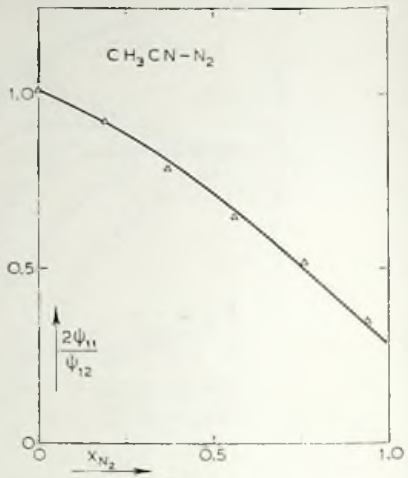

Fig. 30.

Fig. 29. The characteristic parameters for the $\boldsymbol{W}\,\boldsymbol{J}$ and $\boldsymbol{W}[\boldsymbol{J}]^{(2)}$ contribution to $\Delta\lambda^{//}/\lambda_0$ *vs.* X_{N_2} for the system CH_3CN–N_2.

Fig. 30. The decreasing influence of the $\boldsymbol{W}\,\boldsymbol{J}$ contribution, $2\psi_{11}$, with respect to the $\boldsymbol{W}[\boldsymbol{J}]^{(2)}$ contribution, ψ_{12}, with increasing X_{N_2} for the system CH_3CN–N_2.

composition. The calculated half-values are found to be linear in the concentration and for the compositions $X_{N_2} = 0.37$; 0.56; 0.76 and 0.94 the calculated half-values are close to the $(E/p)_{\frac{1}{2}}$ values determined directly from the experimental curves (fig. 23). In fig. 28 the theoretical curves corresponding to the calculated parameters are shown; the curves describe the experimental results well. We notice that the quantity ψ_{12} for pure CH_3CN ($\approx 6 \times 10^{-3}$) is of the same order of magnitude as the corresponding quantity for linear molecules as obtained from experiments performed in a magnetic field[15]). Such a comparison is meaningful since for the extreme prolate molecule CH_3CN, the total angular momentum, J, is nearly perpendicular to the figure axis as happens to be the case for the linear molecules. The ratio $2\psi_{11}/\psi_{12}$ as a function of the concentration of the nonpolar component, see fig. 30, clearly shows a decreasing influence of the $\boldsymbol{WJ}$ term with increasing X_{N_2} *i.e.* decreasing dipole–dipole interactions.

In spite of the above mentioned limitations of the analysis, we conclude that the results look realistic (see also section 6) and are internally consistent.

5*b*. *Comparison with other data.* The positive contribution in the electric field effect for the heat conductivity has also been studied by Borman *et. al.*[5,12]). They investigated the coefficient $\frac{1}{2}(\lambda^{//} + \lambda^{\perp})$ while in the present

article $\lambda^{//}$ is considered. Since in $\frac{1}{2}(\lambda^{//} + \lambda^{\perp})$ and $\lambda^{//}$ the two terms appear in different combinations, see eq. (2.2), a direct comparison of the characteristic values, $(\Delta\lambda/\lambda)_{sat}$ and $(E/p)_{\frac{1}{2}}$, is not useful. In table II the quantities $2\psi_{11}$, ψ_{12} and $(E/p)_{12,\frac{1}{2}}/(E/p)_{11,\frac{1}{2}}$ for CH_3CN obtained from an analysis of $\frac{1}{2}(\lambda^{//} + \lambda^{\perp})$ are compared with those obtained from $\lambda^{//}$. As can be seen from table II, the parameters obtained from $\lambda^{//}$ and $\frac{1}{2}(\lambda^{//} + \lambda^{\perp})$ both show a large

TABLE II

CH_3CN

Quantity	$\psi_{12} \times 10^3$	$2\psi_{11} \times 10^3$	$\frac{(E/p)_{12,\frac{1}{2}}}{(E/p)_{11,\frac{1}{2}}}$
$\lambda^{//}$	5.9	6.0	1
$\frac{1}{2}(\lambda^{//} + \lambda^{\perp})$	4.6	1.4	20

influence from the positive contribution, $2\psi_{11}$. None the less both sets of parameter values show severe discrepancies. Part of these discrepancies may be contributed to the disputability of an analysis based on one single heat conductivity coefficient. Apart from this there are, however, some objections against the theoretical and experimental starting points in refs. 5 and 12.

i) The analysis of the data was made using the simple dispersion function $f = \xi^2/(1 + \xi^2)$ for f_{11} and f_{12}. ii) Only two terms, *i.e.* the $\boldsymbol{WJ}$ and $\boldsymbol{W}[\boldsymbol{J}]^{(2)}$, were taken into account. However, the first-order term $J_\zeta \boldsymbol{J}$ may contribute to $\frac{1}{2}(\lambda^{//} + \lambda^{\perp})$, while it has been shown to be absent for $\lambda^{//}$[10]. iii) Experimentally the investigators use a hot-wire type apparatus with a parallel plate capacitor inside the cell. Since the wire is an equipotential surface, the measured quantity in such a geometry is not exactly $\frac{1}{2}(\lambda^{//} + \lambda^{\perp})$, but according to our estimations rather close to $\frac{3}{5}\lambda^{//} + \frac{2}{5}\lambda^{\perp}$. iiii) The measurements are performed in the far Knudsen region and absolute values of the field effect are obtained by a calibration method with a standard gas. Such a calibration method is only reliable when the measuring gas and the calibration gas have the same Knudsen correction factors.

For CH_3CN Borman *et al.*[12]) also measured the change of $\Delta\lambda(\boldsymbol{E})$ as a function of the field frequency, f. The observed dispersion in $\Delta\lambda$ was ascribed to the disappearance of the positive $\boldsymbol{WJ}$ contribution in the frequency range employed. However, according to theory the dispersion should be a function of f/E, whereas a dependence on f/p is observed. Moreover, the dispersion of the negative $\boldsymbol{W}[\boldsymbol{J}]^{(2)}$ contribution has not been observed although f/p values have been employed up to a factor 200 larger than the characteristic f/p value for the dispersion of $\boldsymbol{WJ}$. This seems incompatible with their static field result, $\tau_{11}/\tau_{12} \approx 20$. Apparently the behaviour of CH_3CN is very complex and as yet not completely understood.

6. *Conclusions.* The foregoing analyses show that the results of the measurements on $\lambda^{//}$ can be explained taking into account two terms, *i.e.* the $\boldsymbol{WJ}$ and $\boldsymbol{W}[\boldsymbol{J}]^{(2)}$ term in the expansion of the non-equilibrium distribution function. The saturation values, $(\Delta\lambda^{//}/\lambda_0)_{\text{sat}} = 2\psi_{11} - \psi_{12}$, as a function of the concentration for the three systems (see fig. 31) indicate a decreasing influence of the positive $\boldsymbol{WJ}$ term as a function of the nonpolar gas concentration. This conclusion is confirmed by the analysis of the CH_3CN–N_2 system which yields a decrease of $2\psi_{11}/\psi_{12}$ with increasing x_{N_2} (see fig. 30). Apparently the $\boldsymbol{WJ}$ contribution is strongly connected to the dipole–dipole interaction. A similar conclusion was made in chap. I, where for a number of polar gases a striking dependence of $(\Delta\lambda^{//}/\lambda_0)_{\text{sat}}$ on the dipole moment was found. The strong connection between the positive $\boldsymbol{WJ}$ contribution and the dipole–dipole interaction is in accordance with the conjecture that with a dipole–dipole interaction between the molecules the collisions will in general have no inverse. In other words, the collision operator is non-self-adjoint, and odd-in-$\boldsymbol{J}$ terms do exist. A more quantitative interpretation of the saturation values, *e.g.* their relation to the intermolecular potential, is not yet possible because of the complicated structure of the theoretical expressions for ψ_{11} and ψ_{12}.

For a full description of the measured field dependences the simple field function, f, is insufficient. This is made clear by fig. 33 where the curves for the highest N_2 concentrations, which have the broadest field dependence, are compared with f such that the curves meet at half height. The reason that earlier measurements on the heat conductivity of pure gases could often be described by one single f is due to the facts that: i) two contributions of opposite sign in general give a steeper field dependence; ii) these measurements generally cover a small E/p range. On the other hand, it has been shown in section 5*a* that for the description of the present measurements weak dispersion functions like f_{pq} are essential. The fact that for the electric-field effects the field dependence is given by an averaged dispersion function, eq. (2.3), rather than by a dispersion function of the averaged quantities, eq. (2.7), has already been shown more directly by measurements on the analogous electric-field effect for the viscosity (chap. I).

The analyses of the results yield equal half-values for both contributions, that is, roughly equal specific relaxation times ($\tau_{11} \approx \tau_{12}$). This is plausible. The types of collisions are specified by the properties of the $\boldsymbol{WJ}$ and the $\boldsymbol{W}[\boldsymbol{J}]^{(2)}$ term. Since both terms are sensitive to elastic and reorientation collisions, the corresponding relaxation times will be roughly equal. Considered in more detail there might be differences because reorientation collisions are rather frequent for polar gases and these collisions might influence differently odd and even terms in $\boldsymbol{J}$.

While the theoretical expressions for the saturation values are too complicated to analyse, the half-values are simply related to the time scales at

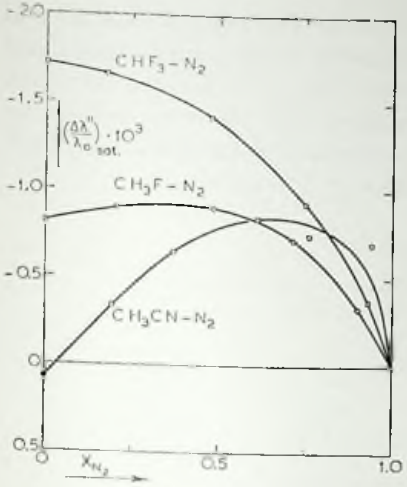

Fig. 31.

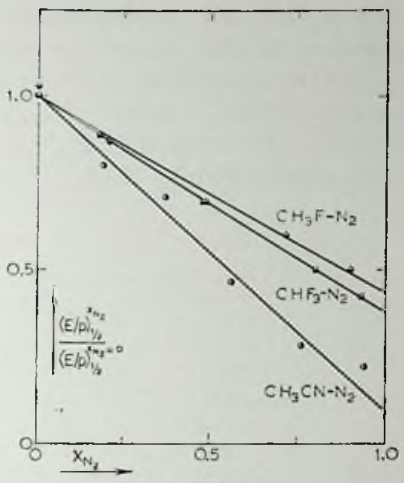

Fig. 32.

Fig. 31. $(\Delta\lambda''/\lambda_0)_{sat}$ *vs.* X_{N_2} for the systems CHF_3–N_2, CH_3F–N_2 and CH_3CN–N_2.
Fig. 32. Reduced half-values *vs.* X_{N_2} for the systems CHF_3–N_2, CH_3F–N_2 and CH_3CN–N_2.

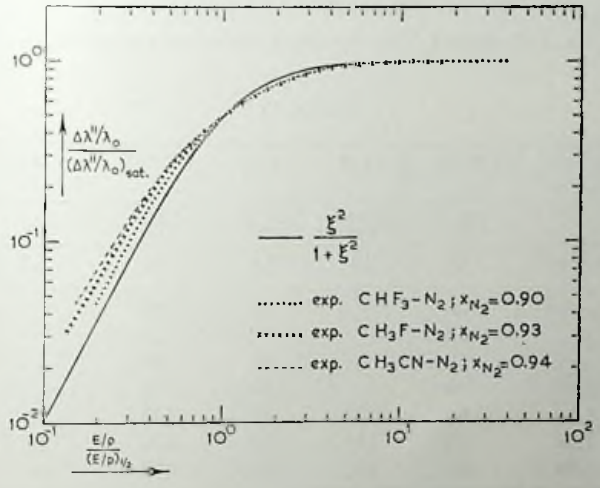

Fig. 33. Comparison between the single dispersion function, *f*, and the experimental field dependence for the three investigated systems at the highest X_{N_2}, to show that the present measurements cannot be described with *f*.

which the relevant polarizations are destructed. The reduced experimental half-values as a function of the N_2 composition for the three investigated systems are shown in fig. 32. Using the eqs. (2.9), (2.10) and the calculated quantummechanical values of $\xi_{pq,\frac{1}{2}}$ (see table III) the cross sections for the polar–polar interaction, $\mathfrak{S}_{pq}^{p-p}$, and the nonpolar–polar interaction, $\mathfrak{S}_{pq}^{n-p}$, can be calculated from $(E/p)_{pq,\frac{1}{2}}^{X_n=0}$ and $(E/p)_{pq,\frac{1}{2}}^{X_n=1}$, respectively.

TABLE III

Gas	$x = \frac{I_A}{I_C}$	$\xi_{02,\frac{1}{2}} = \xi_{12,\frac{1}{2}}$	$\xi_{11,\frac{1}{2}}$
NF_3	0.55	3.16	2.83
CHF_3	0.55	3.16	2.83
CH_3F	6.0	11.9	7.48
CH_3CN	17.3	21.0	13.0

For the systems CHF_3–N_2 and CH_3F–N_2, $\boldsymbol{W}[\boldsymbol{J}]^{(2)}$ is dominant, and if $\boldsymbol{WJ}$ is present, both half-values are probably equal (see section 5*a*). Then it can be assumed that the experimental $(E/p)_{\frac{1}{2}}$ value equals $(E/p)_{12,\frac{1}{2}}$, and therefore, only $\mathfrak{S}_{12}$ has been calculated. Since the $\boldsymbol{WJ}$ contribution decreases with increasing X_{N_2}, the values for $\mathfrak{S}_{12}^{n-p}$ are more reliable than for $\mathfrak{S}_{12}^{p-p}$. For the system CH_3CN–N_2 the quantitative analysis yielded $(E/p)_{11,\frac{1}{2}} \approx (E/p)_{12,\frac{1}{2}}$, and for this extreme prolate molecule $\xi_{11,\frac{1}{2}} = 0.6\xi_{12,\frac{1}{2}}$ (see table III); thus $\mathfrak{S}_{11}$ (= 790 Å) is higher than $\mathfrak{S}_{12}$ by a factor of 1.7. It is important to note that the differences in $\xi_{pq,\frac{1}{2}}$ are due to the different weighting factors, J^{2q}, in formula (2.3) and therefore might be an artifact of the theory. The calculated cross sections are tabulated in table IV, together

TABLE IV*

Tensor polarization →			$[\boldsymbol{W}]^{(2)}$	$J^{-2}J_\zeta \boldsymbol{J}$	$[\boldsymbol{J}]^{(2)}$	$\boldsymbol{W}[\boldsymbol{J}]^{(2)}$	$\boldsymbol{W}[\boldsymbol{J}]^{(2)}$	$J^{-2}J_\zeta \boldsymbol{J}$	$[\boldsymbol{W}]^{(2)}$
Gas		d	$\mathfrak{S}_{20}^{p-p}$	$\mathfrak{S}_{nonres}^{p-p}$	$\mathfrak{S}_{02}^{p-p}$	$\mathfrak{S}_{12}^{p-p}$	$\mathfrak{S}_{12}^{n-p}$	$\mathfrak{S}_{nonres}^{n-p}$	$\mathfrak{S}_{20}^{n-n}$
p	n	debye	Å²	Å²	Å²	Å²	Å²	Å²	Å²
N_2		—	35		21	48			
CO_2		—	52		69				
CF_4		—	63		61	84			
NF_3		0.25	50		63	70			
CHF_3	N_2	1.64	60	93	110	135	38	26	35
CH_3F	N_2	1.86	75	144	160	120	49		35
CH_3CN	N_2	3.94	106	480	480	490	44		35

* $\mathfrak{S}_{pq} = \dfrac{kT}{\langle v_{rel}\rangle p \tau_{pq}}$; $\langle v_{rel}\rangle = \left(\dfrac{8kT}{\pi\mu}\right)^{\frac{1}{2}}$; $\mathfrak{S}_{20} = \dfrac{kT}{\eta_0 \langle v_{rel}\rangle}$.

with similar quantities obtained from $\eta_3(E)$, which is sensitive for $[\boldsymbol{J}]^{(2)}$ polarization[7,13]), and nonresonant absorption[19,20]), which is sensitive for $J^{-2}J_\zeta J$ [21]). To investigate the influence of the dipole–dipole interaction on these cross sections, the cross sections of some typical nonpolar molecules, N_2, CO_2 and CF_4 obtained from $\lambda(\boldsymbol{H})$ (ref. 15) and $\eta(\boldsymbol{H})$ (ref. 22), are also listed in table IV. For comparison the kinetic cross sections, $\mathcal{S}_{20}$, obtained from η_0, are included. Comparing the cross sections it is found that the ratio, $\mathcal{S}_{12}^{p-p}/\mathcal{S}_{20}^{p-p}$, equals 1.4 for the nonpolar molecules and the weakly polar molecule NF_3. The value 1.4 seems to be general for the nonpolar molecules with the exception of the hydrogen isotopes for which inelastic collisions occur rarely[15]). The ratio $\mathcal{S}_{12}^{p-p}/\mathcal{S}_{20}^{p-p}$ tends to be higher than 1.4 for the polar molecules CHF_3 and CH_3F and reaches even the value 4.5 for the strongly polar molecule CH_3CN. For CHF_3, CH_3F and CH_3CN the cross sections for the $[\boldsymbol{J}]^{(2)}$ and $J^{-2}J_\zeta J$ polarizations are also much higher than their kinetic cross sections. Since all three cross sections $\mathcal{S}_{12}^{p-p}$, $\mathcal{S}_{02}^{p-p}$ and $\mathcal{S}_{nonres}^{p-p}$ are sensitive to J-changing collisions, it follows that for these gases J-changing collisions are at least as probable as kinetic collisions. Excluding the strongly polar molecules, it is as yet not clear whether the latter fact is due to the dipole moment or the shape of the molecule, as $\mathcal{S}_{02}^{p-p}/\mathcal{S}_{20}^{p-p}$ is also higher than 1 for the nonpolar, linear molecule CO_2.

If one, finally, compares the cross sections for the nonpolar–polar interactions, then it is remarkable that $\mathcal{S}_{12}^{n-p}$ for CH_3CN–N_2 has a normal behaviour in contrast to the extreme behaviour of $\mathcal{S}_{12}^{p-p}$ for pure CH_3CN. The situation is similar for $\mathcal{S}_{02}^{n-p}$ of the systems CH_3CN–He and CH_3CN–Ar[13]). For the strongly polar molecules the J-changing collisions indeed seem to be a consequence of the dipole–dipole interactions. A comparison between $\mathcal{S}_{12}^{p-p}$ and $\mathcal{S}_{20}^{n-p}$ is as yet not possible since reliable data are not available for the calculation of the latter cross section.

Acknowledgements. The authors wish to thank Dr. H. F. P. Knaap for some valuable comments. The apparatus was constructed by Mr. P. J. M. Vreeburg and Mr. J. M. Verbeek. The assistance of the technical and administrative staffs of the Kamerlingh Onnes Laboratorium is highly appreciated.

This work is part of the research program of the "Stichting voor Fundamenteel Onderzoek der Materie (F.O.M.)" and has been made possible by financial support from the "Nederlandse Organisatie voor Zuiver Wetenschappelijk Onderzoek (Z.W.O.)".

Analysis of the results for the CH_3CN–N_2 mixtures. Assuming the change in the heat conductivity to be made up of two contributions, one positive, the other negative, the theoretical expression for $\lambda^{//}$ has the form:

$$\Delta\lambda^{//}/\lambda_0 = 2\psi_{11} f_{11}(\xi_{11}) - \psi_{12} f_{12}(\xi_{12}), \tag{A.1}$$

where $f_{11}(\xi_{11})$ and $f_{12}(\xi_{12})$ are numerically calculated from the quantum-mechanical expressions for f_{pq}. For the analysis of the experimental results we used the corresponding relation for the integrated field dependences:

$$\delta T/\Delta T = 2\psi_{11} F_{11}(a_{11}\, E/p) - \psi_{12} F_{12}(a_{12}\, E/p), \tag{A.2}$$

where

$$a_{11} = \xi_{11}/(E/p) = \xi_{11,\frac{1}{2}}/(E/p)_{11,\frac{1}{2}} \text{ and } a_{12} = \xi_{12}/(E/p) = \xi_{12,\frac{1}{2}}/(E/p)_{12,\frac{1}{2}}.$$

For convenience E_1 has been replaced by E in eq. (A.2).

In expression (A.2) there are four unknown parameters: ψ_{11}, ψ_{12}, a_{11} and a_{12}, which in principle can be obtained by solving four equations of the form (A.2). Since expression (A.2) is valid for all values of $\delta T/\Delta T$, these four relations can be obtained by choosing four arbitrary values of $\delta T/\Delta T$ at different E/p. The four points, (1), (2), (3) and (4), have in fact been taken at equidistant E/p values distributed over the whole measuring range. For a certain point (i), $(\delta T^{(i)}/\Delta T, E^{(i)}/p)$, eq. (A.2) can be written as

$$\frac{\delta T^{(i)}}{\Delta T} = \psi_{12}\left\{\frac{2\psi_{11}}{\psi_{12}} F_{11}\left(a_{11}\frac{E^{(i)}}{p}\right) - F_{12}\left(a_{12}\frac{E^{(i)}}{p}\right)\right\}. \tag{A.3}$$

Combining eq. (A.3) for points (1) and (2) yields:

$$\frac{2\psi_{11}}{\psi_{12}} = \frac{F_{12}(a_{12}\, E^{(1)}/p)\, \delta T^{(2)}/\Delta T - F_{12}(a_{12}E^{(2)}/p)\, \delta T^{(1)}/\Delta T}{F_{11}(a_{11}\, E^{(1)}/p)\, \delta T^{(2)}/\Delta T - F_{11}(a_{11}E^{(2)}/p)\, \delta T^{(1)}/\Delta T}. \tag{A.4}$$

A similar relation holds for points (3) and (4). Eliminating $2\psi_{11}/\psi_{12}$ from the two equations gives:

$$\frac{F_{11}(a_{11}\, E^{(1)}/p)\, \delta T^{(2)}/\Delta T - F_{11}(a_{11}\, E^{(2)}/p)\, \delta T^{(1)}/\Delta T}{F_{11}(a_{11}\, E^{(3)}/p)\, \delta T^{(4)}/\Delta T - F_{11}(a_{11}\, E^{(4)}/p)\, \delta T^{(3)}/\Delta T}$$

$$= \frac{F_{12}(a_{12}\, E^{(1)}/p)\, \delta T^{(2)}/\Delta T - F_{12}(a_{12}\, E^{(2)}/p)\, \delta T^{(1)}/\Delta T}{F_{12}(a_{12}\, E^{(3)}/p)\, \delta T^{(4)}/\Delta T - F_{12}(a_{12}\, E^{(4)}/p)\, \delta T^{(3)}/\Delta T}. \tag{A.5}$$

Eq. (A.5) is of the form:

$$G_{11}(a_{11}) = G_{12}(a_{12}) \tag{A.6}$$

where G_{11} and G_{12} are known functions.

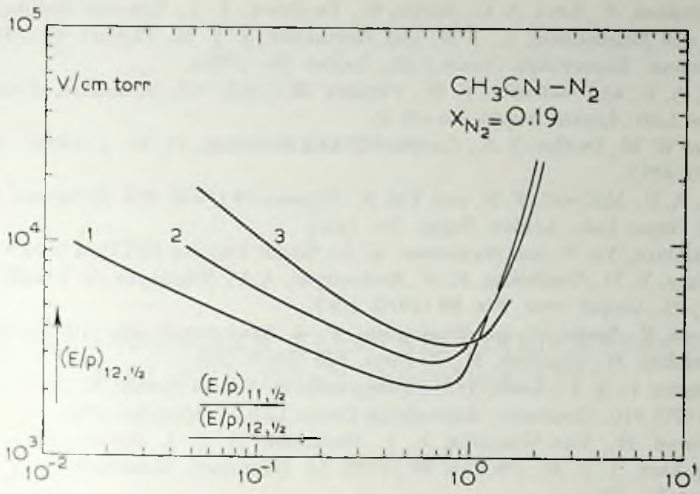

Fig. 34. Graphical solution of the half-values of the W J and $W[J]^{(2)}$ contribution to $\Delta\lambda^{//}/\lambda_0$ for CH_3CN–N_2, $X_{N_2} = 0.19$.

The eq. (A.6) is solved graphically, and thus a relation is obtained between a_{11} and a_{12} or $(E/p)_{11,\frac{1}{2}}$ and $(E/p)_{12,\frac{1}{2}}$. Such a relation obtained from data for $X_{N_2} = 0.19$ is represented by curve 1 in fig. 34. A similar relation is obtained by interchanging points (2) and (3) in eq. (A.5). The solution of the resulting equation is also shown in fig. 34 and is represented by curve 2. Curve 3 represents a third relation between $(E/p)_{11,\frac{1}{2}}$ and $(E/p)_{12,\frac{1}{2}}$ and is obtained by taking two extra points (5) and (6). As can be seen in the figure, the intersections representing the solutions for $(E/p)_{11,\frac{1}{2}}$ and $(E/p)_{12,\frac{1}{2}}$ lie in the region where $(E/p)_{11,\frac{1}{2}}/(E/p)_{12,\frac{1}{2}} \approx 1$. The graphical solution of the four equations in A.3, (see fig. 34) yields one intersection, *i.e.* the solution is unique. Knowing a_{11} and a_{12} the ratio $2\psi_{11}/\psi_{12}$ can be calculated with the aid of eq. (A.4), and ψ_{11} and ψ_{12} are finally obtained from eq. (A.3).

REFERENCES

1) Beenakker, J. J. M., Festkörperprobleme VIII, ed. O. Madelung, Vieweg Verlag (Braunschweig, 1968).
2) Beenakker, J. J. M. and McCourt, F. R., Ann. Rev. Phys. Chem. **21** (1970) 47.
3) Senftleben, H., Ann. Physik **15** (1965) 273.
4) De Groot, J. J., Van Oosten, A., Van den Meijdenberg, C. J. N. and Beenakker, J. J. M., Phys. Letters **25A** (1967) 348.
5) Borman, V. D., Gorelik, L. L., Nikolaev, B. I., Sinitsyn, V. V. and Troyan, V. I., Soviet Physics – JETP **29** (1969) 959.
6) De Groot, J. J., Van den Broeke, J. W., Martinius, H. J. and Van den Meijdenberg, C. J. N., Physica **49** (1970) 342.

7) Tommasini, F., Levi, A. C., Scoles, G., De Groot, J. J., Van den Broeke, J. W., Van den Meijdenberg, C. J. N. and Beenakker, J. J. M., Physica **49** (1970) 299. (Commun. Kamerlingh Onnes Lab., Leiden No. 379*a*).
8) Levi, A. C. and McCourt, F. R., Physica **38** (1968) 415. (Commun. Kamerlingh Onnes Lab., Leiden, Suppl. No 126 *a*).
9) Klein, W. M., Dahler, J. S., Cooper, E. and Hoffman, D. K., J. chem. Phys. **52** (1970) 4752.
10) Levi, A. C., McCourt, F. R. and Tip, A., Physica **39** (1968) 165. (Commun. Kamerlingh Onnes Lab., Leiden, Suppl. No. 126*b*).
11) Mikhailova, Yu. V. and Maksimov, L. A., Soviet Physics-JETP **24** (1967) 1265.
12) Borman, V. D., Gordienko, F. G., Medvedyev, A. V., Nikolayev, B. I. and Troyan, V. I., Zh. eksper. teor. Fiz. **59** (1970) 1067.
13) Levi, A. C., Scoles, G. and Tommasini, F., Z. Naturforsch. **25***a* (1970) 1213.
14) Senftleben, H., Gladisch, H., Z. Phys. **126** (1949) 289.
15) Hermans, L. J. F., Koks, J. M., Hengeveld, A. F. and Knaap, H. F. P., Physica **50** (1970) 410. (Commun. Kamerlingh Onnes Lab., Leiden No. 378*a*).
16) Hulsman, H., Van Waasdijk, E. J., Burgmans, A. L. J., Knaap, H. F. P. and Beenakker, J. J. M., Physica **50** (1970) 53. (Commun. Kamerlingh Onnes Lab., Leiden No. 381*c*).
17) Meeks, J. M. and Craggs, J. D., Electrical Breakdown of Gases, Oxford University press. (London A. C. 4, 1953).
18) Beenakker, J. J. M., Coope, J. A. R. and Snider, R. F., J. chem. Phys. (1971) in print.
19) Birnbaum, G., J. chem. Phys. **27** (1957) 360.
20) Frenkel, L., Kryder, S. J. and Maryott, A. A., J. chem. Phys. **44** (1966) 2610.
21) Tip, A. and McCourt, F. R., Physica **52** (1971) 109.
22) Korving, J., Physica **50** (1970) 27. (Commun. Kamerlingh Onnes Lab., Leiden No. 381*b*).

CHAPTER IV

A SECOND-ORDER ELECTRIC-FIELD EFFECT FOR THE HEAT CONDUCTIVITY

Synopsis

The existence of a second-order electric-field effect for the heat conductivity is experimentally verified. The change of the heat conductivity of a gaseous mixture of NH_3 and N_2 in an electric field is found to be a universal function of the ratio of the square of the field to the pressure. This behaviour is related to the inversion doubling of the NH_3 molecule.

For the dilute polar gases studied so far[1,2]) the changes of the transport properties in an electric field are found to be universal functions of the ratio of field to pressure, E/p (first-order effect). It is the purpose of this study to show a clear example of a case where the heat conductivity is a universal function of E^2/p (second-order field effect). For an analogous study of the viscosity we refer to a paper by the Genova group[3]).

If the change in the transport coefficients is a universal function of E/p, this is indicative for a precession frequency of the molecules proportional to the field: these molecules show spectroscopically a linear Stark effect[4]) and are characterized by a hamiltonian linear in the field.

Many polar molecules, however, exhibit a second-order Stark effect[4]). To this group belong: linear molecules, asymmetric top molecules and molecules with inversion doubling like NH_3 and ND_3. For these molecules deviations from the E/p behaviour will occur. If the field hamiltonian contains only a quadratic term, the transport properties are functions of E^2/p. So far no experimental verification of such a second-order behaviour is available. One of the reasons is that the quadratic effect for the most simple case – linear molecules[5]) – occurs at prohibitively high values of E^2/p (fields beyond the electrical breakdown limit of the gas). For the molecules of the

slightly asymmetric top type, Borman *et al*[6]) pointed out that a transition from a second- to a first-order effect will occur with increasing fields. The asymmetric-top molecules measured so far show a first-order field behaviour, as the experimentally employed fields are too high for a second-order behaviour. The molecules with inversion doubling appear to be more promising. This can be seen by considering the hamiltonian for NH_3 and ND_3[7]):

$$\mathscr{H} = \hbar^2 \frac{J^2}{2I_A} + \left(\frac{1}{2I_C} - \frac{1}{2I_A}\right)\hbar^2 K^2 + \frac{\Delta}{2} \pm \frac{\Delta}{2}\left[1 + \left(\frac{2KM}{J^2}\frac{dE}{\Delta}\right)^2\right]^{\frac{1}{2}}, \tag{1}$$

where I_A, I_C, J, K and M have the usual meaning and $\Delta = h\nu_{\text{inv}}$ is the energy difference between the symmetrical and anti-symmetrical inversion state for $= E\ 0$. From eq. (1) one can obtain the precession frequency in the quasi classical approximation:

$$\omega(J, K, M) \approx \frac{1}{\hbar}\frac{\partial \mathscr{H}}{\partial M} = \frac{K}{J^2\hbar}\, dE\left[1 + \left(\frac{\Delta}{2(KM/J^2)\, dE}\right)^2\right]^{-\frac{1}{2}}. \tag{2}$$

i) In the region $dE \ll \Delta$, $\omega = (2K^2M/J^4\hbar)\ (dE)^2/\Delta$ and the field effect will be a unique function of E^2/p.

ii) In the region $dE \gg \Delta$, $\omega = (K/J^2\hbar)\ dE$, which is the usual form for the symmetric-top molecules, and the field effect is unique in E/p.

For NH_3, $d = 1.47$ debye, $\nu_{\text{inv}} = 24$ GHz, so $dE \ll \Delta$ if $E \ll 3 \times 10^4$ V/cm. For ND_3, $d = 1.50$ debye, $\nu_{\text{inv}} = 1.6$ GHz, so the condition to find a second-order effect becomes $E \ll 2 \times 10^3$ V/cm. This is a factor 15 smaller than for NH_3.

The foregoing considerations remain valid only as long as the energy uncertainty associated with the lifetime of a molecular state is small compared to the relevant level splitting. In the zero-field limit this restriction reads: $\hbar\omega_{\text{coll}} \ll \Delta$ where $\omega_{\text{coll}} = 1/\tau$ with τ the mean free flight time. This condition can be met at low pressures. An estimate for these pressures can be obtained from the shift in the effective inversion frequency as determined from microwave-absorption work of Birnbaum and Maryott[8]). This yields as a condition on the pressure region in which measurements should be done: $p \ll 750$ torr for NH_3 and $p \ll 50$ torr for ND_3.

For a measurement of the heat conductivity with the hot-wire method [chap. III (9)] the pressure region is limited for experimental reasons to about 2 torr $< p <$ 100 torr. The lower limit is determined by Knudsen effects, the higher limit by convection. A measurement of a second-order field effect is therefore not feasible for ND_3. For NH_3, however, condition i) cannot be satisfied. Preliminary measurements on NH_3 yielded for $(E^2/p)_1$ at $p = 20$ torr a value of 2×10^7 V^2 cm^{-2} torr^{-1} and therefore E is too high near saturation.

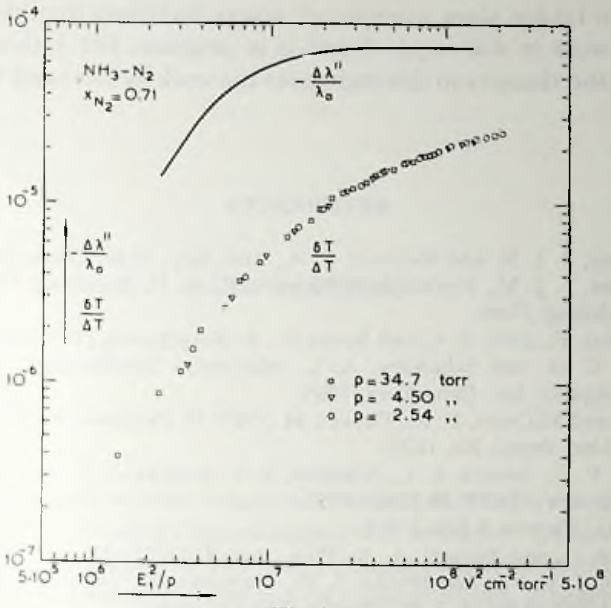

Fig. 1.

To avoid this difficulty we make use of the fact that in a mixture of a polar gas with a nonpolar gas the field effect occurs in general at lower values of E (chap. III). Fig. 1 shows the results, as obtained with the hot-wire method, for the mixture NH_3–N_2 with a 0.71 mole fraction of N_2. One observes that the relative change of the wire temperature, $\delta T/\Delta T$, is indeed a universal function of E_1^2/p, where E_1 is the field strength at the wire. [For completeness the appropriate Knudsen factors (chap. III) are given to be: $K_{\delta T} = -0.7$ torr and $K_{E^2} = 0.7$ torr]. The corresponding behaviour of the heat conductivity is also universal in E^2/p and is obtained from (chap. III):

$$\Delta\lambda''/\lambda_0 = -2af\, \mathrm{d}(\delta T/\Delta T)/\mathrm{d}(\ln E_1^2/p)$$

where $a = \ln (R_1/R_2)$ with R_1 and R_2 the radii of the wire and the cylinder respectively and f is a correction factor for the heat losses. From the curve of $\Delta\lambda''/\lambda_0$ as a function of E^2/p the following characteristic quantities are found: the saturation value, $(\Delta\lambda''/\lambda_0)_{\mathrm{sat}} = -7.5 \times 10^{-5}$, and $(E^2/p)_k = 5.0 \times 10^6$ V^2 cm^{-2} torr^{-1}.

In this paper we have limited our considerations to the experimental proof of the existence of the second-order field effect. A study of the transition between the second-order and the first-order regime is a rather complex task because of the mixing of the high field and the lifetime effects. Measurements on the heat conductivity of ND_3 in this intermediate region, so far

performed in Leiden, show, as expected, severe deviations from the E^2/p law. Additional work is still required and is in progress. For a theoretical description of the viscosity in this regime see the work by Levi and Tommei[10]).

REFERENCES

1) Beenakker, J. J. M. and McCourt, F. R., Ann. Rev. Phys. Chem. **21** (1970) 47.
2) Beenakker, J. J. M., Festkörperprobleme VIII, ed. O. Madelung, Vieweg Verlag (Braunschweig, 1968).
3) Tommasini, F., Levi, A. C. and Scoles, G., Z. Naturforsch. (1971) in print.
4) Townes, C. H. and Schawlow, A. L., Microwave Spectroscopy, McGraw-Hill Book Company, Inc. (New York, 1955).
5) Hess, S. and McCourt, F. R., Physica **44** (1969) 19 (Commun. Kamerlingh Onnes Lab., Leiden, Suppl. No. 127*b*).
6) Borman, V. D., Gorelik, L. L., Nikolaev, B. I., Sinitsyn, V. V. and Troyan, V. I., Soviet Physics – JETP **29** (1969) 959.
7) Polder, D., Physica **9** (1942) 908.
8) Birnbaum, G. and Maryott, A. A., Phys. Rev. **92** (1953) 270.
9) De Groot, J. J., Van den Broeke, J. W., Martinius, H., Van den Meijdenberg, C. J. N. and Beenakker, J. J. M., Physica (1971) in print.
10) Levi, A. C. and Tommei, G. E., Z. Naturforsch. (1971) in print.

SAMENVATTING

In dit proefschrift worden enige onderzoekingen beschreven over de verandering van de transporteigenschappen van verdunde polaire gassen in een uitwendig elektrisch veld. Het werk, weergegeven in het eerste hoofdstuk resulteerde uit een samenwerking van de molecuulfysica groepen te Leiden en Genua. In dit hoofdstuk worden de methoden voor het meten van de verandering in de viscositeit (Genua) en de warmtegeleiding (Leiden) besproken. Voor een geselecteerde groep van moleculen werd de verandering van de beide transporteigenschappen gemeten. Hierbij werd gevonden dat voor zeer sterke polaire gassen de warmtegeleiding toeneemt in een elektrisch veld, terwijl de viscositeit de normale afname laat zien. De toename van de warmtegeleiding is interessant en toont aan dat een beschrijving van het botsingsmechanisme in termen van "direkte" en "inverse" botsingen niet voldoende is. Voor het vergelijken van de experimentele resultaten met de theorie was het noodzakelijk de twee bestaande theorieën nader uit te werken. Door een synthese van beide theorieën werd een goede beschrijving van de experimentele resultaten verkregen.

In hoofdstuk II wordt de betrouwbaarheid van de warmtegeleidingsmetingen onderzocht. Hiertoe werd voor NF_3 met meerdere apparaten zowel de verandering van de warmtegeleiding in een magnetisch veld als in een elektrisch veld gemeten. De experimentele resultaten blijken intern consistent te zijn.

In hoofdstuk III wordt het positieve effect in de warmtegeleiding van de sterk polaire gassen nader onderzocht. Voor dit doel werden een aantal polaire-niet polaire gasmengsels gemeten. Deze experimenten laten duidelijk zien dat het veldeffect voor de warmtegeleiding is samengesteld uit een positieve en een negatieve bijdrage. De positieve bijdrage vertoont een duidelijke samenhang met de dipool–dipool wisselwerking tussen de moleculen. Voorts worden enige effectieve botsingsdoorsneden berekend uit de

experimentele gegevens en vergeleken met die welke bepaald zijn uit het elektrische veldeffect voor de viscositeit en uit absorptie van microgolven.

De hiervoor besproken onderzoekingen beperkten zich tot de gassen die een zogenaamde eerste orde effect vertonen, dwz. hun veldgedrag wordt bepaald door de verhouding van veldsterkte en druk, E/p. Het bestaan van een tweede orde effect (een veldgedrag bepaald door E^2/p) kon experimenteel worden geverifieerd voor een mengsel van NH_3 en het niet polaire gas N_2. Het tweede orde effect van ammonia kan verklaard worden met de moleculaire versie van dit molecuul. Deze onderzoekingen staan beschreven in het laatste hoofdstuk.

Op verzoek van de faculteit der Wiskunde en Natuurwetenschappen volgen hier enige gegevens over mijn studie.

Na mijn Mulo B opleiding van 1954–1957 aan de Titus Brandsma Ulo te Leiden volgde ik het voortgezette onderwijs aan het Sint Bonaventura Lyceum te Leiden en behaalde in 1960 het eindexamen H.B.S.–B. De hierna aangevangen studie aan de Rijksuniversiteit te Leiden werd reeds spoedig onderbroken voor het vervullen van de militaire dienstplicht, 1961–1962. Het kandidaatsexamen met de hoofdvakken natuurkunde en wiskunde met bijvak sterrekunde werd in 1964 afgelegd en het doctoraal examen experimentele natuurkunde met bijvak mechanica in 1967.

Sinds het kandidaatsexamen ben ik werkzaam op het Kamerlingh Onnes Laboratorium bij de werkgroep Molecuulfysica, die onder leiding staat van Prof. Dr. J. J. M. Beenakker. Gedurende twee jaar assisteerde ik Dr. L. J. F. Hermans, eerst bij metingen aan het verschil in polariseerbaarheid van de waterstofisotopen, daarna bij een onderzoek naar het bestaan van een dwars-warmtetransport in een magnetisch veld. In 1965 werkte ik gedurende enkele maanden in het „Instituut voor Lage Temperaturen en Technische Fysica" te Leuven.

In 1966 werd ik assistent op het natuurkundig practicum.

Vanaf 1966 ben ik in dienst van de Stichting voor Fundamenteel Onderzoek der Materie, F.O.M., eerst als wetenschappelijk assistent, later als wetenschappelijk medewerker.

Eind 1966 begon ik samen met Drs. A. van Oosten aan het onderzoek, dat in dit proefschrift beschreven staat. Een belangrijk aandeel in het verdere onderzoek hadden mevrouw Drs. M. Wisse-Schouten en de heer J. W. van den Broeke, terwijl in verschillende stadia van het experimentele werk meewerkten de heren Drs. H. Moraal, Drs. W. Schippers en H. J. Martinius. De ervaring van Drs. W. Schippers met chemisch actieve stoffen was van veel

nut. De constructie van de apparaten werd gerealiseerd door de heren P. J. M. Vreeburg en J. M. Verbeek. De nodige technische hulp werd verleend door de heer J. Turenhout en zijn medewerkers. De heer J. C. A. de Goede, van het Centraal Reken-Instituut van de Universiteit te Leiden, was behulpzaam by het opstellen van een aantal computerprogramma's.

De samenwerking met de leden van de Molecuulfysica groep van de Universiteit van Genua, Prof. A. C. Levi, Prof. G. Scoles en Dr. F. Tommasini is van veel belang geweest voor het vergelijken van experiment en theorie. In het kader van deze samenwerking werkte ik in 1969 gedurende een maand aan het „Istituto di Fisica" van de Universiteit te Genua.

Veel profijt heb ik eveneens gehad van de discussies met Dr. H. F. P. Knaap.

Mej. A. M. Aschoff en mej. S. M. J. Ginjaar brachten het manuscript van dit proefschrift in getypte vorm en de heer W. F. Tegelaar vervaardigde de tekeningen.

STELLINGEN

I

Door de verandering van een transporteigenschap van een gas in een electrisch veld te vergelijken met die in een magnetisch veld, kan, met behulp van de waarde van het elektrische dipoolmoment, het effectieve magnetische dipoolmoment worden bepaald. Uit de in hoofdstuk II gegeven resultaten voor het elektrische en magnetische veldeffect voor de warmtegeleiding van NF_3 volgt dat de effectieve moleculaire g-factor van dit molecuul $\pm$ (0.047 $\pm$ 0.005) is.

Beenakker, J. J. M. en McCourt, F. R., Ann. Rev. Phys. Chem. **21** (1970) 47.

II

De berekende theoretische snelheidsafhankelijkheid van de totale botsingsdoorsnede, die Winicur e.a. gebruiken om hun experimentele resultaten voor het systeem Ar–Kr te beschrijven, is onjuist.

Winicur, D. H., Knuth, E. L. en Rodgers, W. E., Entropie **30** (1969) 154.

III

De conclusie van Watson e.a., dat er voor supergeleidende V_3X verbindingen een verband bestaat tussen de toestandsdichtheid der geleidingselectronen aan het Fermi oppervlak en de elektrische veldgradient ter plaatse van de vanadiumkernen is aan twijfel onderhevig.

Watson, R. E., Gossard, A. C. en Yavet, Y., Phys. Rev. **140** (1965) A 375.

IV

Door Borman e.a. is experimenteel aangetoond dat de verandering van de warmtegeleiding van polaire gassen in een elektrisch wisselveld afhankelijk is van de veldfrequentie. In het gebied waar de verandering van de warmtegeleiding evenredig is met het kwadraat van de verhouding van veldsterkte en druk, kan deze techniek, in een aantal gevallen, worden gebruikt voor het bepalen van een effectieve botsingsdoorsnede.

Borman, V. D., Gorelik, L. L., Nikolaev, B. I. en Sinitsyn, V. V., JETP Letters **5** (1967) 85.

V

Bij het publiceren van botsingsdoorsneden en botsingsgetallen is het wenselijk de gebruikte definitie van deze grootheden op te geven.

Holmes, R., Jones, G. R. en Pusat, M., Trans. Faraday Soc. **60** (1964) 299.
Tommasini, F., Levi, A. C., Scoles, G., De Groot, J. J., Van den Broeke, J. W., Van den Meijdenberg, C. J. N., Beenakker, J. J. M., Physica **49** (1970) 299.

VI

Dave e.a. concluderen uit de door hen bepaalde viscositeits-coëfficiënten van gassen dat de moleculen CH_4, CF_4, en SF_6 een niet sferische interactie hebben. Deze conclusie is aanvechtbaar.

Dave, R. A. en Smith, E. B., J. chem. Phys. **52** (1970) 693.
Dave, R. A., Maitland, G. C., Rigby, M. en Smith, E. B., Trans. Faraday Soc. **66** (1970) 1955.

VII

Terecht merkt Schmidt op dat het in principe niet nodig is éénkristallen te gebruiken om overgangen te detecteren tussen de spincomponenten van de fosforescerende triplettoestand van organische moleculen in afwezigheid van een magneetveld. Het is evenwel niet duidelijk waarom hij geen gebruik maakt van dit voordeel.

Schmidt, J., proefschrift, Leiden, 1971.

VIII

Gezien de in dit proefschrift beschreven resultaten voor polaire gassen en mengsels van polaire met niet-polaire gassen is het interessant om na te gaan welke eigenschappen voor de botsingsoperator van deze gassen volgen

uit de symmetrie-eigenschappen van de dipool-dipool wisselwerking en de dipool-quadrupool wisselwerking.

IX

De door Borman e.a. gebruikte formule voor het afschatten van de gemiddelde precessiefrequentie van polaire symmetrische tol-moleculen in een electrisch veld, is ontoereikend voor dit doel.

Borman,, V. D., Gordienko, F. G., Medvedeyev, A. V., Nikolaev, B. I. en Troyan, V. I., Z.E.T.F. **59** (1970) 1067.

X

Om het springen van flessen, welke koolzuurhoudende frisdrank bevatten, te voorkomen, is het o.a. gewenst een aan de kwaliteit van de fles aangepaste veiligheidsdop wettelijk voor te schrijven.

N.S.D.A. rapport "Bottle Performance Guide Lines".